Catarina Pereira Amado

Licenciada em Ciências da Engenharia Biomédica

Diving into the depth of primary motor cortex

A high-resolution investigation of the motor system using 7Tesla fMRI

Dissertação para a obtenção do Grau de Mestre em Engenharia Biomédica

Orientadora: Doutora Wietske Van der Zwaag, CIBM, EPFL

Co-orientador: Doutor Roy Salomon, LNCO, EPFL

Co-orientador: Professor Doutor Mário Forjaz Secca, FCT/UNL

Júri:

Presidente: Doutora Carla Quintão

Arguente: Doutora Rita Nunes

Vogal: Doutor Mário Forjaz Secca

FACULDADE DE CIÊNCIAS E TECNOLOGIA
UNIVERSIDADE NOVA DE LISBOA

Diving into the depth of the Primary Motor Cortex: a high-resolution investigation of the motor system using 7-Tesla fMRI

Acknowledgements

First of all I would like to express my sincere thanks to my co-supervisor Dr. Roy Salomon, who has proposed this fascinating theme. Your regular feedback, enthusiasm, patience, attention, encouragement and guidance have been essential in the development of this project. Thanks also to my supervisor, Dr. Wietske Van der Zwaag, despite the short presence, without your knowledge, advice and suggestions; this study would not have been successful. It was a privilege working with both of you and once again thank you for sharing your knowledge with me.

I gratefully acknowledge the assistance of Dr. Aaron Schurger in the final stage of this study. Thanks for your contribution, feedback and support. Your participation had a great importance for this study.

I wish to express my gratitude to both labs, CIBM and LNCO, and all volunteers for your collaboration and availability since the very beginning of this study until its conclusion.

I also wish to thank Professor Doutor Mário Secca, who created this amazing master degree of biomedical engineering and encouraged me to be a part of this project in EPFL.

To all my friends, thanks for your supportive attitudes, not only during this work, but also during other life stages. Especially to Inês and Patricia, thank you for your inexhaustible encouragement and the part you both played in helping me get to this point.

No words can describe the support given by my family, specially my parents, brothers and grandparents, that in different ways made this work possible with all the love, care and comprehension. I know that I can always count with you anywhere for everything.

Lastly, but by no means least, to my life partner THANKS for the fine moments that you provided me during these last months. This journey has been truly challenging but with your assistance and advice I have managed to never lose my path. I will never be able to express how much you mean to me.

To everyone who made this work possible, **THANK YOU!**

Abstract

Human behaviour is grounded in our ability to perform complex tasks. While human motor function has been studied for over a century the cortical processes underlying motor behaviour are still under debate. Central to the execution of action is the primary motor cortex (M1), which has previously been considered to be responsible for the execution of movements planned in the premotor cortex, yet recent studies point to more complex roles for M1 in orchestrating motor-related information.

The purpose of this project is to study the functional properties of primary motor cortex using ultra-high fMRI. The spatial resolution made possible by using a high field magnet allows us to investigate novel questions such as the existence of cortical columns, the functional organization pattern for single fingers and functional involvement of M1 in motor imagery and observation.

Thirteen young healthy subjects participated in this study. Functional and anatomical high resolution images were acquired. Four functional scans were acquired for the different tasks: motor execution; motor imagery; movement observation and rest. The paradigm used was a randomized finger tapping. The images analysis was performed with the Brainvoyager QX program. Using the novel high resolution cortical grid sampling analysis tools, different cortical laminas of human M1 were examined.

Our results reveal a distributed pattern (intermingled with somatotopic “hot spots”) for single fingers activity in M1. Furthermore we show novel evidence of columnar structures in M1 and show that non motor tasks such as motor imagery and action observation also activate this region.

We conclude that the primary motor cortex has much more un-expected complex roles regarding the processing of movement related information, not only due to their involvement in tasks that do not imply muscle movement, but also due to their intriguing organization pattern.

Key-words: Primary Motor cortex, high-resolution fMRI, fingers organization, motor imagery, movement observation, cortical columns

Resumo

O comportamento humano está na sua base ligado à nossa capacidade de realizar tarefas complexas. Apesar do funcionamento do sistema motor humano ter sido estudado até agora por mais de um século, os processos corticais que consistem na base de todo esse comportamento estão ainda em debate. Um dos elementos principais no que toca à execução de ações é o cortex motor primário (M1), que foi primeiramente considerado responsável pela execuçao de movimentos previamente planeados pelo cortex premotor, contudo recentes estudos indicam para um maior e mais complexo envolvimento deste cortex no processamento de informações relacionadas com o movimento.

O objectivo deste projecto é estudar as propriedades funcionais do cortex primário motor usando a técnica de fMRI de alta resolução. A resolução espacial produzida pelo uso de um elevado campo magnético permite a investigação de novas questões como a existencia de colunas corticais, assim como o padrão da organização funcional do movimento de um único dedo e ainda o envolvimento funcional do M1 na imaginação motora e observação.

Treze jovens saudáveis participaram neste estudo. Foram adquiridas imagens funcionais e anatomicas de alta resolução. As quatro aquisições funcionais foram realizadas para diferentes tarefas: execução motora, imaginação motora, observação do movimento e descanço. O paradigma utilizado corresponde ao batimento aleatório de um único dedo. A análise de imagens foi realizada com o programa Brainvoyager Qx. Usando uma nova ferramenta de alta resolução para amostragem de grelhas corticais foram examinadas diferentes laminas do cortex motor primário humano.

Os resultados mostram um padrão distribuido (misturado com centros somatotópicos) para a actividade de dedos no M1. Adicionalmente, apresentam evidencias de estruturas colunares no M1 e ainda que tarefas não motoras como imaginação motora e observação de acção também activam esta região.

Conclui-se que o cortex motor primário tem muitos mais inexperados papeís no que toca ao processamento de informação relacionada com movimento, não só devido ao seu envolvimento em tarefas que não implicam interação com músculos, mas também pele seu intrigante padrão de organização.

Palavras Chave: Cortex Motor Primário, fMRI de alta resolução, organização de dedos, imaginação motora, observação de movimento, colunas corticais

Contents

List of Figures

List of Tables

Abbreviations and Acronyms

ANOVA	Analysis of Variance
BOLD	Blood Oxygen Level Dependent
CBF	Cerebral Blood Flow
CBV	Cerebral Blood Volume
$CMRO_2$	Cerebral Metabolic Rate of Oxygen
CSF	Cerebrospinal Fluid
E	Local Oxygen Extraction Fraction
EEG	Electro-Encephalography
EPI	Echo-Planar Imaging
EV	Extra-vascular BOLD component
FDR	False Discovery Rate
FFT	Fast Fourier Transform
FG1	Thumb Finger Grid
FG3	Middle Finger Grid
FID	Free Induction Decay
FM1	Thumb Activity Map
FM2	Index Finger Activity Map
FM3	Middle Finger Activity Map
fMRI	Functional Magnetic Ressonance
FOV	Field of View
FSTC	Finger Specific Time Course
G_{FE}	Frequency Encoding Gradient
G_{PE}	Phase Encoding Gradient
G_{SS}	Slice Selection Gradient
GRE	Gradient Echo
GLM	General Linear Model
GM	Grey Matter
HRF	Hemodynamic Response Function
IIC	Intensity Inhomogenity Correction
IV	Intra-Vascular BOLD component
M1	Primary Motor Cortex
ME	Motor Execution
MEG	Magneto- Encephalography
MP-RAGE	Magnetization Prepared Rapid Gradient Echo
MO	Movement Observation
MRI	Magnetic Ressonance Imaging
MT	Middle Temple Visual Area
NMR	Nuclear Magnetic Ressonance
OD	Ocular Dominance
PD	Protonic Density
PMC	Premotor Cortex

rER	Rough Endoplasmatic Reticullum
RF	Radiofrequency
ROI	Region of Interest
SE	Spin Echo
SMA	Supplementary Motor Area
SNR	Signal to Noise Ratio
STS	Superior Temporal Sulcus
T_1	Longitudinal Relaxation Time
T_2	Apparent Transverse Relaxation Time
T_2^*	Transverse Relaxation Time
TE	Time to Echo
TMS	Trans-cranial Magnetic Stimulation
TR	Time to Repetition
V1	Primary Visual Cortex
V2	Prestriate Cortex
V4	Visual area located in the extrastriate cortex
V5	Visual area MT
WM	White Matter

μ	Magnetic Moment
γ	Gyromagnetic Ratio
B_0	External Magnetic Field
J	Angular Momentum
M_0	Net Magnetization
v_0	Larmor Frequency

1 Introduction

1.1 Project Presentation

Due to a powerful tool - the advent of functional magnetic resonance imaging (fMRI), the knowledge related with the human brain has been exponentially increased. Most notably, novel techniques using ultra-high fields allow astounding data quality, with resolutions capable of imaging different cortical laminas; bringing a brighter future not only for neuroscience, but also to other science fields like medicine.

Allying this and other techniques, cognitive neuroscience has accomplished a new level of knowledge, especially regarding the functioning of the motor system.

The capacity to perform a complex sequence of movements, linking all the basic actions is the main component of voluntary motor behaviour. To process such detailed information, the brain uses different regions, for instance primary motor cortex (M1). From a classical view, M1 is responsible for the final cortical output of movement commands, while recent studies point to more complex roles for M1 in orchestrating motor-related information.

Several conflicting theories and findings have shown different features for imagery and visual activity in M1 or even for somatotopy (the idea that body representations follow a specific and ordered pattern) in the primary motor cortex. Additionally no studies have been performed in humans to analyze the existence of cortical columns structures in M1.

Therefore, the purpose of this project is to study the primary motor cortex in a laminar level using ultra-high fMRI. The complex functioning of M1 was studied in three different tasks: movement, observation and imagery of fingers tapping. Furthermore, different cortical laminas of human M1 were analyzed for the first time: providing a better understanding of somatotopy and cortical connections in depth. Accordingly, this study aims to answer to the following questions:

- Is there a somatotopic or distributed representation for fingers in M1?
- Are there any depth structures in human M1?
- Is M1 activated by action observation?
- Is M1 activated by motor imagery?

1.2 Structure of the thesis

The present thesis is divided in seven chapters, involving a theoretical background for a better understanding of the current work; a description of the images acquisition process and the data analysis, as well as a result's discussion and final conclusions.

This thesis begins by providing some background theory in Chapters 2 and 3, describing the basic biological and physiological aspects of brain function in the second chapter, with special focus in primary motor cortex (M1). The physics behind Magnetic Resonance Imaging (MRI) are explained in

the third chapter, as well as the functioning of Functional Magnetic Resonance Imaging (fMRI). The same chapter also includes a report about ultra-high field MRI.

In order to summarize all the scientific information related with this project, Chapter 4 consists in a literature review.

The methodology used for this study is described in Chapter 5. It includes the methods applied for the acquisition and processing of the images, as well as the ones used to analyze the results (measures and statistics). The obtained results are presented in Chapter 6.

The results discussion is provided in the Chapter 7. Finally, the main conclusions drawn from this work are exposed in Chapter 8.

2 Neuroanatomy

The human brain has fascinated and baffled people throughout the centuries, from nowadays scientists to our prehistoric ancestors. During the last decades, researchers have developed novel techniques to improve the knowledge about human brain functioning and its structures.

Even though, the attempt to understand the functional organization of the brain has proven to be a daunting challenge. Mostly, due the slow development of the experimental tools to measure and map brain activity, because its structures are minute and highly complex.

Since this work focuses on the brain's cortical motor network the following section presents some general considerations about this organ.

2.1 Brain Structure

As the *maestro* of the body, with 100 billion nerve cells, brain has a complex anatomy and a tiered structure.

The normal adult human brain in average weights 1.4 Kg and which corresponds to only 2% of the body weight. Yet the energy-consuming processes account for approximately 25% of total body glucose utilization(Carter et al., 2009a; Squire, 2013).
From a gross point of view, this organ can be subdivided into the cerebrum, the brain stem and the cerebellum. The scheme bellow (Figure 2.1 - Subdivision of the brain structures) shows a detailed division and in Figure 2.2 there is an anatomical representation.

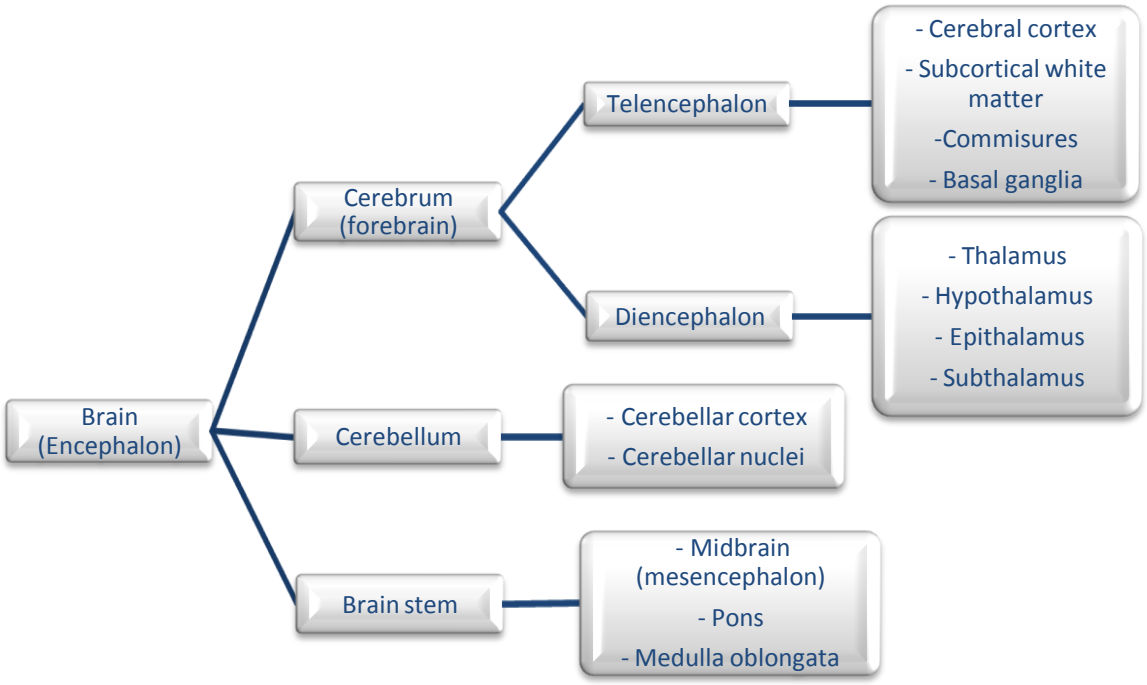

Figure 2.1 - Subdivision of the brain structures (adapted from Snell, 2010)

The most complex functions occur in the cerebrum(Carter et al., 2009b).
For instance, the hypothalamus has many vital roles such as conscious behavior, emotions and instincts, and automatic control of body processes. The thalamus screens and preprocesses all the flux of sensory information and sends it on to the cerebral cortex.
Finally, the cortex is responsible for conscious, discriminative aspects of sensation; and cognitive activity, including language, reasoning, and many aspects of learning and memory.

On other hand, the brain stem and cerebellum main functions are essential to complement the brain functioning.
For example, subconscious or autonomic regulation mechanisms are controlled by the brain stem. In medulla stand the centers for respiratory, cardiac and vasomotor monitoring and command. Even the pons is involved in learning and remembering motor skills.
Finally, body movement coordination (like balance and posture) is ordered by cerebellum(Carter et al., 2009a; Snell, 2010).
Most of mammal's cortical brain networks have been described, although structural connection data for the human brain is largely missing (Crick and Jones, 1993).

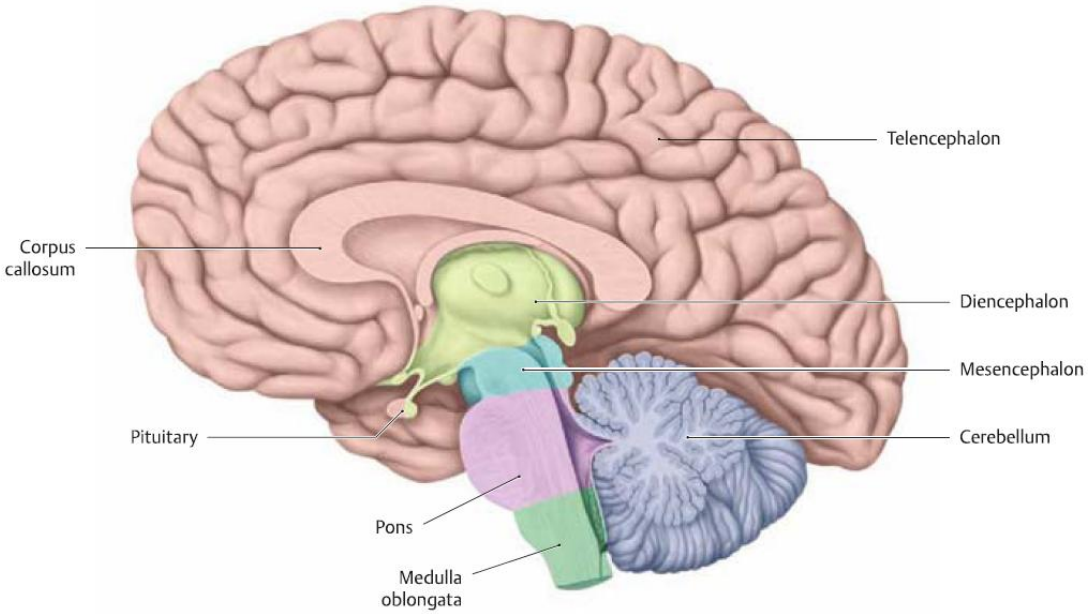

Figure 2.2 - Representation of brain anatomic structure – main divisions (Schünke et al., 2010)

Note that: in the Figure 2.2 are two structures, that haven't been yet referred - corpus callosum and pituitary.

The largest commissure[1] of the brain, corpus callosum, contains more than 200 million nerve fibers that link the cerebral hemispheres.

Pituitary is an endocrine gland, which is regulated by hypothalamus. It thus controls a variety of bodily functions, such as growth, heart rate, muscle contraction, sexual behavior among others (Carter et al., 2009a; Snell, 2010).

1 - A commissure is a bundle of fibers which usually interconnects similar structures of the two sides of the brain, but sometimes is merely a location where fibers intercept to dissimilar locations.

2.2 Cerebral Hemispheres

The cerebrum constitutes more than three-quarters of the brain's total volume and is divided in two cerebral hemispheres (telencephalon), which include the cerebral cortex, the cerebral white matter (comissures and subcortical white matter) and a complex of deep gray matter masses, the basal ganglia.

Basically, the cerebrum has two types of tissue – white and grey matter (Figure 2.3).
The gray matter consists of neuronal cells bodies and gial cells[1], axons[2], dendrites[3] and synapses[4].
While, the white matter (WM) contains axons and theirs associated gial cells. Many axons are myelinated[5], allowing rapid nerve impulse conduction and giving WM its pale appearance (Snell, 2010; Squire, 2013).

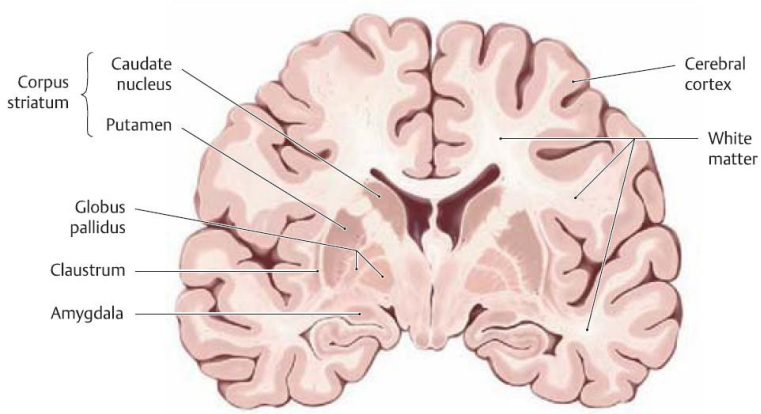

Figure 2.3 -Coronal section showing the distribution of the grey and white matter in the brain (Schünke et al., 2010)

According to Figure 2.3, the structures of the telencephalon compound by grey matter are:
- Cerebral cortex;
- Basal ganglia: the caudate nucleus and putamen (collectively called the corpus striatum) and globus pallidus;
- Other grey matter nuclei that are not included among the basal ganglia: claustrum and amygdale (often considered a transitional form between the two types of gray matter – cortex and basal ganglia)(Schünke et al., 2010).

The surfaces of the cerebral hemispheres contain many gyri[6], sulci and fissures, in a way that more than 50% of the cortex's area (approximately 0.8 m^2) is hidden within the grooves[7].

Therefore, their presence, in a pattern that is relatively constant from brain to brain, allows to separate different cortical areas: frontal, parietal, occipital and temporal, insular and limbic lobes (Figure 2.4). In some naming systems, the limbic and insular lobes are distinguished as separate from other lobes (Krieg, 1946; Carter et al., 2009a; Schünke et al., 2010; Snell, 2010).

1- These cells appear to play important roles in supporting and protecting neurons, like myelin formation or guidance of developing neurons.
2- Specialized structure that conducts electrical signals from the initial segment (near the cell body) to the synaptic terminals.
3- Extensions of neurons that stretch out from the cell body; they receive incoming synaptic information and thus, together with the cell body, constitute the receptive pole of the neuron.
4- Interneuronal complex responsible for the communication between neurons.
5- Covered with myelin (multiple concentric layers of lipid-rich membrane which functions as an insulator).
6- Rounded bulges of the cortex;
7- Grooves are termed sulci when relatively shallow and fissures when deeper

The cerebral hemispheres are separated by the main and deepest groove- the longitudinal fissure. The central sulcus, also known as the fissure of Rolando, arises about the middle of the hemisphere and separates the frontal lobe from the parietal lobe.

Note that, the insular lobe lies deep within the lateral sulcus.

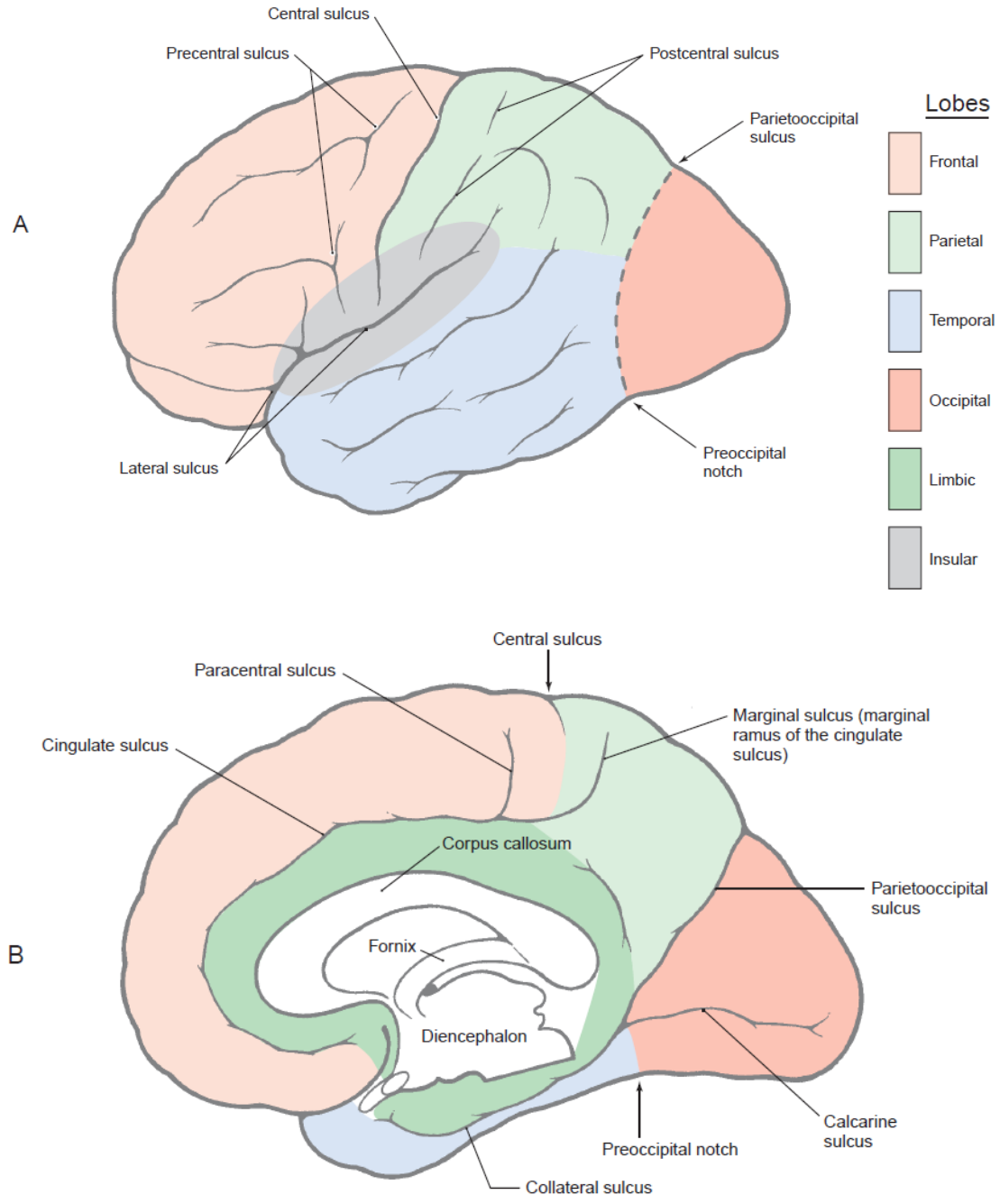

Figure 2.4 - Left lateral (A) and medial (B) views of the cerebral hemisphere showing the landmarks used to divide the cortex into its main lobes (Haines, 2012)

2.3 Cerebral cortex

The cerebral cortex is the outer layer of the cerebrum, constituting about 40% of the brain by weight and contains an average of 16 billion neurons (Herculano-Houzel, 2009).

There are two types of cortices:

- Allocortex (three layered cortex, mostly found in the limbic system cortex)
- Neocortex (more frequently found in most of the cerebral hemisphere and contains six layers)

There is also mesocortex (a form of neocortex), which makes the transition between the allocortex and isocortex. It contains three to six layers and it includes such regions as the cingulate gyrus and the insula.
The allocortex and mesocortex incorporate the limbic lobe, while the neocortex consists of the cortex of all the cerebral lobes, excluding the allocortex (Snell, 2010; Strominger et al., 2012).

2.3.1 Organization of the neocortex

As already referred, the neocortex consists of six layers parallel to the cortical surface, each of which is usually named after its predominant cell type.

Main Neurons of the Neocortex

There are four main types of cells arrange in this layered structure: pyramidal, stellate, granulate and spindle (fusiform) cells (Brodal, 2010; Economo and Triarhou, 2009; Schünke et al., 2010; Snell, 2010).

Pyramidal cells usually contain well-developed Nissl bodies[1]. They have a triangular shape, being elongated in the vertical direction. Their size may vary substantially, so, there are: small and large pyramidal neurons.

The small pyramidal neuron is a cell with a long axon that usually ends within the cortex, either as:

- Association fiber (axon links two different cortical areas within the same hemisphere);
- Commissural fiber (axon passes in the corpus callosum and connects areas in opposite hemisphere but in a cortical area of similar function)

These types of pyramidal cells have the property to project neurons whose axons end within the cortex. On other hand, the large pyramidal neuron is a cell with a very long axon that projects outside the cortex, even for distant structures.

The stellate neuron has a short axon to process local information. They have inhibitory (aspiny neurons) and excitatory (spiny stellate cells) properties. Stellate cells exhibit a variety of shapes, such as: double bouquet cells, tuft cells, chandelier cells and basket cells.

Stellate and pyramidal cells can also be distinguished by the arrangement of their dendrites. Pyramidal cells have an apical dendrite[2] and basilar dendrites[3]. While, the stellate cells (star shaped) have dendrites exending in all directions.

1- Large clumps of rough endoplasmic reticulum (rER) in the cytoplasm of neurons, also called tigroid granules
2- Dendrite reaching from the upper end toward the cortical surface
3- Dendrite extending horizontally from the cell body

Granule cells are round or polygonal, often triangular (similar to the stellate cell morphology). This is the generic term for a small neuron; in fact it has a very short cytoplasm, because the nucleus occupies most of the cell.

Fusiform cells are long and spindle shaped with an apical dendrite together with numerous dendrites radiating from the cell body. These cells combine the features of both stellate and pyramidal cells (Brodal, 2010; Economo and Triarhou, 2009; Schünke et al., 2010; Snell, 2010).

Layers of the Neocortex

The neurons of the neocortex are arranged in six well-defined layers (Figure 2.5), or laminae, known generally from the outside inward (from the surface of the cortex to the WM) as the molecular, external granular, external pyramidal, internal granular, internal pyramidal and multiform layers matter (Brodal, 2010; Economo and Triarhou, 2009; Schünke et al., 2010; Snell, 2010; Strominger et al., 2012) .

The outermost cortical layer - the molecular layer (I) - is abundant in fibers, that come from within the cortex or from the thalamus. The neurons in this layer are few in number, apart from that, layer I also contains apical dendrites of pyramidal cells in the deeper layers.

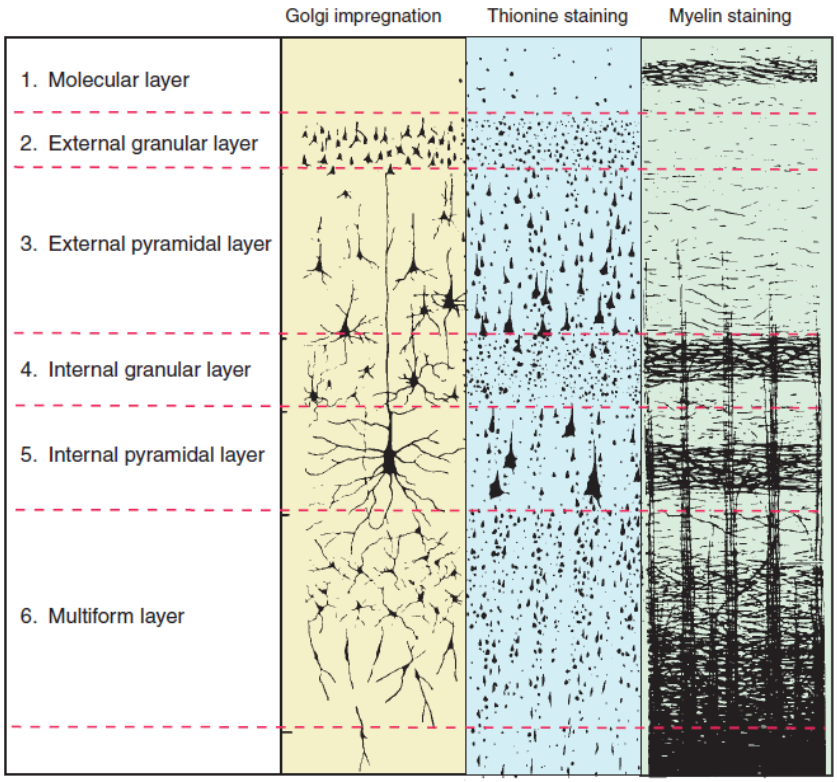

Figure 2.5 - The basic six-layered structure of neocortex - The three columns show perpendicular sections to the cortical surface to different staining[1] methods. Left: Appearance in Golgi-stain[2]. Middle: A thionine-stained section[3]. Right: Appearance after myelin staining[4]. (Brodal, 2010)

1- Auxiliary technique used in to highlight contrast in the microscopic image
2- Type of staining, also known as silver impregnation, in which the cell bodies and some of the dendrites can be seen.
3- With this staining method only the cell bodies are visible

4- Another kind of staining, in which the major pattern of the myelinated axons is clear, where perpendicular bundles of fibers are entering the cortex, and the ones horizontal are interconnecting close regions of the cortex.

The second layer is the external granular layer (II). It is a fairly dense layer comprised of numerous small granule cells. The name of this layer is misleading because it is largely populated by small pyramidal neurons.

Right beneath layer II is the pyramidal cell layer (III). It is thick and pyramidally shaped cells prevail (they are larger in size, not in number), but it also contains another kinds of cell types.
The size of neurons increase with depth, which means that the ones located deeper in this layer are typically larger than those located more superficially.

Layer IV, the internal granular layer, usually a thin layer, is made up primarily of granule cells, its densely packed somata is similar to the one in layer II.

The internal pyramidal layer (V) mainly consists of pyramidal cells, these are typically larger than those in layer II.

The last layer (VI) is called the polymorphic/fusiform/multiform layer, due to its heterogeneous somata, main of which belongs to spindle-shaped cell bodies. This layer forms the deep limit of the cortex, whose axons go through the adjacent WM (Brodal, 2010; Economo and Triarhou, 2009; Schünke et al., 2010; Snell, 2010; Strominger et al., 2012).

The layers diverge regarding to their connections - afferent and efferent.

Generally, layers II and IV are receiving, when in fact layers III and V are essentially efferent. The afferents connections extend from the thalamus to lamina V, whereas layer V is the starting point to subcortical tracts to the cord, brain stem and basal ganglia. Layers II and III receive and send out their axons primarily to other areas of the cortex (association and commissural fibers). The layer VI is also largely efferent and sends many axons to the thalamus (Brodal, 2010).

2.3.2 Functional areas

The details of layer's functional organization vary throughout the cortex. So, the cortex has been divided in various ways, the most used demarcation system is that of Brodmann (1909), who took advantage of Nissl-stained preparations to visualize the distribution of the neurons in different layers of neocortex (cytoarchitectonics) and number the functional areas of neocortex. More than 40 areas are distinguished on the lateral (Figure 2.6) and medial surfaces of the brain (Schünke et al., 2010; Strominger et al., 2012).

Cortical Microstructure: Columns

While morphological considerations separate the cerebral cortex into horizontal layers, functional considerations guide to its division into distinct units or modules.

At a microstructural level, the cortical neurons appear to be organized into small modules formed by cylinders or columns of tissue extending perpendicular to the surface of the cortex. These modules of tissue contain neurons whose salient physiological properties are identical.
A predisposition for cortical neurons to be arranged in perpendicular rows is noticeable from thioninestained sections (Figure 2.5) (Brodal, 2010; Mountcastle, 1997; Schünke et al., 2010).

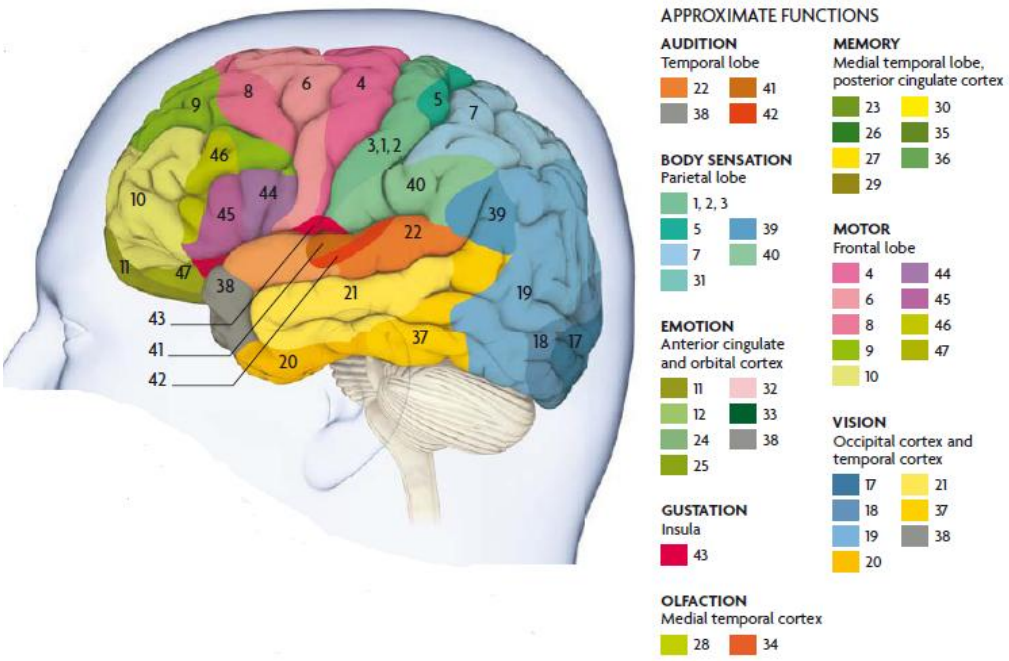

Figure 2.6 - Lateral Brodmann's areas (Carter et al., 2009)

2.4 Primary motor cortex (M1)

Brodmann area 4 is the primary motor cortex, located on the anterior wall of the central sulcus.

Not all cortical regions have the same laminar organization. For example, the precentral gyrus, also known as M1, has almost no internal granule layer (layer IV) and thus is called agranular cortex. The lack of prominence of layer IV can be understood because of its connections with the thalamus. Layer IV is where the sensory information arrives from the thalamus. The motor cortex is principally an output area of the neocortex, therefore slightly receives sensory information directly from the thalamus (Kandel et al., 2000).

There are also changes within cortical regions related to layer's constitution. For instance, exceptional large pyramidal neurons, known as Betz cells, are restricted to cortical lamina V of M1. These cells are in charge of voluntary movements on the opposite side of the body, with the impulses traveling over their axons.

M1 has a somatotopic organization, which means that M1 has specific regions in the cortex to control the movement of different parts of the body. Homonculus is the cartoon that magnifies some parts of the body with respect to cortical territory, by distorting the size of body parts relative to their normal proportions (Penfield and Boldrey, 1937; Squire, 2013).

The motor homunculus, illustrated in Figure 2.7, shows the somatotopy of the primary motor cortex where the fingers, hands, and face are represented extremely large conforming to their participation in tasks that involve highest precision and finest control.

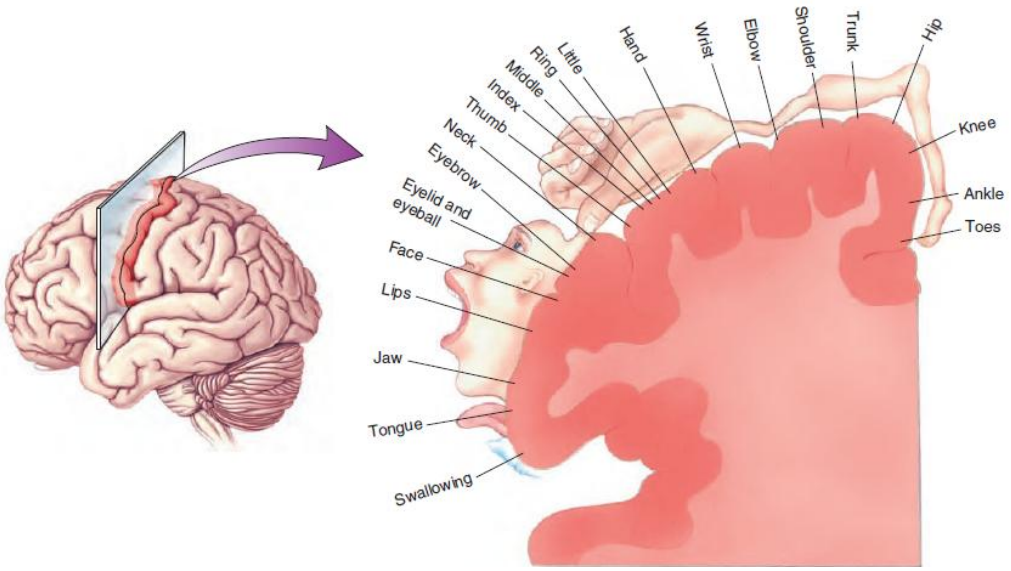

Figure 2.7 – A somatotopic map of the human precentral gyrus (M1): showing the specific regions in this cortex to control the movement of different parts of the body (Squire, 2013)

2.5 Blood vessels of the head

As expected, the brain and all our body are critically dependent on an uninterrupted supply of oxygenated blood. Nearly 20% of the blood body circulates in the brain, which represents 2% of the body weight. Brain vessels (Figure 2.8) provide the means for this uninterrupted blood supply (Snell, 2010).

There are variations among individuals in the vessel's size, positioning and even in their number.

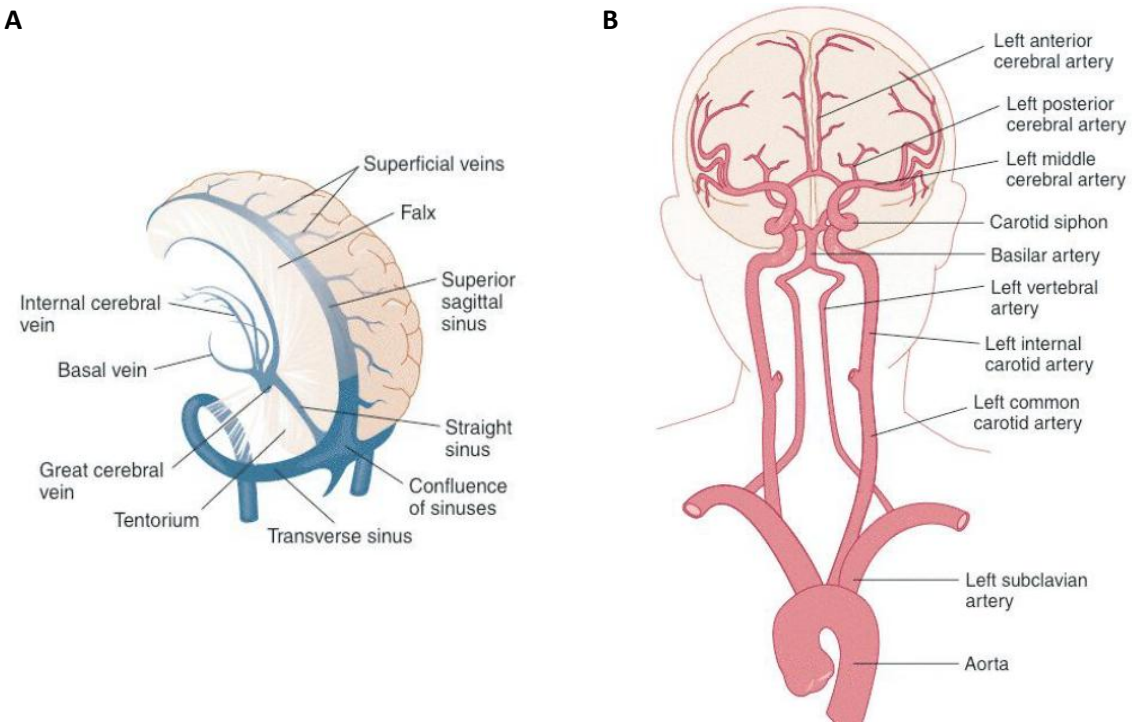

Figure 2.8 - Main vessels of the brain: Three dimentional view of veins and sinuses[1] of the brain (A); Major cerebral arteries, Circle of Willis (B) (Brodal, 2010)

1-Venous sinuses are venous channels of the dura mater (one of the three brain's connective tissue layers)

The blood transports oxygen, nutrients, and other necessary substances to keep the brain tissues working properly. The arteries carry the oxygenated blood with all the nutrients and the veins carry the deoxygenated blood.

Cerebral veins have no valves and rarely accompany the matching the cerebral arteries (Snell, 2010).

3 Magnetic Resonance Imaging (MRI)

Magnetic resonance imaging has become an important tool for neuroscientists, because it can be used non-invasively to obtain high-quality images of the brain or other organs/structures of the body without radiation, as is necessary for X-ray imaging. The technology behind this technique is complex, but it is essential to understand in order to entirely appreciate MR images of the brain.

3.1 Basic Principles

As the name suggests, magnetic resonance imaging uses the magnetic properties of tissue to produce an image.

3.1.1 Nuclear Magnetic Resonance and Equilibrium Magnetization

All magnetic resonance imaging relies on a few physical principles that were discovered by Rabi, Bloch, Purcell and others (Geva, 2006). They performed the first successful experiments, demonstrating the phenomenon of NMR – Nuclear Magnetic Resonance. Certain nuclei have an intrinsic magnetic moment and, when placed in a magnetic field, they rotate with a frequency proportional to the field (Buxton, 2009).

Consider a single hydrogen atom. In regular conditions, thermal energy lets the proton to spin about its axis (Figure 3.1A); his precession motion has two effects: first its spin creates superficial electrical current, which origins a magnetic source. The strength of this magnetic source per unit of magnetic field is the magnetic moment (μ). Second, because the proton has an odd atomic mass number, its spins results in an angular momentum (J). Due to the right-hand rule, both μ and J are vectors pointing in the same direction (Huettel et al., 2009).

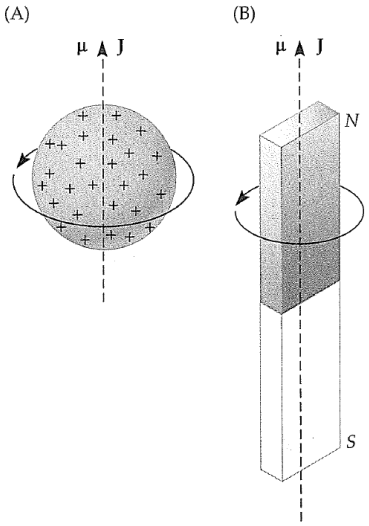

Figure 3.1 - Similarities between spinning proton (A) and spinning magnet (B): both have angular momentums (J) and magnetic moments (μ) (Huettel et al., 2009)

Basically, as the nuclei spins, the changing magnetic field produces a magnetic moment and the moving mass results in angular momentum.

For a nucleus to be useful for MRI, it must possess nuclear magnetic resonance properties – have both a magnetic moment and an angular momentum.

Only a few atoms have the required properties - ^{1}H, ^{13}C, ^{19}F, ^{23}Na and ^{31}P; the hydrogen is the most used, due to its abundance in the living organisms, for example an average person contains approximately $5x10^{27}$ hydrogen protons (Huettel et al., 2009).

These hydrogen protons can be thought of as little magnets (Figure 3.1): they spin about an axis and their spinning positive charge induces a minuscule magnetic field. In absence of an external magnetic field (B_0), due to different axis of precession, the magnetic fields of individual protons orient in random directions and the equilibrium magnetization[1] – M_0 – is null, because *x*, *y* and *z* components cancel each other (Figure 3.2A) (Carter and Shieh, 2010).

1-The net magnetization is the sum of all the magnetic moments of each of the H nuclei within a system

Now consider one of these spins located in an external magnetic field (B_0). This external field exerts a torque on the proton that would tend to align the proton spin with B_0.

However, because the nucleus also has angular momentum, it instead gains a gyroscopic motion known as precession (Figure 3.2C). This movement is analogous to a spinning top in a gravitational field. In this case, the spin precesses around an axis parallel to the main magnetic field, maintaining a constant angle.

The precession frequency - Larmor frequency, v_0, is the resonant frequency of a spin within a magnetic field and is proportional to the strength of the applied field (B_0):

$$v_0 = \gamma B_0 \qquad \textbf{Equation 3.1}$$

Where:

- γ is the gyromagnetic ratio (constant for a given type of nucleus) and it corresponds to the ratio between the charge and mass of a spin. For the hydrogen nucleus it corresponds to 42.58 MHz/T (Buxton, 2009).

There are two states for precessing spins (Figure 3.2B): one low energy state (parallel to the magnetic field, spin = -½) and one high energy state (anti-parallel to the magnetic field, spin = ½). Thus, more energy is required for the anti-parallel direction, which translates into a (small) preference for the parallel alignment.

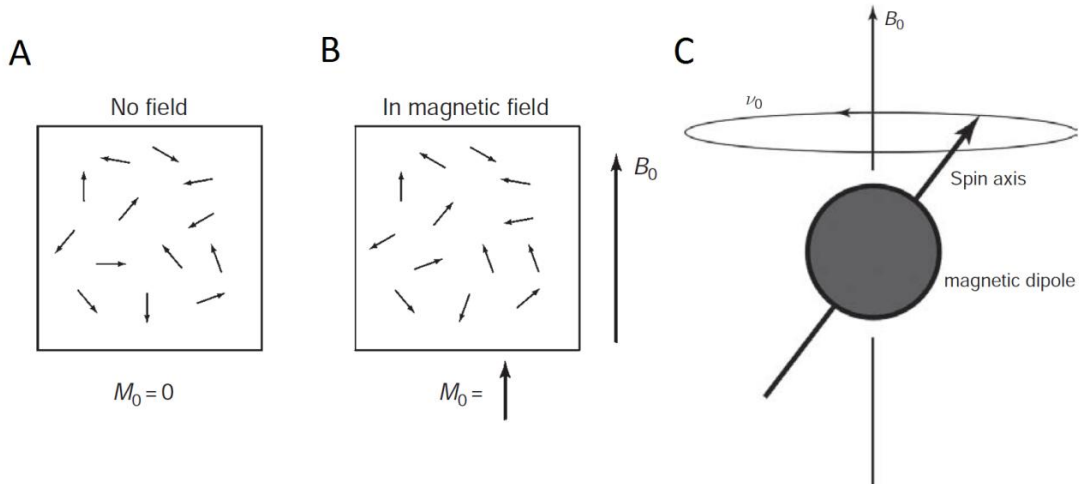

Figure 3.2 – Magnetic fields cause the alignment of nuclei that have the NMR property: In absence of an external magnetic field, protons orient in random directions (A); When an external magnetic field is applied, protons aligned either in a parallel or anti-parallel direction**.** (B); Precession of a magnetic dipole in a magnetic field B_0 (C) (Buxton, 2009)

As a result, when a system of these nuclei, for example the human body, is placed in a magnetic field (B_0) the net magnetization is no longer null, because in the equilibrium state there are slightly more spins aligned in the parallel direction (Figure 3.2B). This small difference creates a weak magnetization in the same direction of B_0. Since the protons involved don't spin in phase, the resultant vector, M_0, doesn't show any transversal (xy axis) component (Carter and Shieh, 2010).

Even though this weak magnetization is not directly observable, in certain conditions it can be measured and it is the basis of all observable NMR signals.

3.1.2 Excitation and Detection

The resonance phenomenon corresponds to an exchange of energy between two systems at a specific frequency. Hence, in order to measure M_0, a radiofrequency (RF) pulse oscillating at Larmor frequency is created producing a magnetic field B_1 perpendicular to B_0. This RF pulse is generated by a transmitter coil.

The new field, B_1, is several orders of magnitude smaller than B_0. Nevertheless, this causes disturbances among the parallel aligned protons, because some of them, gradually, will absorb the electromagnetic energy and jump to the high-energy state, process known as excitation. The effect is that with each precessional rotation M_0 tips farther away from B_0, tracing out a widening spiral (Figure 3.3).

These RF pulses are regularly characterized by the flip angle (α) they make. The flip angle can be controlled by the strength and duration of the RF pulse. The new magnetization (tipped M_0) is represented by M (Figure 3.3).

Basically, during excitation, longitudinal magnetization decreases and a transverse magnetization develops (excluding for a 180° flip angle).

Longitudinal magnetization is due to a difference in the number of spins in parallel and anti-parallel state. Transverse magnetization is due to spins getting more or less phase coherence (Imaios, 2013).

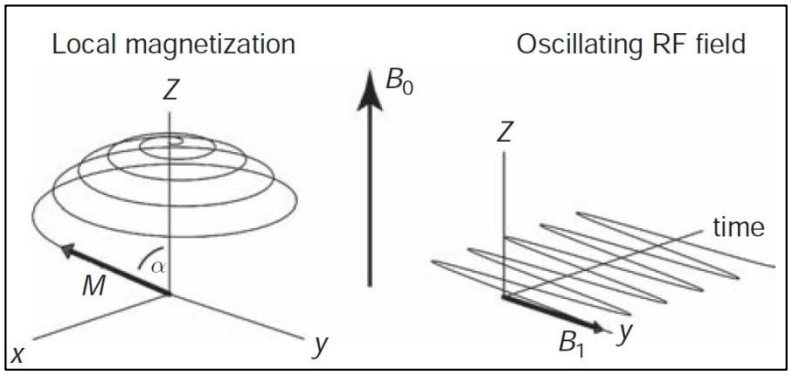

Figure 3.3 – Tipping over the net magnetization with excitation by radiofrequency pulse (Buxton, 2009)

A 90º degree excitation pulse results in an equal numbers of spins in low and high energy states. This can be seen as the rotation of the net magnetization from the longitudinal direction (z axis) into the transverse plane (xy axis). In this case, the application of a 90º RF pulse also brings the spins to complete phase coherence (Imaios, 2013).

When the net magnetization is along the longitudinal axis, the individual spins precession cannot be measured in detector coils. But when the net magnetization acquires a transverse compound via excitation, its precession around the main magnetic can generate an oscillating electric current in reception coils with the scanner (applying the Faraday's law of induction) (Huettel et al., 2009; McRobbie, 2007).

Note that typically, the coil is used as both a transmitter and a receiver. During the transmit phase of the experiment, an oscillating current is applied to the coil for a brief time. During the receive phase of the experiment, the coil is connected to a detector circuit that senses the small oscillating currents in the coil.

3.1.3 Relaxation times

The MR signal detected through receiver coils does not remain stable forever. After a time, the RF field is turned off and the spins will eventually return into the equilibrium state in a process known as relaxation.

The relaxation mechanisms depend on spins interaction with the surroundings and behaves differently in different tissues. The relaxation of excited spins combines two different mechanisms: longitudinal relaxation and transverse relaxation (Imaios, 2013).

Longitudinal relaxation

Longitudinal relaxation or spin-lattice relaxation refers to a phenomenon of energy exchange between the spin system and the surrounding environment. As spins pass from a high energy state to a low energy state, RF energy is released back to re-establish thermal equilibrium.

These energy transferences give rise to the recovery of the longitudinal magnetization: an increasing in the longitudinal component of the flipped net magnetization vector from *M* to M_0 (Imaios, 2013).

The recovery rate is characterized by the tissue-specific time constant T_1, which corresponds to the time taken for the magnetization to recover to 63% of its equilibrium value(McRobbie, 2007). According to the Bloch equations, the amount of longitudinal magnetization, M_z, present at time *t* following an RF pulse is given by:

$$M_z(t) = M_z(0)exp\left(\frac{-t}{T_1}\right) + M_0\left[1 - exp\left(\frac{-t}{T_1}\right)\right] \qquad \textbf{Equation 3.2}$$

Transverse relaxation

Transverse relaxation or spin-spin relaxation results from spins losing their phase coherence. As spins collectively move, their magnetic fields interact (spin-spin interaction), vaguely changing their precession rate. These interactions incite a cumulative loss in phase coherence producing transverse magnetization decay.

The transverse relaxation is characterized by a time constant represented as T2 - the time taken for the transverse magnetization to drop to 37% of its initial size (Imaios, 2013).

According to the Bloch equations, the amount of longitudinal magnetization, M_{xy}, present at time *t* following an RF pulse is given by:

$$M_x(t) = \left[M_x(0)\cos\omega_0 t + M_y(0)\sin\omega_0 t\right] \cdot exp\left(\frac{-t}{T_2}\right) \qquad \textbf{Equation 3.3}$$

$$M_y(t) = \left[M_y(0)\cos\omega_0 t + M_x(0)\sin\omega_0 t\right] \cdot exp\left(\frac{-t}{T_2}\right) \qquad \textbf{Equation 3.4}$$

Where M_x is the transverse magnetization in the *x* axis and M_y is the transverse magnetization in the *y* axis.

In biological tissue, the transverse magnetization quickly loses coherence and the longitudinal magnetization slowly recovers. This means that T_2 is always shorter than T_1.

The decay of transverse magnetization arises from magnetic field inhomogeneities. These inhomogeneities may be intrinsic or extrinsic, i.e. internal to the proton system or external in the scanner. Note that, only the intrinsic inhomogeneities contribute to T_2 (McRobbie, 2007).

An extrinsic source of differential spin effects is the external magnetic field, which is usually inhomogeneous. Each spin precesses at a frequency proportional to its local field strength; as a result, spatial variations in field strength provoke spatial differences in precession frequencies. This additional decay caused by extrinsic inhomogeneities has been called T_2'decay (Buxton, 2009; Huettel et al., 2009).

The combined effects of cumulative phase differences (intrinsic inhomogeneities) and local magnetic field inhomogeneities lead to signal loss known as T_2* decay, characterized by the time constant T_2*:

$$\frac{1}{T_2^*} = \frac{1}{T_2} + \frac{1}{T_2'} \qquad \textbf{Equation 3.5}$$

During relaxation, protons re-radiate the absorbed energy: this will induce a current in a nearby coil, creating a measurable signal that is proportional to the magnitude of the transverse magnetization. This detected signal is called free induction decay (FID) and is illustrated in Figure 3.4.

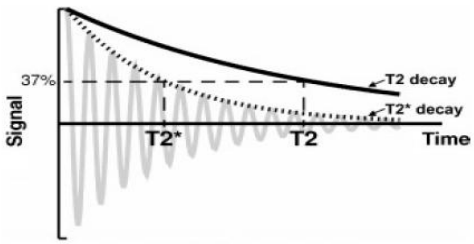

Figure 3.4 – Free Induction Decay after a 90° RF pulse (Edelman, 2006)

This signal decays away exponentially and the time constant for this decay is:

T_2 in a perfectly homogeneous magnetic field;
T_2^* in an inhomogeneous magnetic field.

3.2 Image Acquisition

3.2.1 Signal Detection: Spatial Localization

In the theory described above the magnetic resonance signal is introduced as a global signal from a sample. In order to create MR images signal must be divided into components with different frequency parameters in a method known as spatially encoding; so it can be detected from different spatial locations.

Spatial encoding relies on successively applying magnetic field gradients. To resolve spatial information in three dimensions (x, y and z), we need at least three gradient fields. Therefore in an MR scanner, there are three gradient coils in addition to the RF coils and the coils of the magnet itself. Each gradient coil produces a magnetic field that varies linearly along a particular axis (Buxton, 2009).
Spatial localization is made in three steps: slice selection, phase encoding and frequency encoding; each step is related with one gradient: slice selection gradient (G_{SS}), phase encoding gradient (G_{PE}) and frequency-encoding gradient (G_{FE}). The different gradients have identical properties but are applied at distinct moments (Imaios, 2013).

In the first step (slice selection), a gradient (G_{SS}) is turned on along the slice selection axis (z, perpendicular to the desired slice), consequently the precession frequency of the protons varies linearly along the z direction. An RF wave is simultaneously applied with a bandwidth that contains the range of precession frequencies in the desired slice plane. This causes a shift in the magnetization of only the protons on this plane. As no protons located outside the slice plane are excited, they will not emit a signal.(Buxton, 2009; Imaios, 2013)

The phase encoding consists of applying a magnetic field gradient (G_{PE}) in the vertical direction (y axis) of the slice selected in the first step. While it is applied, it modifies the spin resonance frequencies, inducing dephasing, which persists after the gradient is interrupted (Imaios, 2013). After this step, all the protons precess in the same frequency but each local precessing magnetization is marked with a phase offset proportional to its y-position.
During frequency encoding, a magnetic field gradient (G_{FE}) is applied in the horizontal direction (x axis) of the slice selected in the first step. This gradient modifies the spin resonance frequencies along the horizontal direction. It thus creates proton columns, which all have an identical Larmor frequency. This gradient is applied during the data acquisition period.

The repeated combination of the three gradients allows the formation of a 3D image.

Note that, the imaging coordinate system can have any orientation relative to the magnetic field, even though both the direction of B_0 and the axis perpendicular to the image plane are usually referred to as the z-axis. (Buxton, 2009)

Any spatial localization method has resolution limits, in this case these limits can be represented in terms of a volume resolution element (voxel) with dimensions (Δx, Δy, Δz) (Buxton, 2009).

3.2.2 Image Formation

The collected data from the same slice - a mix of RF waves with different amplitudes, frequencies and phases, containing spatial information - is stored in the k-space (Fourier space) and requires a 2D inverse Fourier Transform to form an image of the slice plane, as illustrated in Figure 3.5.

Fourier transform is a mathematical procedure that allows the transformation of a time domain signal into a frequency domain signal (a spatial frequency in the case of fMRI) (Imaios, 2013).

The central portion of k-space describes the low-spatial-frequency components, which in image space is traduced in the lowest intensity change. On other hand, the outer edges describe the high frequencies, which determine image brightness, but no detail (Buxton, 2009; McRobbie, 2007).

There are several ways to fill the k-space, like linear filling, centric or spiral. The easiest way to fill the k-space is to use a line-by-line rectilinear trajectory. One line of k-space is fully acquired at each excitation, containing low and high-horizontal-spatial-frequency information (contrast and resolution in the horizontal direction). Between each repetition, there is a change in phase-encoding-gradient strength, corresponding to a change in k_y-coordinate.

However, the most used is the interleaved slice acquisition. In order to minimize the influence of excitation pulses on adjacent slices, the collection of data is performed in an alternating order (Huettel et al., 2009).

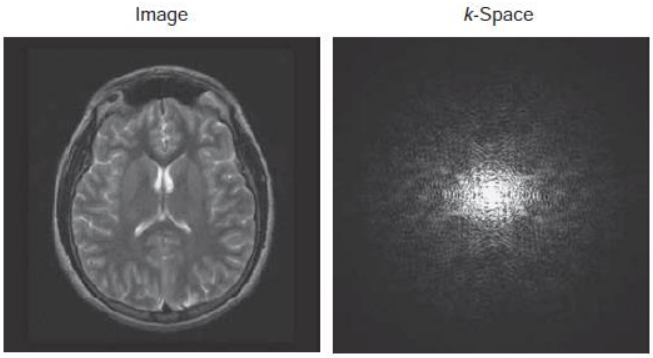

Figure 3.5 – Image space (left) and k-space (right): Any MR image can be represented as a matrix of intensities on the image space or as a matrix of spatial frequencies on the k-space (Buxton, 2009)

3D imaging

The methods described so far, using a slice selection to define each single slice, are all intrinsically two-dimensional methods, but true three-dimensional imaging also can be performed.

The principle is simply to excite a complete volume, rather than one thin slice and to apply a second phase-encode axis in the third dimension (z axis).

This translates in particularities in k-space, now a 3D space: in order to fill this new space the number of repetitions increases in a factor equal to the number of « slices» (partitions) in the third dimension. Obviously, the image reconstruction is performed by an inverse 3D Fourier Transform (Imaios, 2013).

The advantages of 3D acquisitions consist in getting thinner and more slices with better profiles, and better signal to noise ratio (SNR) for an equivalent slice thickness. The disadvantages are longer acquisition time and possible artifacts[1] (McRobbie, 2007).

While the majority of MRI data is multi slice, the anatomical data acquired for this project were 3D acquisitions.

3.2.3 MR pulse Sequences

The arrangement of radiofrequency pulses and magnetic gradients used to collect a given type of MR image is known as a pulse sequence. The basic format of a pulse sequence diagram consists of a series of horizontal lines, each representing how a different component of the scanner changes over time (Huettel et al., 2009).

The essential components for any imaging sequence are: an RF excitation pulse; gradients for spatial encoding (2D or 3D); signal reading. When performing an image acquisition, the user must choose the sequence parameters. One essential parameter is echo time (TE) - the time between the 90° RF pulse and MR signal sampling, corresponding to maximum of echo. The other is the repetition time (TR) - the time between two pulse sequences applied (Imaios, 2013).

1 - An artifact is any component that appears on the image which is not present on the original object.

There are several types of sequences; the aims are to find the best compromise between contrast, spatial resolution and speed. New pulse sequences are being created every day, but there are two main sequence families: spin echo (SE) and gradient echo (GRE) sequences.

Spin Echo

SE sequences are made up of a series of events. First, a 90° RF pulse is applied to tip the magnetization into the transverse plane. Due to field heterogeneities spins star to lose phase coherence. So, in order to compensate this dephasing effect at one-half of the echo time a 180° RF pulse is applied. With this rephasing pulse, the signal is characterized in T_2 and not in T_2^*. Finally, the signal reading is performed at TE (Imaios, 2013).

Gradient Echo

GRE sequences (Figure 3.6) differ from SE sequences in regard to: the RF pulse applied, which has a variable flip angle, usually below 90° and the absence of a 180° RF rephasing pulse.

As GRE techniques use a single RF pulse and no 180° rephasing pulse, the signal obtained is thus characterized in T_2* rather than in T_2. In this case the gradients are used to dephase and rephase the transverse magnetization.

The gains of low-flip angle excitations and gradient echo techniques are faster acquisitions, new contrasts between tissues and a stronger MR signal in case of short TR (Imaios, 2013).

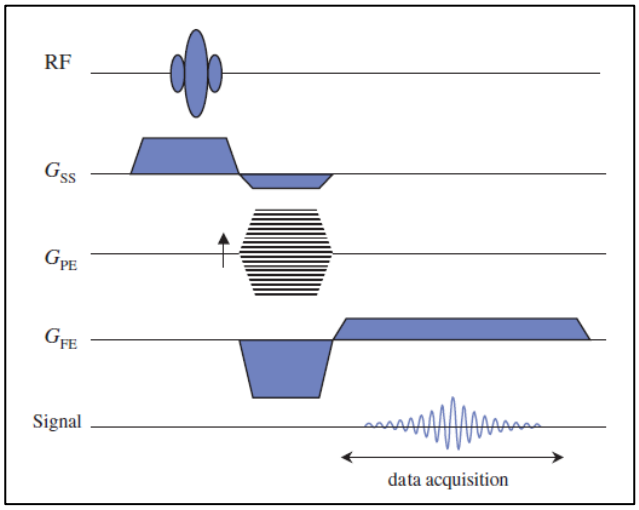

Figure 3.6 - Basic gradient echo sequence subdivided into from top-to-bottom: radiofrequency pulses (RF); slice selection (G_{SS}), phase encoding (G_{PE}), frequency encoding (G_{FE}) and signal acquisition (McRobbie, 2007)

Fast Imaging

New image acquisition techniques have allowed to significantly reduce the acquisition time.

One method to do it is to collect the data corresponding to more than one phase-encoding step from each excitation. There are a number of schemes for doing this; one of them is echo planar imaging (EPI).

EPI is the fastest acquisition method in MRI, but has a limited spatial resolution. It is based on: an excitation pulse; continuous signal acquisition in the form of a gradient echo train, to acquire total or partial k-space (single shot or segmented acquisition); readout and phase-encoding gradients

adapted to spatial image encoding with some possible trajectories to fill k-space (constant or intermittent phase encoding gradient, spiral acquisition etc.) (Imaios, 2013).

There are several EPI possibilities, like: GRE-EPI (gradient echo EPI) and SE-EPI (spin echo EPI), among others (Edelman, 2006). In the figure below (Figure 3.7) one variance of GRE-EPI is represented.

Another fast imaging technique is MP-RAGE (magnetization prepared rapid gradient echo) a 3D-imaging sequence, which combines a periodic inversion pulse[1] (to enhance the signal characteristic in T1) with a rapid GRE acquisition to produce images of high spatial resolution with good contrast between gray matter and WM (Buxton, 2009).

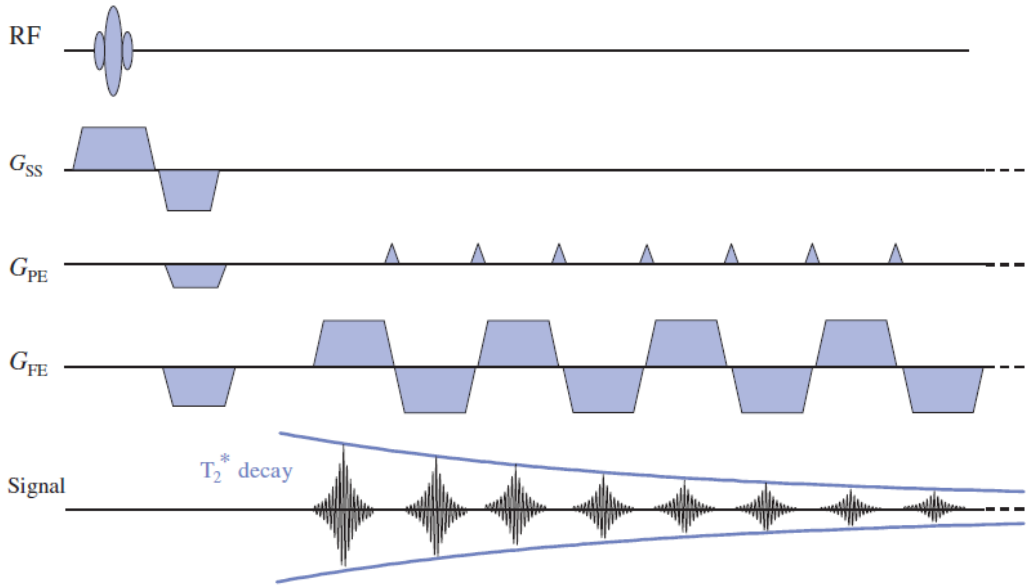

Figure 3.7 – Blipped GRE-EPI sequence: an intermittent (blipped) phase encoding gradient translates in a regular path to fill k-space, making reconstruction easier and quicker than with a constant phase encoding gradient, which produces an irregular zig-zag path to fill k-space (McRobbie, 2007)

3.2.4 Contrast and Weights

In MR images, the contrast depends on the acquisition method used. The intensity difference of the obtained signal between the different measured tissues is called contrast. It also can refer to the physical quantity being measured (T_1, T_2, T_2^*, PD[2]).

Each tissue has characteristic relaxation times (T_1 and T_2) and different proton density. In the Table 3.1 are presented a few typical values of T_1 and T_2 of some brain tissues

Table 3.1 Rough values for the relaxation times at field strength of 1.5 T (Buxton, 2009)

	Gray Matter	White Matter	Cerebrospinal Fluid
T_1	900 ms	600 ms	>2000 ms
T_2	100 ms	80 ms	2000 ms

1 – The inversion pulse corresponds to a 180° RF wave which flips longitudinal magnetization in the opposite direction. Due to longitudinal relaxation, longitudinal magnetization will increase to return to its initial value, passing through null value. (Imaios, 2013)

2 – PD refers to proton density (the number of protons present within each voxel)

The image weighting depends on the main parameters (TR and TE) of the applied sequence: a long TR and short TE sequence is usually called PD –weighted; a short TR and short TE sequence is generally called T_1-weighted; finally, a long TR and medium long TE[1] sequence is usually called T2-weighted.

A tissue with a long T_1 and T_2 (like water) is dark in the T1-weighted image and bright in the T2-weighted image. Thus, a tissue with a short T_1 and a long T_2 (like fat) is bright in the T1-weighted image and gray in the T2-weighted image (Imaios, 2013).

Note that, like T_2-weithted images, T_2^* contrast is provided by pulse sequences with long TR and medium TE values. An additional requirement is that these pulse sequence use magnetic field gradients to generate the signal echo, instead of refocusing pulses, which eliminate field inhomogeneity effects (Huettel et al., 2009).

3.2.5 Image Parameters

The images obtained by magnetic resonance are created in a bi-dimensional grid of numerous pixels in different intensities. The acquisition matrix and the field of view (FOV) characterize the image.
This matrix corresponds to the number of pixels along the frequency-encoding (FE) and phase-encoding (PE) axes (Edelman, 2006). Because the imaging process collects data from a certain slice thickness, there is a volume associated with each pixel, called a voxel (from "volume element") (Buxton, 2009).
FOV is the area that contains the object of interest, thus it defines the size of spatial encoding.
The smaller the voxels are, the higher the spatial resolution will be. However, it is important to realize that a high level of spatial resolution is useless if there is insufficient SNR to support it.
We can calculate the voxel size in all three dimensions from the field of view (FOV), matrix and slice thickness (McRobbie, 2007):

$$FE\ voxel\ size = \frac{FE\ FOV}{FE\ matrix}$$

$$PE\ voxel\ size = \frac{PE\ FOV}{PE\ matrix}$$

$$Slice\ voxel\ size = slice\ thickness$$

3.2.6 Point Spread Function

The modification between what is measured and reality is presented by the point spread function (PSF).

Consider imaging a single, small point source, ideally, the result would be only a single pixel lit up. Instead, the point source is spread out over many pixels in the image.

An ideal, true image of a continuous distribution of magnetization would specify an intensity value for every point in the plane. However, the resulting image is a convolution of the true image with PSF (Buxton, 2009).

Researchers have developed some models to recover the original image and diminish this blur effect.

1 – A medium long TE is to ensure that the signal haven't disappeared

3.3 Functional Magnetic Resonance

One of the remarkable developments on MRI work - functional MRI (fMRI) - is an indirect method of imaging brain activity at high temporal resolution. The principle relies on detecting changes in the metabolic state of the brain with MR signal. Since early 1990's, this technique has grown explosively to become an indispensable tool in neuroscience research (Ogawa et al., 1990).

Note that, the term functional MRI or fMRI has become synonymous with brain activation imaging using the BOLD effect.

3.3.1 Physiological basis of brain activation and BOLD effect

In a typical fMRI experiment the goal is to map patterns of neuronal activation in the subject's brain while the same performs specific tasks. However, fMRI does not measure the neuronal activity itself. In its place, it creates images of physiological changes that are correlated with neuronal activity.

Neuronal activity provokes an increase in oxygen consumption and an even higher increase in cerebral blood flow (CBF). In addition, the blood volume (CBV), the cerebral metabolic rate of oxygen ($CMRO_2$) and blood velocity increase. So, local oxygen extraction fraction (E) diminishes. As a result, the O_2 content of the capillary and venous blood is increased. This process is shown in Figure 3.8. Therefore, neuronal activity is expressed as a relative increase in oxyhemoglobin compared to deoxyhemoglobin (Buxton, 2009; Imaios, 2013).

Even before the discovery of nuclear magnetic resonance itself, Pauling and Coryell found that the magnetic state of hemoglobin changes with its state of oxygenation. In 1982, Thulborn and colleagues demonstrated T_2^* relaxation rate changes in blood samples due to the magnetic susceptibility[1] variations caused by the presence of paramagnetic deoxyhemoglobin (Edelman, 2006).

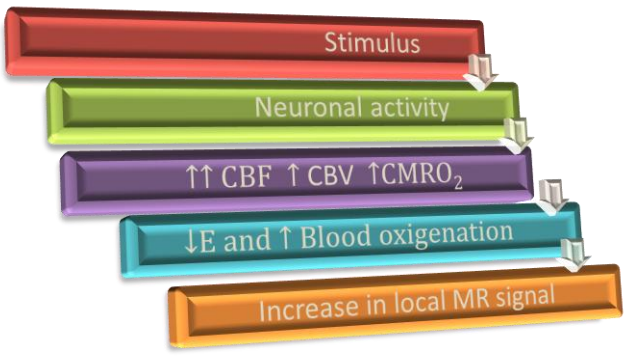

Figure 3.8 – An overview of the physiological changes leading to fMRI data (adapted from Buxton, 2009)

1 –Magnetic susceptibility refers to the tendency of a material to become magnetized in the presence of an applied magnetic field. The applied magnetic field is distorted in the presence of a material of different susceptibility. Materials that are paramagnetic have a slightly greater field than in vacuum, while diamagnetic materials have a slightly lesser field. Ferromagnetic materials have a much higher field. Most of body tissues are diamagnetic.

Thus, the relative increase in oxyhemoglobin concentration can be detected by MRI as a weak transient rise in the T_2* weighted signal. This signal change is called blood oxygenation level dependent (BOLD) effect. However, the existence of a BOLD effect on the MR signal does not necessarily lead to a way of measuring brain activation. The BOLD contrast obtained is very poor (low percentage of signal variation). So, acquisitions need to be repeated in time (Edelman, 2006).

In a typical study to map patterns of brain activation based on the BOLD effect, a series of dynamic images is acquired while the subject alternates between periods of performing a task (the activity to study) and performing a reference task (usually rest), the last one is referred as baseline (Buxton, 2009).

This type of study was performed for the first time in 1992 with a blinking light(Kwong et al., 1992; Ogawa et al., 1992). The time course of BOLD hemodynamic response evoked by a single stimulus event was demonstrated in the end of the same year, Blamire and colleagues used short stimulus to conclude that the first observable change in BOLD signal within the visual cortex occurs, on average, 3.5 seconds after the stimulus (Blamire et al., 1992).

The changes in blood flow are relatively slow; consequently the BOLD signal is a blurred and delayed representation of the original neural signal. As shown in Figure 3.9, this signal does not increase instantaneously and does not return to baseline immediately after the stimulus ends (Poldrack et al., 2011).

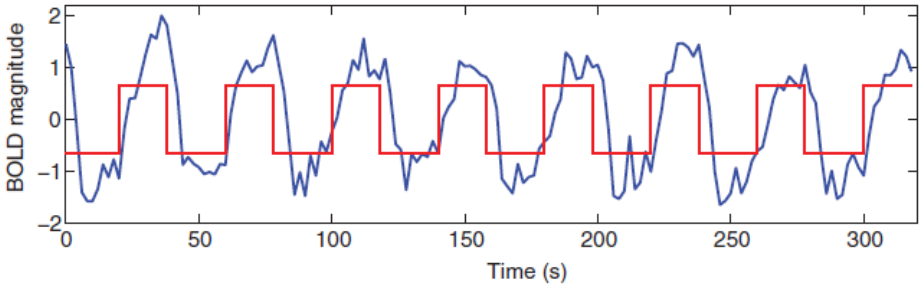

Figure 3.9 – Illustration of BOLD fMRI time series in active voxel: the BOLD signal is represented in blue and the stimulus time series in red (Poldrack et al., 2011)

The time series for each image voxel is then analyzed to determine if the signal shows a significant correlation with the stimulus. Those pixels that do show a correlation are displayed in color on a regular anatomical MR image as the areas activated by the stimulus. (Edelman, 2006)

To cope with the constraints of temporal resolution and T_2* sensitivity, functional MRI sequences are generally of the ultrafast echo planar type (GRE-EPI) (Edelman et al., 1994; Deichmann et al., 2003).

The limitations and disadvantages of BOLD contrast functional MRI are linked to: the distance between activated neurons and blood oxygenation ratio; movement artifacts and magnetic susceptibility (signal distortion and loss at interfaces with the bones, the air) (Imaios, 2013).

Overall, the BOLD signal consists of an intravascular (IV) and an extravascular (EV) component, both of which can arise from small and large blood vessels. Spin-echo acquisition suppresses EV BOLD from large veins and reflects predominantly blood T_2 changes and EV BOLD signal from small blood vessels. On other hand, gradient-echo signal accounts IV and EV components (Ogawa et al., 1993).

3.3.2 fMRI data, GLM and statistical maps

In fact, the signal acquired by the scanner corresponds to: effects of interest and effects of no interest.

BOLD responses to different stimulus correspond to the effects of interest, whereas baseline, slow drift (psychological effect) and noise are disinteresting effects. Other typical effects of no interest are head motion effects.
Mathematical models have been developed to extract BOLD responses from the fMRI data.
The most used is the General Linear Model (GLM) (Friston et al., 1994). This model makes use of a mathematical formulation of the ideal, noiseless change in MR signal on T_2^* images following neuronal activity correspondent to a brief stimulus – hemodynamic response function (HRF). This function and its characteristics are presented in Figure 3.10 (Buxton, 2009; Huettel et al., 2009; Poldrack et al., 2011).

BOLD signal is an indirect measure of brain response. HRF bridges between neural response and BOLD signal. This usually is done by assuming a fixed-shape for HRF. However, there is substantial variability in HRF characteristics across brain areas and across individuals.

In event-related fMRI, the hemodynamic response itself is estimated for each voxel by treating the response at each time point after an event as a separate model function (Buxton, 2009). Assuming a fixed shape for HRF, the BOLD signal corresponds to a convolution between HRF and the stimulus onset time series. The relationship between the neural response and the BOLD signal exhibits *linear time invariant*[1] (LTI) properties.

In order to detect and exclude the effects of no interest, other model functions must be taken to account in GLM to predict this effects. Usually, no model functions are made to predict noise. (Buxton, 2009)

Basically, GLM produces the solution for linear regression:

$$y = X\beta + \varepsilon \qquad \textbf{Equation 3.6}$$

Where:
- y is the signal time series (fMRI data);
- X is a matrix of model functions;
- β is an amplitude vector;
- ε is the noise vector

The best-fit estimates of the amplitudes in β are calculated from the design matrix, X. The objective is to find the point in the model space that is closest to the data point defined by Y, and this point is the projection Y_X on to the model plane. A critical question is whether the estimated amplitudes are statistically significant. There are two related ways to address this question. The first is to estimate the SNR of the measurement, the ratio of the measured amplitude to the expected variance in that measurement. The second approach is to define a t-statistic (Buxton, 2009). The most used is the t--statistic. In its simplest form, the signals measured from a particular voxel are treated as samples of

1 - The meaning of *linearity* is that if a neural response is scaled by a factor of *a*, then the BOLD response is also scaled by this same factor of *a*. This term also implies additivity, for instance if two events occur close together in time, the resulting signal would be the sum of the independent signals. *Time invariant* means that if a stimulus is shifted by *t* seconds, the BOLD response will also be shifted by this same amount.

two populations (active and rest); the t-test is used to assess whether there is a significant difference between the means of the two groups.

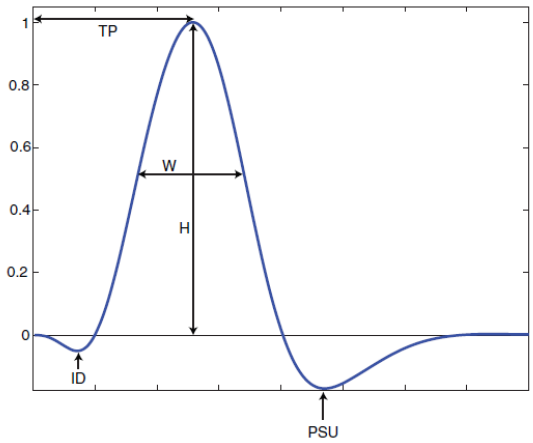

Figure 3.10 –Characteristics of the HRF: time from the stimulus until peak (TP); height of response (H), the width of the HRF at half height (W), post stimulus undershoot (PSU) and initial dip (DIP) (Poldrack et al., 2011)

This is quantified with the t-distribution, from which one can calculate the probability that a particular value of t could arise from random noise. A threshold value of this probability can be chosen, such as $p < 0.01$. The voxels whose t-value passes the threshold are then displayed in color on an underlying map of the anatomy. (Buxton, 2009)

3.3.3 Experimental Design

Depending on what the researcher is interested in measuring, different study designs are required. In majority of experiments, the aim is to detect and estimate the magnitude of activation. But sometimes, purpose is to estimate the precise shape of the hemodynamic response associated with the task.

The task sequence and mode of repetition constitute the activation paradigm. It involves at least one reference task (usually rest), and another task whose only difference is in the activity we wish to study. (Imaios, 2013)

The theoretical curves of the hemodynamic response and the BOLD signal depend on the type of design chosen. There are two types: block design and event-related design. There are also mixed designs, containing both events and blocks.

In the block design, the activities are organized into blocks of several seconds (each block lasts for more than one TR), alternating at regular intervals. Within the same block, the hemodynamic responses will overlap (Figure 3.11A). On other hand, event-related design is related to a pseudo-random sequence of activities, to avoid anticipation. Each event lasts for one TR at maximum. The hemodynamic response of this type of design is presented in Figure 3.11B; in this case the response tends to be weaker, since fewer overlaps occur. (Imaios, 2013)

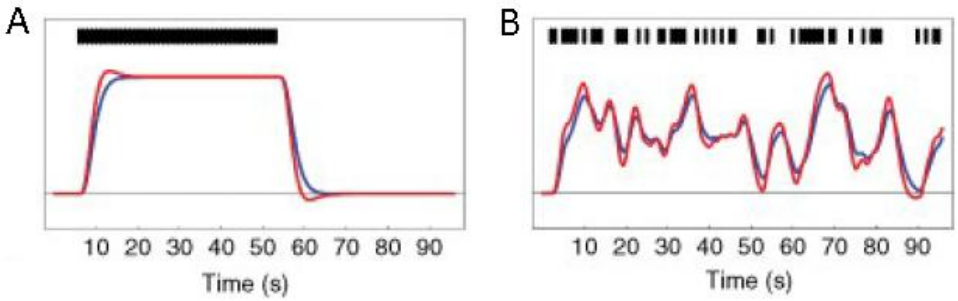

Figure 3.11 –Assumed fixed-shape of hemodynamic response for different experimental designs: Block design (A); Event-Related design (B); the stimulus pattern is presented in black (Edelman, 2006)

3.4 Ultra-High Field MRI

During the last two decades, MRI has under gone substantial at advances, both in the quality of the data and in the sort of applications used for studying the brain. These developments have in part been augmented by increasing the magnetic field strength.

The higher the magnetic field strength is the better the image quality. High fields improve signal-to-noise ratio, thereby permitting a significant progress in spatial resolution (Vaughan et al., 2001) and also reduce acquisition time (Duyn, 2012). Apart from all the advantages, there are a few limitations, from economical to technological and biological levels.

MRI field is considered to be high when its strength is greater than 3.0 T and ultra-high when equal or greater than 7 T (Graham et al. 2001).

3.4.1 Anatomic Neuroimaging at high field

Structural MRI has profited from the resolution amplification and contrast offered at high magnetic fields.

Just the jump from 1.5 T to 3 T has enhanced the separation of grey and WM, and allowed quantification of cortical volume. At ultra-high fields from 7 T to 9.4 T, magnetic susceptibility weighted techniques have permitted visualization improvements of small anatomical structures (Bourekas et al., 1999). Also, at a resolution of a few microns white matter fibers, vascular structures and the layer structure of cortical gray matter (Marques et al., 2010a) are revealed (Graham et al. 2001).

Regarding technical problems at high magnetic fields in MP-RAGE sequences, in 2010 was created an extension of this sequence – MP2RAGE (Marques et al., 2010). In the same study is also shown that this new sequence has a better contrast in 7 T than in 3 T.

3.4.2 High-field functional magnetic resonance imaging

Ultrahigh fields provide bigger sensitivity and specificity for fMRI applications, allowing a better understanding of functional networks (De Martino et al., 2011).

In fact, the early work done in fMRI was greatly facilitated by the availability of magnets with fields substantially higher. For instance, Ogawa's first fMRI study in a human was performed at 4 T (Ogawa et al., 1992).

An additional aiding in the initial development of fMRI was the use of the fast imaging technique EPI(Blamire et al., 1992). Although, at a high magnetic fields this type of imaging acquisition showed some issues, like increased distortions and reduced T_2^*, until 2008, when Speck and colleagues solved those problems(Speck et al., 2008). In large part because of the increased magnetic susceptibility contrast at high field that underlies the BOLD effect, several major fMRI research sites now own 7 T human scanners (Duyn, 2012).

The gain of ultra-high magnetic fields in sensitivity, specificity, and resolution is related in several fMRI studies (e.g. De Martino et al., 2011; Triantafyllou et al., 2005).

The combination of such data with high resolution anatomical data available offers unique opportunities for the study of the relationship between structure and function in the human brain.

4 State of art

Over the last century the motor cortex has been one of the most extensively studied brain areas, yet the neural correlates of movement are not well understood.

4.1 Somatotopy

During some years, the idea that body representation followed a specific and ordered pattern in the primary motor cortex (M1) has been fruit of mere speculation, based in Jackson's study in 1863.

With later research (using electrical stimulation) this idea gained some shape to culminate in the description of human (Penfield and Boldrey, 1937; Penfield and Rasmussen, 1950) and primate (Woosley et al., 1952) representation sequences (somatotopy) for the M1, a well-known tool for nowadays neuroscience – the homunculus (Figure 4.1).

Basically, M1 somatotopy consists in the existence of systematically organized cortical regions to control movements of different body parts. In visual cortex, there is an analogous phenomenon; in this case the cortical regions are organized to map the receptor cells of the retina – retinotopy (Tootell et al., 1982). There are a few factors that influence retinotopy, for example color (Hadjikhani et al., 1998) and spatial attention (Tootell et al., 1998). So, following this analogy, M1 somatotopy should be coded by movement factors, such as direction, force and muscle synergies.

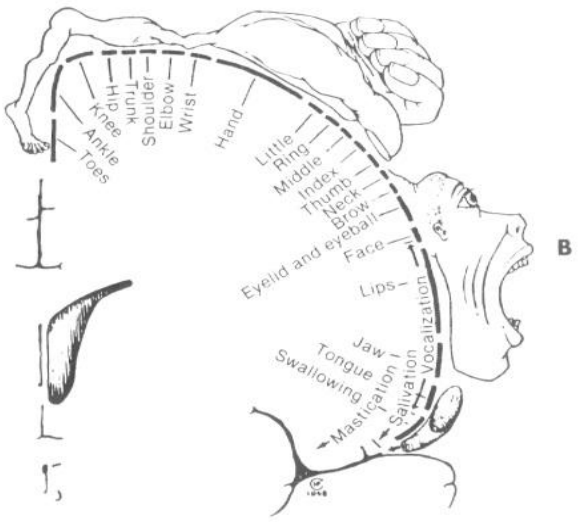

Figure 4.1 - Human M1 homunculus: the order of body representation in the primary motor cortex (Penfield and Rasmussen, 1950)

The early and some subsequent ones generally show big similarities between the representation patterns of humans and nonhuman primates. Although, a polemic involving the somatotopic sequence of within-limb segments has risen, especially in upper limb area.

It is clear that representations of large limb segments, such as head, upper extremity, and lower extremity are sequential and largely separated. The discussion is about whether representations of these small body parts preserve distinct homuncular locations or overlap with each other, as studied in primates (Figure 4.2) for the fingers (Kwan et al., 1978; Schieber and Hibbard, 1993).

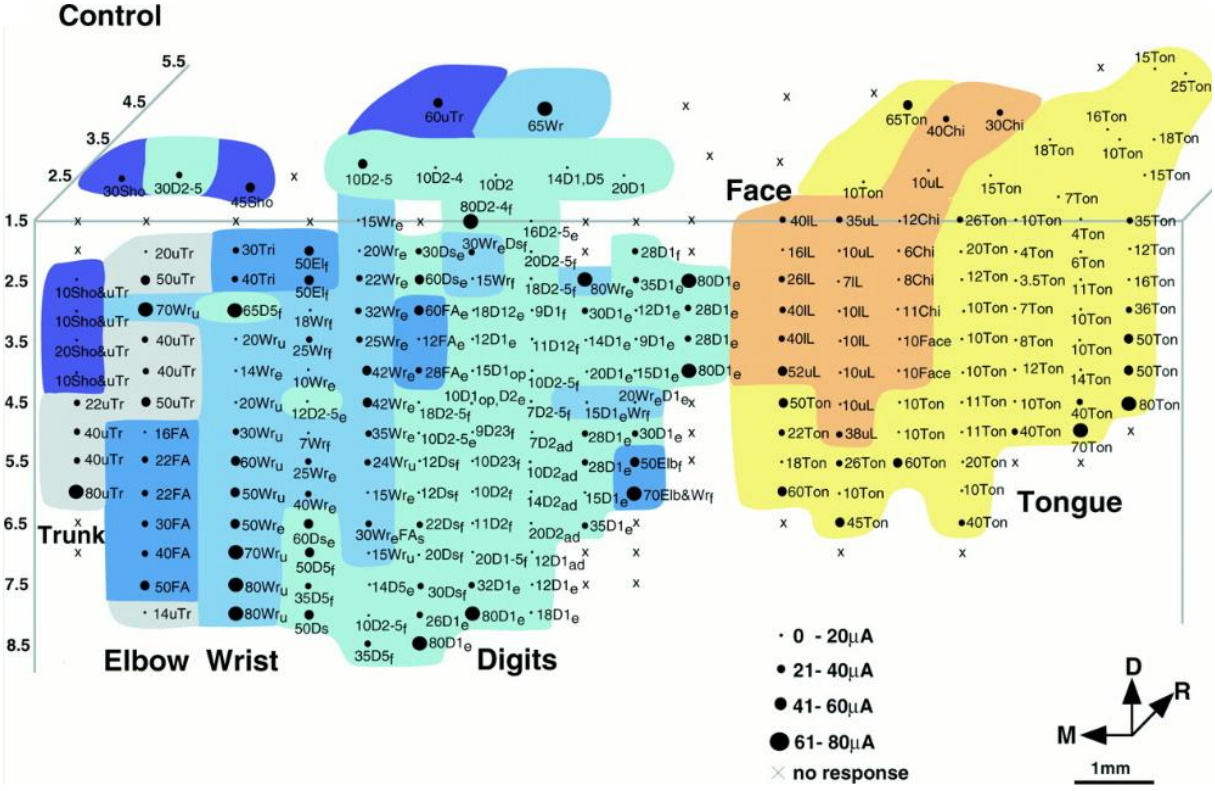

Figure 4.2 - Organization of motor cortex of a normal macaque monkey: movement and current thresholds for stimulation sites from face to upper trunk, the digits area is coded by D1-5, digit 1,2,3,4,5 (from thumb to little finger); different types of movements were performed being ab, abduction; ad, adduction; dep, depression; e, extension; el, elevation; f, flexion; mr, Medial rotation; opp, opposition; p, pronation; r, radial deviation; s, supenation; u, ulnar; the orientation vectors correspond to D, dorsal; M, Medial; R, Right. (Qi et al., 2000).

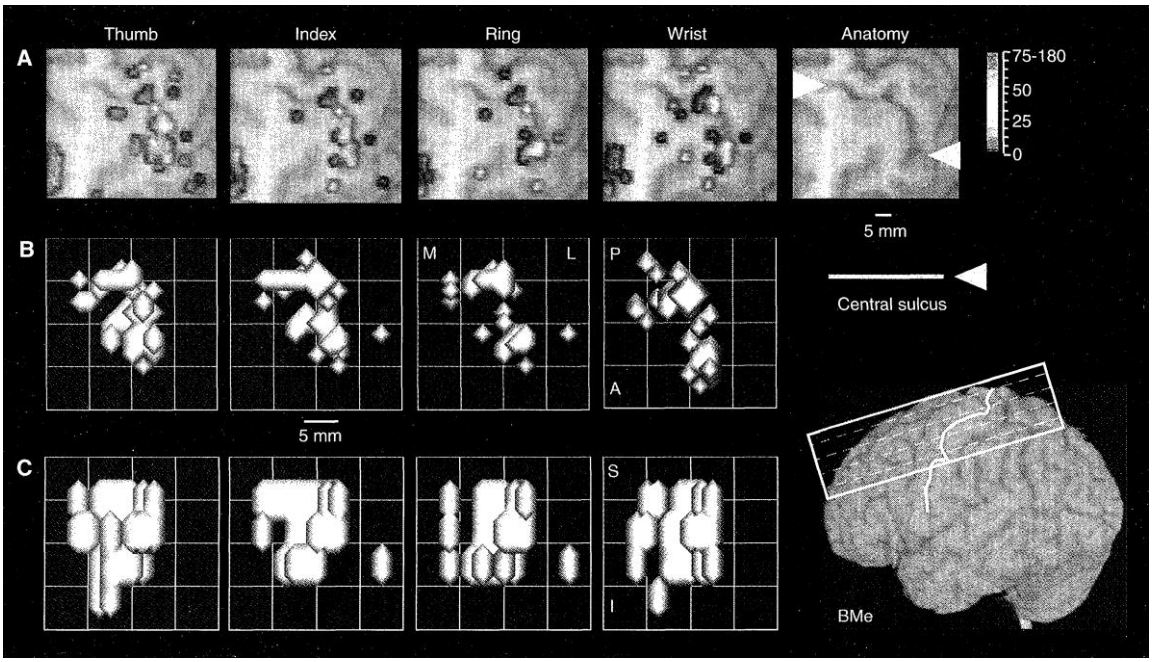

Figure 4.3 - Movement representation overlap: single slices of different fingers or writ activity maps during movement (A); three dimensional reconstructions of the significantly activated voxels extracted from M1 for two angles: same angle of the A slices, the sagital view (B) and the other one corresponds to a coronal view (C) (Sanes et al., 1995).

This nonsomatotopic organization for the hand area (specifically the fingers) in nonhuman primate M1 is supported by some studies employed in humans (Grafton et al., 1991; Indovina and Sanes, 2001; Sanes et al., 1995; Schieber, 1999) (Figure 4.3). Besides the experimental results, there are a several arguments used by those who consider the overlap has the hallmark of M1: convergence of cortico-spinal input from multiple locations, horizontal connections or even divergence of cortico-spinal output to multiple segments (Schieber, 2001). M1 codes panoply of finger movements with different features regarding the strength, direction and muscle synergies; additionally, single finger movements, normally, depend on coincident contractions of multiple muscles (Schieber, 1995), the muscles needed for one type of movement can be located in different cortical regions of M1. The main argument is that somatotopy would reduce the capacity to access different combinations of muscles contractions. Following, Schieber's comparison of a piano keyboard with M1, in order to play one tunes a combination of notes is made; he supposes, that the same happens in the cortical area of M1, to easily produce such a diverse variety of movements, different combinations of neurons have to be effortlessly encoded. To facilitate the achievement of different combinations, the piano keyboard is a mixture of white and black keys (white and black keys contain different groups of notes); similarly, Schieber states that M1 processes a distributed organization.

By contrast, recent studies have indicated discrete centers in the homuncular order for finger movement representation, despite the overlap existence between adjacent representations (Beisteiner et al., 2001; Dechent and Frahm, 2003a; Hluštík et al., 2001; Lotze et al., 2000). The majority of these recent studies was done using higher resolution functional MRI methods. In this case, the explanation is that shared regions allow multi-joint coordination and the discrete centers are related with the specification of the movement control.

All the debate about fingers somatotopy can possibly be explained with several neuroimaging factors: spatial resolution, magnetic field strength, paradigm, data analysis.

For example, a low spatial resolution allied with a low magnetic strength could have induced to evidences of overlap between finger representations (Sanes et al., 1995); on the other hand, a high spatial resolution of 1.6 mm^2 (in-plane) and 3mm of slice thickness (Hluštík et al., 2001) or a high magnetic field strength (Beisteiner et al., 2001) probably indicated fingers somatotopy.

Another aspect is the paradigm itself: when the baseline corresponds to rest the activity map (direct paradigm) could embrace shared regions with the next-door representations (Indovina and Sanes, 2001); whereas if the defined baseline used corresponds to another finger movement (differential paradigme) (Dechent and Frahm, 2003a) the results could lead to strong somatotopy (for instance, in Dechent study the two paradigm approaches were used, they concluded that differential paradigms reveal more segregated and somatotopically ordered activations, apart from the somatotopy dependency on the baseline finger).

Still focusing on the paradigm, there are different factors regarding with the task. The referred studies have used different tasks: flexion-extension movements of fingers (Sanes et al., 1995; Beisteiner et al., 2001; Indovina and Sanes, 2001; Hluštík et al., 2001); tracking of one moving target with fingers (Grafton et al., 1991); finger tapping (random or thumb sequential opposition movements) (Lotze et al., 2000; Dechent and Frahm, 2003). Note that, only flexion-extension movement task shows incongruence between the results.

The final factor, data analysis is related with the measurement of activity. First, a difference between two methods - center of mass (average location of representation) and peak of activity - is patent (Lotze et al., 2000). In last, the characterization of the active regions can be done using the GLM (Indovina and Sanes, 2001), or use a cross correlation technique which a-priori excludes overlap (Beisteiner et al., 2001)).

Combining both theories – distributed and somatotopic organization, we predict that there is a distributed pattern (intermingled with somatotopic "hot spots") for fingers encoding in M1. This means that like a piano keyboard, in order to flexibly access to a huge amount of different movements, all possible neuronal combinations (regarding the finger's movements) can be made within each finger's cortical specified region. Inside the finger specific region the majority of neurons function should code movements related with this finger, however in the same area there should also exist neurons that encode some features of other fingers movements. Moreover, we also hypothesize that this distributed pattern (intermingled with somatotopic "hot spots") varies with the cortical layers. Following No's (Lorente De Nó, 1938a) idea that M1 superficial cortical layers are more receptive, functioning in stimulus reception, whereas the deeper layers are more efferent, functioning as an effector organ, it would make sense that the somatotopy characteristic is more evident in deeper layers.

Finally, in order, to avoid neuroimaging dependency of the data, the used method relies in high resolution fMRI to map the activity of finger tapping.

4.2 Depth Structures

The capacity to perform a complex sequence of movements, linking all the basic actions is the main component of voluntary motor behaviour. The processing of such detailed information is estimated to include neuronal ensembles at the cortical column level (Lorente De Nó, 1938b). Thus, in order to understand the functioning of the cortex it is fundamental to know this structure at its basic architectural level.

Soon the idea of elementary cortical unit's existence in the cortex (Lorente De Nó, 1938b) gained support from animal studies (Hubel and Wiesel, 1959; Mountcastle, 1957). Mountcastle described his observation (Figure 4.4) stating that there is an elementary unit of organization in the somatic cortex made up of a vertical group of cells extending through all the cellular layers, intermingled in a mosaic-like fashion, he called this unit a column. Basically, they are clusters of neurons that share physiological properties.

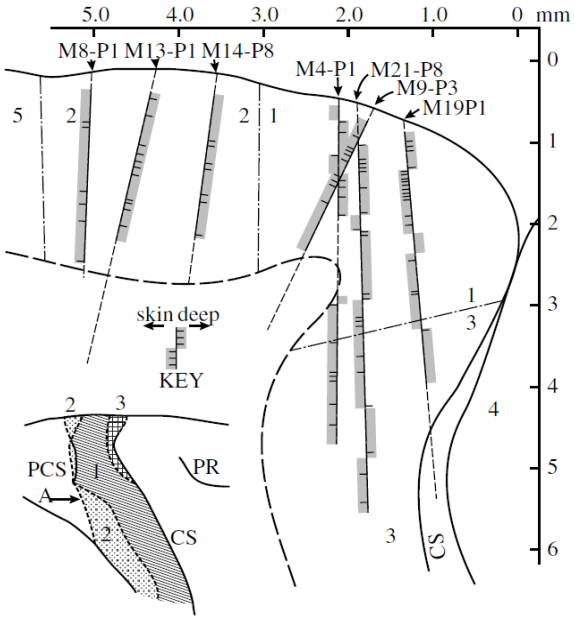

Figure 4.4 - Reconstruction of some electrode penetrations performed by Mountcastle in the Brodmann areas 1, 2 and 3
(Powell and Mountcasle, 1959)

Since their discovery, cortical columns have been extensively studied in animals, due to their promise of simplifying the understanding of one of the most intriguing structures in biology, the cerebral cortex.

All this effort induced a big development in the characterization of such fine structures, among a several parts of the neocortex (visual, temporal, auditory and frontal cortices).

To identify this organization in primary visual cortex (V1) many studies were performed to evaluate different types of factors, like ocular dominance - OD, which is the preference to left or right eye, contour orientation, direction of motion and spatial frequency (Blasdel and Salama, 1986; Bonhoeffer and Grinvald, 1991; Hubel and Wiesel, 1959, 1977; Hübener et al., 1997; Shmuel and Grinvald, 1996; Weliky et al., 1996).
In order to describe the pattern of cortical columns (modules) orientation, processing modules have been studied in different animals for different factors, not only for V1, but also for other areas like V2(Tootell et al., 1983), V4 (Ghose and Ts'o, 1997), V5/MT, inferior temporal (Desimone et al., 1984) cortex and frontal cortices (Goldman-Rakic and Schwartz, 1982).

With the development of noninvasive neuroimaging techniques, Yacoub and colleagues showed the ability to map the ocular dominance columns of the human visual cortex using fMRI (Yacoub et al., 2007). In the same study, a difference between the performance of two techniques (spin-echo (SE) and gradient-echo (GE)) was evaluated. Their conclusion points that SE signal can uniformly resolve columnar patterns better than GE, mainly due to their different susceptibility regarding the vascular signal: while SE BOLD corresponds to the intravascular signal, GE BOLD accounts all the vascular components (intra and extra vascular) (Ogawa et al., 1993). This susceptibility difference allied with the demonstration that large vessels influence the columnar specificity of cerebral blood flow(Duong et al., 2001); indicate the way to be successful in mapping columnar structures using the positive BOLD effect, which is the avoidance of large vessel contributions in the data. This approach was used in earlier studies that attempted to map columns in humans using GE. (Dechent and Frahm, 2000; Goodyear and Menon, 2001; Menon et al., 1997)

Other approaches have been instigated: suppression of large vessel contributions during the data acquisition (using spin echo sequences), to better discern their location as well as their influence in the BOLD signal (using bipolar gradients (Boxerman et al., 1995; Song et al., 1996) and phase specific information (Menon, 2002) or even by their removal (for example: masking of voxels demonstrating high-amplitude responses (Cheng et al., 2001; Shmuel et al., 2007).
On other hand, looking at these two methods of BOLD imaging, SE has a lower SNR then GE, which is a precious advantage in the activity detection.

Lately, ultra-high magnetic fields solved some problems related with GE BOLD fMRI, by the enhancement of the tissue's signal and thus, providing a higher SNR (Yacoub et al., 2001).

In addition, evidence of cortical columns has been found in the language cortex in humans (Galuske et al., 2000). In fact, these structures have been most frequently found in sensory areas, however they also appear in motor areas. For instance, in 2003, a study with primates culminated in the founding of clusters of cells differentiated by the preferred direction vector of motion (Amirikian and Georgopoulos, 2003).

Even though, in M1 cortical columns still fit in *unknown M1 fields*: to date, no evidence of such structures has been found in humans M1.

Recent studies have performed an analysis to this elementary cortical unit in humans: in V1, the existence and spatial features of orientation selective columns in humans has been proved (Yacoub

et al., 2008); in the middle temporal area was collected the first direct evidence for large-scale axis of motion selective feature organization closely matching predictions from topographic columnar-level simulations (Zimmermann et al., 2011a). This last one is based in a novel high resolution cortical grid sampling analysis tools, being able to investigate the functional properties in multiple layers at the columnar level.

From the anatomical point of view, it is known that Betz cells, huge pyramidal cells, are exclusively found in layer V of M1 (Scheibel et al., 1977); in non-humans, cortical surface electrical stimulation provokes a discharge in Betz cells (Asanuma and Rosén, 1972; Jankowska et al., 1975). Considering this and the existing evidence of columnar structures in monkey M1 (Amirikian and Georgopoulos, 2003), we predict that these structures also exist in human M1. Therefore, allying high resolution fMRI with the novel cortical sampling method now is possible to evaluate their existence.

4.3 Visual Responses in M1

The discovery of mirror neurons was originally found in monkey area F5 of the premotor cortex, these neurons also showed responses for visual stimulation. They discharge when the monkey does a particular action (with hands or face) and also when it observes the same action being performed by another individual (monkey or human) (Gallese et al., 1996; di Pellegrino et al., 1992; Rizzolatti et al., 1996a). Mirror neurons belong to a larger class of neurons – the visuomotor family - that also includes canonical neurons, which respond to object's presentation(Rizzolatti and Luppino, 2001).

The finding of a new family of neurons – visuomotor neurons – induced new theories about the role played by the motor system: mirror neurons might be involved in understanding the actions of the others (Rizzolatti et al., 2001), learning how to perform such actions (Rizzolatti and Craighero, 2004) and might, therefore, be related with an ancient communication system based on recognition of gestures (Rizzolatti et al., 1996a).

These earlier studies also stated that mirror neurons only respond to movements related with objects, pointing that the view of an object alone or even the sight of an agent making intransitive (non-object directed) actions are all unsuccessful; this theory was refuted by succeeding studies (Fadiga et al., 1995, 2005; Maeda et al., 2002).

The presence of mirror neurons is also evident in the superior temporal sulcus (STS) of monkeys (Jellema et al., 2000; Perrett et al., 1989, 1992).
To date, only one study provides direct evidence of this kind of neurons in humans (Mukamel et al., 2010). There is, although, a good amount of data from neurophysiology and brain imaging experiments demonstrating, indirectly, the existence of mirror-neuron system in humans.

In the 50s, the first raw evidence that only the observation of an action also provokes activity within the motor system was discovered (Cohen-Seat et al., 1954; Gastaut and Bert, 1954). They found that de-synchronization of an electro encephalograph (EEG) signal occurs when subjects perform two tasks - movement and observation of the movement. Latter studies have confirmed this finding: some using EEG recordings (Cochin et al., 1998, 1999) and other one applying the magneto encephalographic (MEG) technique (Hari et al., 1998). Hari's experiment associated the origin of the de-synchronization with the central sulcus.

Other kind of neurophysiological study performed in humans is transcranial magnetic stimulation (TMS). The results show that the observation of both transitive and intransitive actions provoke an

increase of the motor-evoked potentials (MEPs) measured in the extremity of contralateral muscles (Fadiga et al., 1995, 2005).

With these discoveries, Baldissera and colleagues decided to do a study to investigate the influence of action observation in the spinal cord. Their results point the existence of an inhibitory process to avoid the performance of an observed movement (Baldissera et al., 2001).

There are other experiments using TMS technique showing the existence of a relationship between movement execution and movement observation (Gangitano et al., 2001; Strafella and Paus, 2000). Besides the existence of such relationship, TMS studies stated a difference between mirror-neurons of humans and monkey. In the human species, not only goal-directed actions but also intransitive actions provide mirror neurons activation (Fadiga et al., 1995, 2005; Maeda et al., 2002).

Looking at brain imaging experiments, a considerable number showed that the visualization of movement induces responses in several areas: besides the usual visual areas - occipital, temporal and parietal, other cortical regions more related with motor functions are also responsive (Figure 4.5).

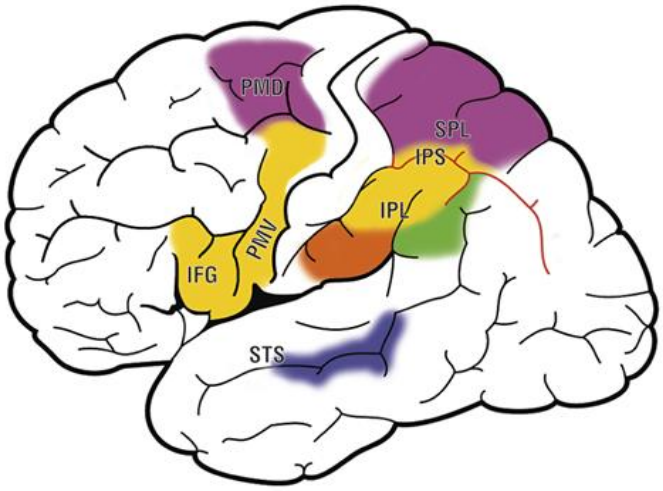

Figure 4.5 – Cortical areas related to the mirror system responding to different types of motor acts: yellow indicates transitive distal movements; purple, reaching movements; orange, tool use; green, intransitive movements; blue portion of the superior temporal sulcus (STS) responding to observation of upper-limb movements. IFG indicates inferior frontal gyrus; IPL, inferior parietal lobule; IPS, intra pareital sulcus; PMD, dorsal premotor cortex; PMV, ventral premotor cortex and SPL, superior parietal lobule (Cattaneo L and Rizzolatti G, 2009).

Focusing in the cortical regions a-priori associated with motor tasks, a part of the experiments states that a visual-movement stimulus provokes activity in diverse premotor areas (Buccino et al., 2001; Rizzolatti et al., 1996b). Other studies show that apart from the premotor regions activity, there is also a response from M1: related with hand movement visualization (Grezes, 1998; Nishitani and Hari, 2000) and also related with lips movement visualization (Nishitani and Hari, 2002). Grèzes shows that the cerebral blood flow in M1 varies between meaningless and meaningful actions, being increased with the last one.

From the biology, it is known that M1 superficial cortical layers are more receptive, functioning in stimulus reception, whereas the deeper layers are more efferent, functioning as an effector organ (de No, 1938). Therefore, we hypothesize that observation of movement activates mostly the superficial layers of M1, apart from the biology support, this hypothesis is based in the few studies that have showed the existence of such activity (Grezes, 1998; Nishitani and Hari, 2000). Noone of

these studies have used fMRI, thus we expect that the high resolution wonders of this technique will bring more certainty about the relation between movement observation and M1. In addition, following the finger somatotopy distribution ideal for the motor activity in M1, we theorize that also the observation of fingers movement shows the same pattern.

4.4 Imagery in M1

Motor imagery can be defined has the consciousness access to the content of the intent to perform a movement, in other words this cognitive state results in the mental simulation of a given action.

Early mental simulation theories defended that motor imagery and action observation are based in the same processes has motor execution (Decety, 1996; Jeannerod, 1994, 2001; Jeannerod et al., 1995). They have founded this theory on the basis that the motor imagery state corresponds to the conscious motor preparation process; there are two types of motor imagery visual and telekinetic.

The visual motor imagery is based on a visuospatial processing, so relies on the third person perspective. On other hand the telekinetic motor imagery leans on the first person perspective, in the sense that is constructed with motor-kinesthetic information processing. The majority of the studies use telekinetic motor imagery.

Later, it has been demonstrated that motor imagery and motor execution (ME) responses are comparable, but not equal (Gerardin et al., 2000). The premotor cortex (PMC) and the supplementary motor area (SMA) are the brain areas that show the strongest relationship with motor imagery, their contribution during this task has been consistently shown among the literature (e.g. Nair and colleagues, using fMRI, demonstrated the involvement of PMC and SMA in fingers motor imagery (Nair et al., 2003)). On other hand, there is a debate about the involvement of M1 in motor imagery.

Some experiments related with finger movement imagery show no participation of M1 during motor imagery (Binkofski et al., 2000; Hanakawa et al., 2003), while others point to activation of M1 during the exact same task (Figure 4.6) (Porro et al., 2000; Roth et al., 1996; Sharma et al., 2008). There is also an in-between position, for those who propose a weak transient activation of M1 (Dechent et al., 2004; Kuhtz-Buschbeck et al., 2003; Wriessnegger et al., 2008).

Recent studies state that different factors can influence M1 activity during motor imagery, such has: imaginer quality - only poor imaginers show responses (Guillot et al., 2008); active mental training – activation increases after mental training (Sacco et al., 2006); type of imagery (visual or telekinetic) – no activity during visual motor imagery (Solodkin et al., 2004).

Basically our predictions for motor imagery are similar to the ones described in the movement observation, although we theorize that these two tasks (telekinetic motor imagery and movement observation) are not related.

Thus, once again following the different functions of superficial and deeper cortical layers regarding the receptive ad efferent features (being the superficial layers more receptive and the deeper ones more efferent) (de No, 1938), we conjecture that motor imagery activates mostly the superficial layers of M1 due the existence of a motor related stimulus.

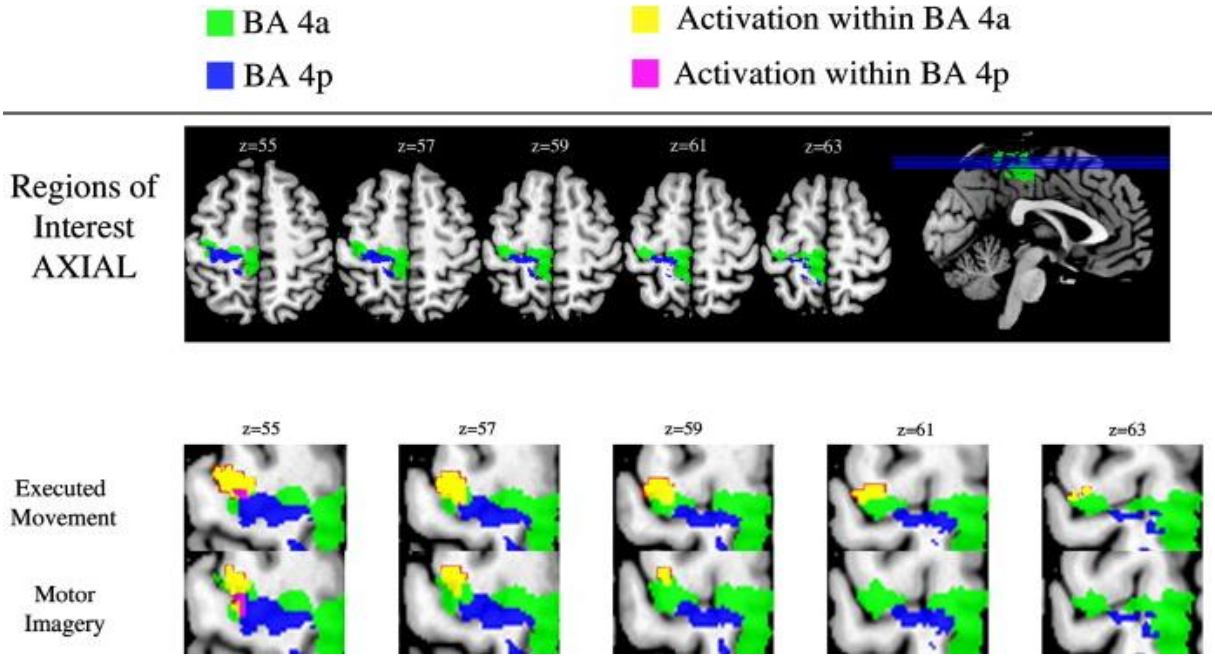

Figure 4.6 – Illustration of M1 activity during fingers motor imagery and movement execution: the BA 4a and BA 4p correspond to the ROI's illustrated in the first row (Sharma et al., 2008).

Apart from the biology support, this hypothesis is based in some studies that have revealed motor imagery activity in M1 (Porro et al., 2000; Roth et al., 1996; Sharma et al., 2008). However, these last studies have used a finger-thumb opposition blocks sequence for both tasks - motor imagery and motor execution; which is a quite different approach from single finger tapping blocks sequence (the one implemented in this project). Also these projects have applied the fMRI method, yet none of them made use of high resolution fMRI, thus we expect that the high resolution marvels will get to a better understanding of the relation between motor imagery and the M1 in a totally different approach. Moreover, any of the studies that showed a transient M1 activation in motor imagery have made use of single finger tapping blocks sequence. Ultimately, following the finger somatotopy distribution ideal for the motor activity in M1, we also predict that fingers motor imagery pursues the same organization model.

5 Methods

5.1 Participants

Thirteen healthy subjects (9 male, 4 female, ages 20 –32) participated after giving written, informed consent. No volunteer had a history of neurological or psychiatric illness. Experimental procedures were approved by the local ethics committee.
In total, 5 participants performed all the four tasks: visualization of movement (VM), motor imagery (MI), motor execution (ME) and rest. All the 13 subjects performed ME, 7 of them also participated in MI and rest tasks, from the 13 subjects only 5 performed VM task.

5.2 Paradigm

Before entering the fMRI stage of the research, all subjects experienced a preliminary session in which adequate task compliance was assured.

During the experiment, participants were installed inside the scanner in the supine position with their right arm comfortably set to perform finger movements.

Motor Execution task (ME)

Volunteers were instructed to move their thumb, index or middle finger when a visual cue appeared. Finger movements were blocked with 20 movements per block at 1 Hz, followed by 10s of rest (Figure 5.1A). Each participant was scanned twice at high and ultra-high resolution.

Motor Imagery task

Participants were instructed to imagine the movement of their thumb, index or middle finger when a visual cue appeared. The experiment design of this task is the same of the one used for ME: 20s of MI for different fingers depended on the visual cue, interspersed with 10 s of no stimuli (Figure 5.15.1B).

Action Observation (AO)

Subjects were instructed to watch a video presenting the movement of different fingers (thumb, index and middle) from a human hand. The paradigm used for this video corresponds to the one used in MI and in ME: except that this time there is no visual cue to instruct the participant. Instead of imagining or moving the fingers, like in the other two paradigms, the subject is just watching the respective finger move at 1 Hz during 20s, the movement period is intermingled with 10s of rest (Figure 5.1C).

Rest

While being scanned the participants were asked to close their eyes and not think of anything specific for 5 min (Figure 5.1D).

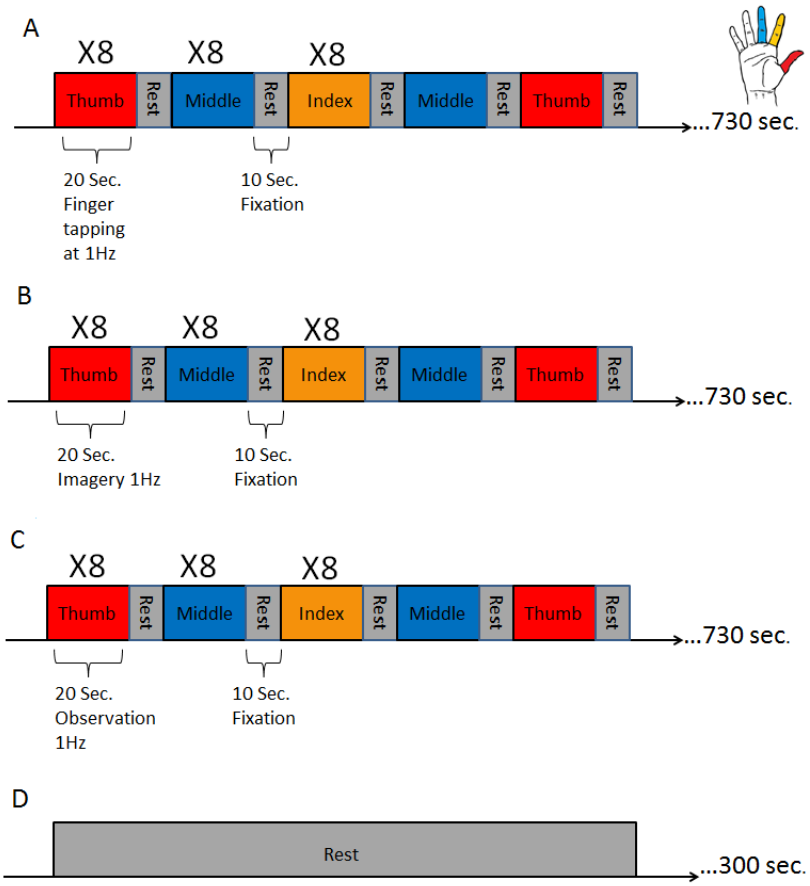

Figure 5.1 - Experimental design used for all the different tasks: Motor Execution (A); Motor Imagery (B); Action Observation (C); Rest (D) [Note that each finger has 8 blocks of 20 s for A, B and C]

Note that for motor imagery, AO and rest tasks the subjects were only scanned once with ultra-high resolution.

All videos used for stimuli were produced in the ExpyVR software, which provides precision control of stimulus presentation during fMRI experiments. The images were projected on a screen and then displayed via a mirror fixed in place with a cranial coil. Overall, the order of the fingers stimuli/images used in the video was randomized, but the same order was used to the different tasks to assure the same level of practice effects in all subjects.

5.3 Image acquisition

Imaging was performed with a 7 T MR system (Siemens, Germany) located at the Centre d'Imagerie BioMedicale (CIBM) in Lausanne, Switzerland. The scanning session included anatomical and Blood oxygenation level-dependent (BOLD) functional imaging.

The improved signal-to-noise ratio and the continuing access to BOLD signal with ultrahigh magnetic field systems (bigger than 3 T) allow the use of reduced voxel sizes in fMRI. Also, the signal strength of venous blood is diminished due to a reduced relaxation time, confining activation signals to the cortical gray matter and therefore enhancing the spatial specificity of the BOLD signal (van der Zwaag et al., 2009).

All data was acquired using a 32-channel head coil. fMRI images were collected using an gradient-echo echo-planar imaging (EPI) sequence with sinusoidal readout (Speck et al., 2008)) with the next parameters: TR=2500 ms, TE=29 ms, flip angle=75°, 28 oblique slices parallel to bi-commissural plane covering the whole motor cortex, these first parameters were used for high (HR) and ultra-high (UHR) resolution scans, differing in the spatial resolution factors - matrix size, FOV and slice thickness (HR: matrix size=96× 96, FOV 125 × 125 mm^2, which corresponds to 1.3 × 1.3 mm^2 in-plane resolution, slice thickness=1.3 mm; UHR: matrix size=154 × 154, FOV 115 × 115 mm^2, leading to 0.75 × 0.75 mm^2 in-plane resolution, slice thickness=1 mm). Functional runs of 730 s with 292 volumes each were acquired per volunteer for VS, MI and ME tasks. During rest, images were collected for 300 s resulting in 120 volumes per subject.

A T1-weighted high-resolution 3D anatomical image was acquired for each subject using the MP2RAGE pulse sequence optimized for 7 T MRI(Marques and Gruetter, 2013; Marques et al., 2010; Tanner et al., 2012). The anatomical data had the following parameters: TR=5500 ms, TE=2.82 ms, 176 slices, matrix size=256× 240, FOV 256 × 240 mm^2, which corresponds to 1 × 1 mm^2 in-plane resolution, slice thickness=1 mm. These images were prearranged based on a sagittal localizer and covered the whole brain.

5.4 Imaging Data Analysis

The collected data was processed using BrainVoyager QX 2.8 software package.

5.4.1 Preprocessing

Preprocessing of functional scans involved 3D motion correction, low -frequency drifts removal and temporal high-pass filtering with a cutoff frequency of 0.0005 Hz for the rest condition (Salomon et al., 2011). Anatomical scans preprocessing was based on intensity inhomogeneity correction.

5.4.1.1 Functional Images Preprocessing Steps

3D motion correction

The quality of fMRI data is robustly dependent in the presence of head movements. It is expected that each voxel represents one specific location in the brain, thus, if there is any movement, the signal correspondent of one single voxel will now represent a mixture of signals from different parts of the brain.

Consequently, motion correction is a strong tool to improve the quality of the data, minimizing the false positive activations and increasing sensitivity to true task-related activations.

In general motion correction combines the estimation of the movement based on one reference volume (in this case the first volume) and the consequent application of the estimated movement parameters (translation along the x, y and z-axes and rotation around these axes) to the data to realign the time series of brain to the reference. It is highly recommended to apply this method to small movements, that's why all that subjects that showed any translational or rotational movement above 3mm were excluded from this analysis (Jenkinson et al., 2002).

The 3D motion correction process applied in this study was the T*ri-linear sinc Interpolation*. Linear interpolation is used during motion detection, while sinc interpolation is used for the actual motion

correction step. Therefore, this method brings the highest possible quality to the corrected image. In this project all the subjects showed movements bellow a radius of 3 voxels.

Low-frequency drifts removal

Voxel time courses of fMRI data frequently have low-frequency drifts, which are believed to be produced by physiological noise as well as by physical (scanner-related) noise

These signal drifts cut significantly the power of statistical data analysis, besides they also nullify event-related averaging, which assumes stationary time courses.

Consequently, the removal linear trend is one important preprocessing step and should be always implemented.

Since the signal drifts are slowly rising and falling, these drifts are removed by using a high-pass filter.

The process used to perform this filtering was the *GLM with Fourier basis set*. The presence of low frequencies in a voxel's time course is estimated using GLM. The projected time course from a GLM based on the predictors (in this case sines and cosines for low frequencies) will then be subtracted from the original data resulting in a filtered time course. In this analysis 2 predictors were used, in other words 2 pairs of sines and cosines (Woolrich et al., 2001).

Temporal high-pass filtering cutoff

The high pass filter cutoff controls the longest temporal period allowed, this means the amount of filtering can be defined by the cutoff value, thus frequencies below that value are removed. This type of filtering is used to remove low frequency artifacts.

The method used in this study to implement this filter was *Frequency-space filter (FFT).* Applying a FFT the time course of a voxel is transformed into the frequency domain and the undesired low frequencies can be easily removed. Then the resulting data is transformed back in the time domain. In this experiment, the frequencies were cutoff above 0.0005 Hz.

Note that this type of filtering was only used for rest task (Senden, 2012).

5.4.1.2 Anatomical Images Preprocessing Steps

Intensity Inhomogeneity Correction (IIC)

Intensity inhomogeneities in MR images can diminish the exactitude of some imaging data analysis methods, like segmentation and co-registration. Modern scanner software has shown solutions for this; however high resolution scanning techniques amplified again the dimension of this problem: images reveal significant intensity inhomogeneities across space (Figure 5.2A).

The method of IIC used is based on a *surface fitting* methodology (Vovk et al., 2007): low-order polynomials are used for estimation of low frequency intensity variation through 3D image, also known as a bias field (Figure 5.2C); this field is then removed from the data producing a homogeneous intensity image (Figure 5.2B).

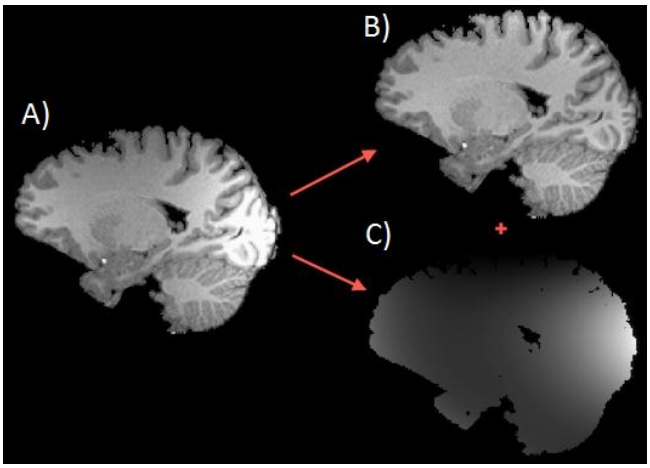

Figure 5.2- Intensity differences before and after IIC: anatomical image before IIC (A)**;** anatomical image after IIC (B); low frequency intensity fluctuations (C)

5.4.2 Co-registration

Functional images were aligned with anatomical volumes using the scanners positional information followed by manual fine alignment, and both were transformed to the Talairach coordinate system (Talairach and Tournoux, 1988). In order to overcome the different size of voxels between anatomical and functional images a tri-linear interpolation was applied turning the voxel's size to 0.5 mm^3.

Talairach Coordinate System

The Talairach coordinate system is a well-known tool used to rescale the brain structure into defined spatial coordinates, solving the problem of brain's size differences between subjects. The reference anatomical points are anterior and posterior commissures, as well as lateral, vertical and front-occipital edges.

5.4.3 Segmentation

For each subject, cortical surface representations were generated from the anatomical images, the procedure included gray and white matter segmentation.
This method allows the cortical tissue segmentation along the inner (WM) and outer (CSF) boundary. Different intensities values were defined for the inner and outer grey matter (GM) boundary. Applying Laplace's partial differential equation, a smooth transition of intensities between the distinct tissues is made, basically by keeping the values at the boundaries fixed and by smoothing the ones located in the GM (Lim and Pfefferbaum, 1989).

5.4.4 Statistical parametric maps

Three-dimensional statistical parametric maps[1] (SPM) (Figure 5.3) were calculated separately for each subject and for different runs using GLM with a linear predictor for each experimental stimulus conditions convolved with a standard hemodynamic response function (HRF) - onset of response and undershoot 5 s and 16 s, respectively, dispersion 1 s, response to undershot ratio 6. The false discovery rate (FDR) correction was used to correct for multiple comparisons (Benjamini and Hochberg, 1995).

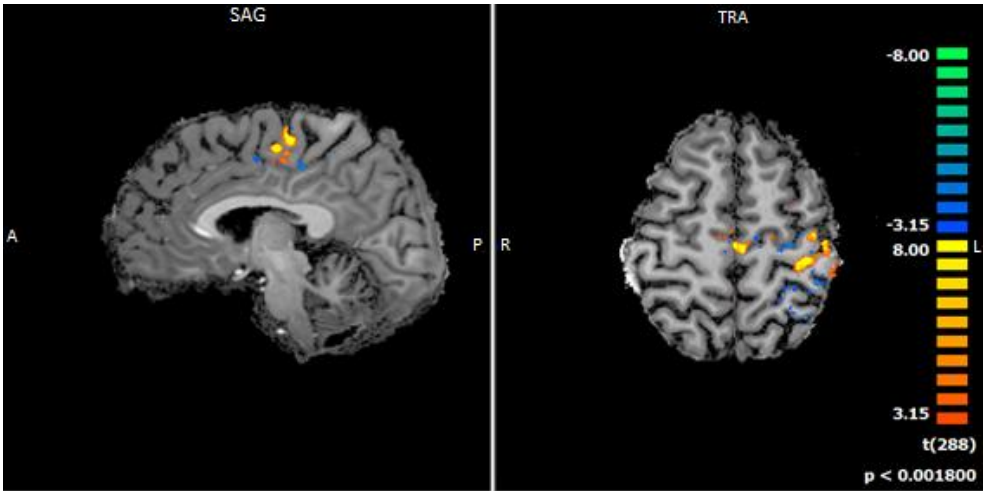

Figure 5.3– Three dimensional activity map (FDR corrected) of middle finger during motor task for lower resolution scan: in sagittal (SAG) and transversal (TRA) planes [Subject S13].

Multiple comparisons

The problem of searching the brain volume for significant activation is related with probability: by chance 5% of voxels are expected to have significant p-values, known as uncorrected p-values, and thus they must be corrected (Nichols and Holmes, 2002).

FDR

FDR is one of the available methods to correct for multiple comparisons. Operating simultaneously on all voxel wise test statistics to determine which tests should be considered statistically significant. This implicitly corresponds to a threshold selection that adjusts to the properties of the given data set(Genovese et al., 2002).

Regions of interest (ROI's)

Since the present study is related with the primary motor cortex- M1, the regions of interest are located inside this cortex; two types of ROI were select for each subject: the first associated with the thumb activity focus; the other one associated with the middle finger activity cluster (Figure 5.4).

1 – For each finger's task (motor, imagery and visual), two types of activity maps were created, differing in the baseline used: direct paradigm - finger vs rest; differential paradigm - finger vs the other fingers.

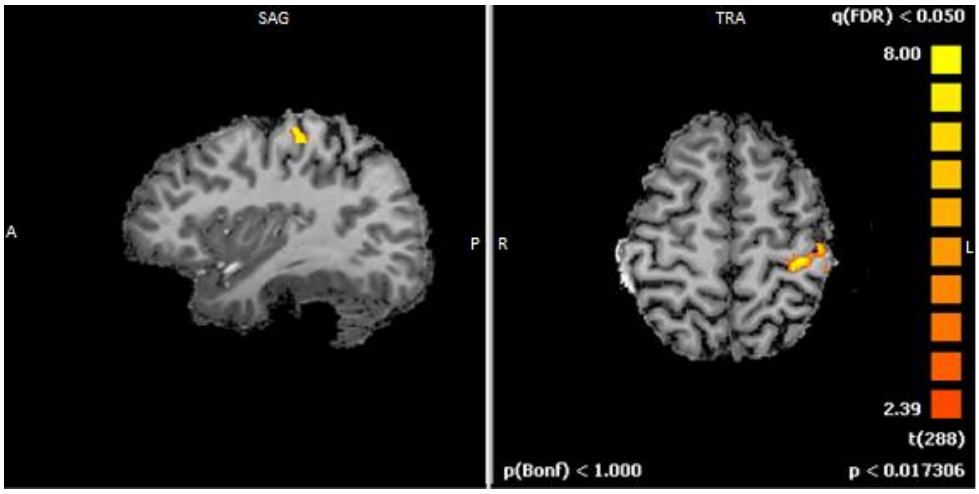

Figure 5.4 – ROI selected from the three dimensional activity map presented in Figure 5.3: in sagittal (SAG) and transversal (TRA) planes [Subject S13].

5.4.5 Cortical grid sampling

Using a novel cortical depth sampling approach, cortical grids were created in volume space for each subject, making possible to map the functional activity for different cortical laminas, in this case different relative depths of the cortical thickness.

To construct a grid at a certain relative depth, step-sizes were performed orthogonal to the cortical thickness of GM in two orthogonal directions resulting in regularly spaced grid sample points at any initialized relative depth value (Zimmermann et al., 2011a).

If, for example, the initialized depth value is 0.5, one grid axis will trace a curved line along the middle of GM; at regular intervals through this first line, other orthogonal lines will be started in orthogonal direction providing regularly spaced grid points along the second axis at the same relative depth level (Zimmermann et al., 2011a). This process is executed for each chosen relative depth level.
The position of the cross within the anatomical sets the start point of the grid sampling; logically, this start point needs to be located in GM, if not the grid sampling process will be cancelled. Note that, in the end the center of the grid will correspond to the starting point.

To sample the co-registered functional activity maps, high resolution cortical grids were created at three depth planes covering specific areas in M1; in order to obtain smooth curvature boundaries, three dimensional up-sampling with 2 data points per actual voxel was used.

The placement of the grids was defined by the motor activity maps resultant from the lower resolution scan (Figure 5.5A). Two cortical grids were made for each subject: the first one was centered in the voxels highly related with the thumb activity (FG1); the second grid was placed in the center of the middle finger activity (FG3).

Figure 5.5B shows the flattened results of the high resolution cortical grid sampling of middle finger activity for subject S2 at three relative cortical depth levels (0.25, 0.5 and 0.75 percent of 1.5 mm mean cortical thickness) with an area of 85.94 mm^2 (13.75 mm right-left 6.25 mm inferior-superior).

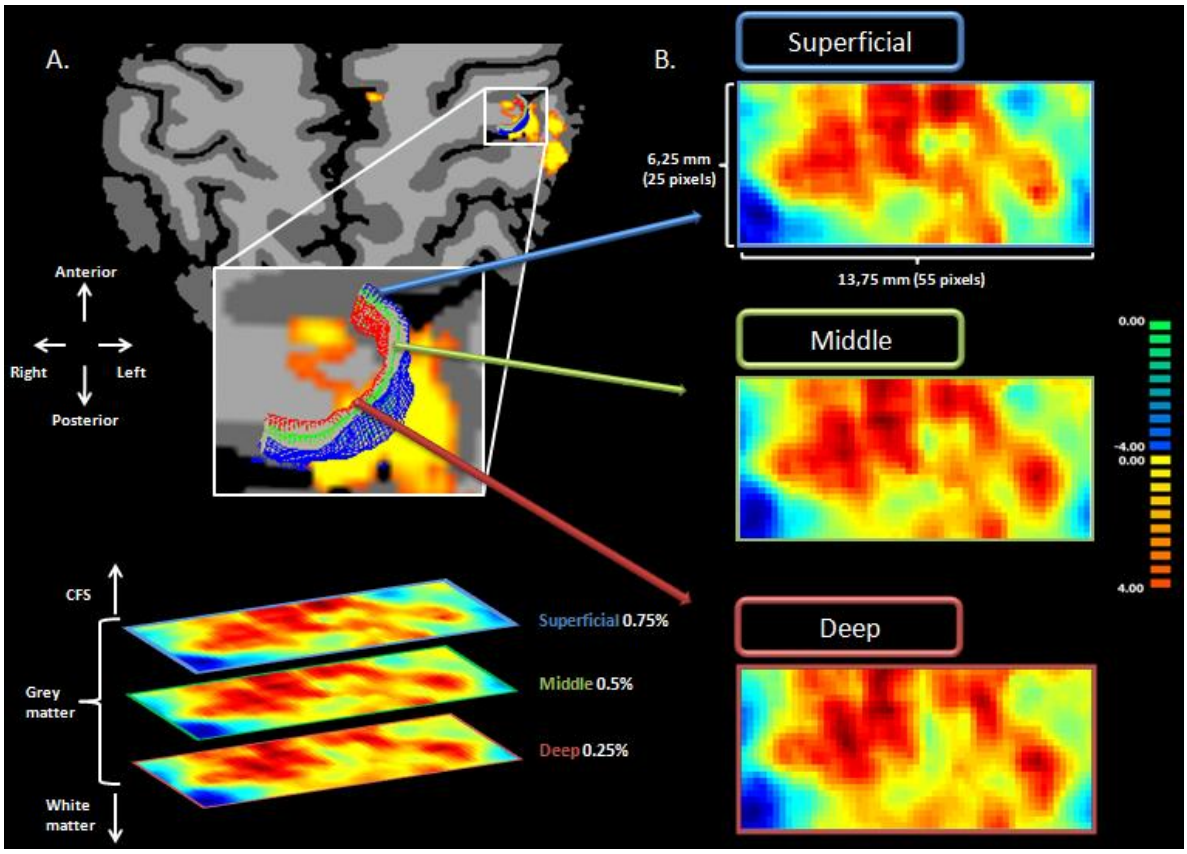

Figure 5.5 – Illustration representing the cortical mapping approach exemplary in subject S2: SPM of motor activity (lower resolution) is projected onto the cortical reconstruction. High resolution cortical grid sampling performed -zoomed in view with overlaid streamlines at three relative cortical depths (0.25, 0.5 and 0.75%) (A); Results of the high resolution cortical grid sampling for the motor activity of middle finger from the higher resolution run in the three sampled layers (Superficial, Middle and Deep) (B)

In each cortical grid is possible to plot any statistical map created. For instance, in FG1 the activity pattern for all the three fingers: thumb, index and middle fingers, during different tasks (imagery, motor or visual), can be mapped. In this study for each cortical grid FG1 and FG3, all activity maps were plotted, including the differential and direct paradigms for imagery, motor and visual tasks.

Due to the three dimensional up-sampling used in this process, one pixel of these cortical maps have 0.25 mm^2.

5.4.6 Veins

In order to not suffer from contribution of superficial blood vessels, veins detection and treatment methods were used.

Veins detection

Using the functional images from the high resolution run a visual inspection was performed to detect any vessels involved in the cortical grid sampling area. The fMRI images are analyzed along the central sulcus ROI in order to determine which ones represent a vein (if a black dot is only present in one slice, it is not counted as a vein, however if a black dot appears in the same location in the adjacent slices, one vein has been found (Figure 5.6).

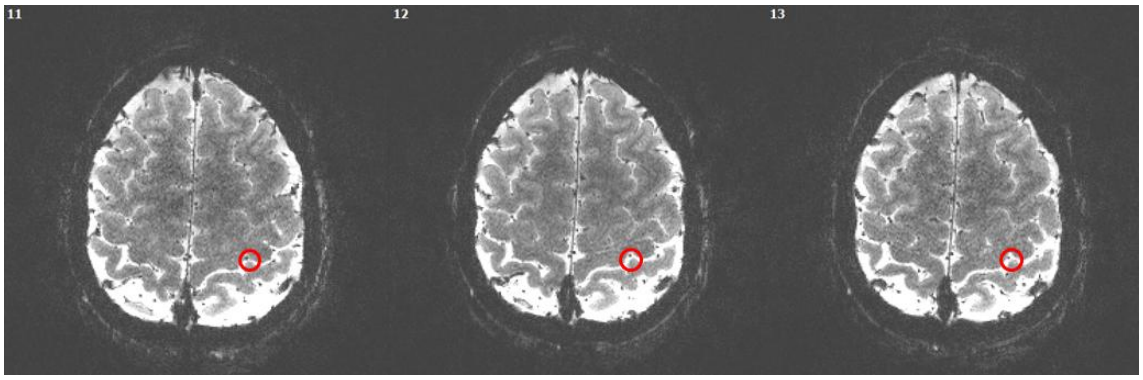

Figure 5.6 - Veins detection: three functional slices from motor high resolution run of S12 are shown (11, 12 and 13); inside the red circle there is a black dot, which is clearly one vein.

Veins treatment

When veins involvement was found in the ROI, the time course signal of the vessels was saved.
The criteria used to determine a single pixel contamination was the correlation level between the pixel's and vein's signal. Thus, a threshold of 0.3 was applied for the correlation level, which means that all the pixels that show a vein correlation level above 0.3 were removed.

From the 13 subjects, 6 suffered from vessels contamination, 3 of them in both grids (FG1 and FG3). The number of pixels correlated with vessels signal was always smaller than 30% of all the grid's pixels.

5.4.7 Types of data and measures

For each pixel of cortical grids there are two types of data: the time course signal (Figure 5.7A) and the activity level (Figure 5.7B), in form of t-value. Both categories are layer specific: for different layers specific t-values and signals. Note that for the fMRI data of resting state (RS-fMRI) there isn't any activity info.

Therefore, the measures performed are split according with the data category and based in single subject analysis approach.

Activity level related measures

To analyze the activity maps of the data, two main kinds of measures were used: active pixels and correlations (Lee Rodgers and Nicewander, 1988).

One pixel was considered active if the correspondent t-value was above 3 (FDR correction threshold).

For each subject's grids (FG1 and FG3) the number of active pixels was measured. Different kinds of active pixels were then defined: shared and specific pixels. Shared active pixels are the ones activated by more than one finger; specific active pixels are only active in one finger activity map.

Using the activity maps, diverse correlations measurements were executed, they are divided into: within and between tasks.

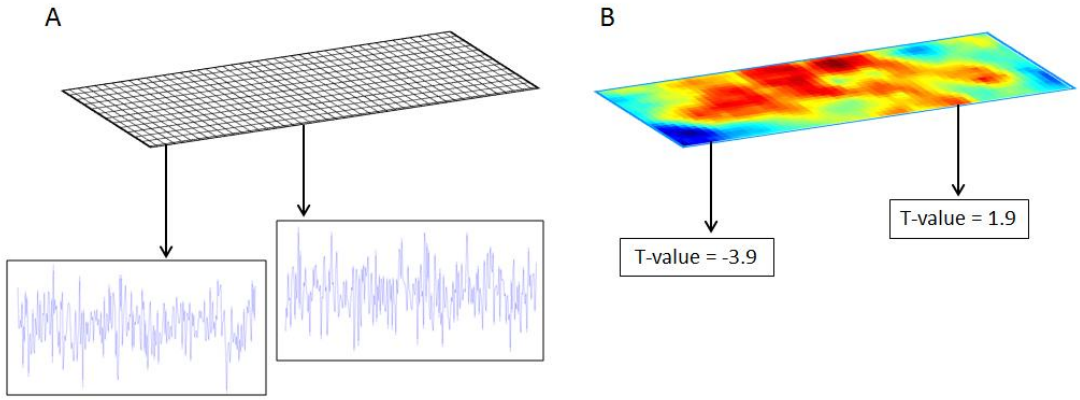

Figure 5.7 – Cortical grid's info: time course signal (A); activity map (B)

Within task correlations were performed between different finger maps and between different depths, for all the possible combinations.

In the same pattern as within task correlations, between tasks correlations were executed to evaluate the relation of motor, imagery and observation tasks in fingers and depths level.

Time course signal related measures

To analyze the time course signal, three main kinds of measures were used: mean time course per layer, event related averaging and correlations.

The mean time course per layer was used to study correlations between different layers and also to perform the event related averaging (Buckner, 1998), in other words the percent signal change also known as BOLD response.

According with the paradigm, finger specific time courses were determined. Considering the delay of BOLD response, the signal was only set as finger specific 5s after the first stimulus. Thus, during the next 35s, after the delay, the signal was acquired (Figure 5.8). After eight times the finger specific time course (FSTC) is created.

The percent signal change is given by:

$$\%\ Signal\ Change\ (i) = \frac{FSTC(i) - \overline{baseline}}{\overline{baseline}} \times 100$$

Where:
i is a time data point;
$\overline{baseline}$ is the average baseline (all the first values of each pre stimulus period - green circles in Figure 5.8 - over the whole time course are averaged).

Therefore, the mean BOLD signal was determined for each finger specific time course layers. The peak of the percent signal change was calculated and correlations were performed between BOLD's signal layers.

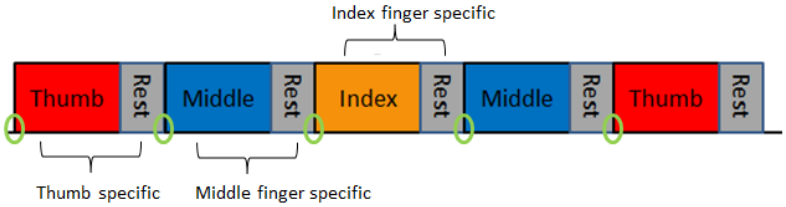

Figure 5.8- Illustration of finger specific time courses selection according with the paradigm and baseline data points (green)

Since one pixel corresponds to half a voxel, time course correlations were performed between blocks of four pixels in three dimensions - x, y and z (Figure 5.9) – to avoid inflating the correlation due to the up-sampling data.

Using MATLAB software (v.8.0, The MathWorks Inc., Natick, MA, 2000), all these measures were performed for each subject's grids (FG1 and FG3). In order to simplify the data analysis, an automatized procedure was created to determine all these measures for all the subjects. In the end, each kind of measure has a correspondent matrix with the entire subject's results.

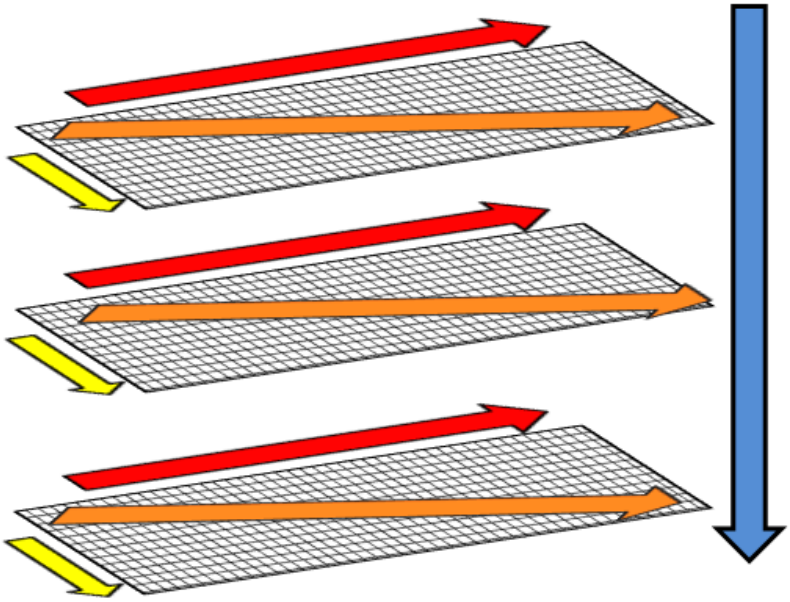

Figure 5.9 – Scheme of the dimensions used for time course correlation: red arrow corresponds to the x dimension; yellow represents the y dimension; orange arrow symbolizes the xy dimension; the blue arrow corresponds to the z dimension.

5.4.8 Statistical Analysis

Statistical analysis is a form of showing the veracity or falsity of the assumptions made about the data.
The performed measures were analyzed with STATISTICA software (v.10, StatSoft Inc., Tulsa, OK, USA), allowing to acquire essential information for the results analysis and discussion.

The statistical test used was repeated measures Analysis of Variance (Huck and McLean, 1975). This method is used when all members of a random sample are measured under a number of different conditions, therefore is ideal for this study.

Analysis of Variance (ANOVA) is a statistical method used to test differences between two or more means by analyzing their variance.

Repeated measures ANOVA is the equivalent of ANOVA independent group's analysis, but for related groups. This indicates that the same subjects are tested more than once, because they are present in more than one group, thus each subject has been measured on all occasions on the same dependent variable. This particular test requires one independent variable (in this case: subjects) and one dependent variable.

For the statistic tests, the confidence interval is 95%, which means that with 95% of certainty the real value of the factor is inside the estimated interval. The confidence interval is associated with a significance level (p-value). For example, a confidence interval of 95% corresponds to a significance level of 5% (p-value: 0.05).

Once a confidence interval is defined, the tests that show a p-value above or below the significance level, in this case 0.05, are considered statistically insignificant and significant, respectively.

Inside the statistically significant, there are very significant ($p\text{-value}<0.01$) and extremely significant ($p\text{-value}<0.001$) considerations.

In order to apply ANOVA statistics correlation measures were corrected with fisher z correction (Hotelling, 1953).

6 Results

In this chapter the results are reported according to the different themes of this project: somatotopy, depth structures, imagery in M1, visual activity in M1 and task related differences.

6.1 Somatotopy

In this subchapter we will address the question of the somatotopic organization for single fingers within M1 and for different cortical depths. While an ordered somatotopic organization has been suggested for single fingers, both human and primate data have challenged this view advocating a distributed representation of limbs along M1. Here we addressed this question by examining: 1. The number of activated pixels and the peak of the BOLD response for each finger in each grid. 2. The functional representation of single fingers between different cortical depths. 3. The spatial relationship between different finger presentations using grid correlations.
We hypothesized that 1. The organization for single fingers within M1 is based in distributed pattern (intermingled with somatotopic "hot spots"): different finger grids (FG1 and FG3) would show finger specificity (somatotopic "hot spots"), but also each finger grid area would be responsive to other fingers as well. 2. This organization pattern varies with the cortical layers being more distributed in the superficial layers and more specific in the deeper layers. 3. All the fingers show a strong relation due to the hypothesized distributed like pattern, although considering the somatotopic feature of our theory, we also expect that neighbour fingers are more related than distant fingers.

6.1.1 Grids Specificity

A grid is defined as finger specific if it shows a larger response to movements of one finger, this response can be measured by the number of active pixels and also by the peak of signal percent change (BOLD response).

In order to be certain about the grids specificity, their placement is dependent on the lower resolution activity and the sampled maps correspond to the high resolution run. We predicted that grids would show specificity for the finger upon which they were placed in the lower resolution scan (e.g. a grid placed in the thumb representation would be more thumb specific). However, following previous work in humans (Indovina and Sanes, 2001; Sanes et al., 1995; Schieber, 1999, 2001) and monkeys (Kwan et al., 1978; Schieber and Hibbard, 1993) we hypothesize that, besides the grid specificity, each grid will also contain response evidences from other fingers.

Even though grids were placed according with the lower resolution activity map, when the higher resolution activity map is plotted a relation between the activity pattern of different fingers and the finger used in grid's placement is evident. From all the finger activity maps plotted in one finger grid, the finger that shows a big activity patch in all the layers is the one used in the grid's placement.

The thumb grid (FG1) specificity is visible in the two paradigms: differential (in this case the baseline corresponds to the other fingers, which means that the t-value measure is related with the activity of one finger versus the other fingers) (Figure 6.1) and direct (for this paradigm the baseline corresponds to the resting state) (Figure 6.2). In both paradigms, there is a high selectivity of the FG1 to thumb movements and the existence of intermingled patches responsive to other fingers. Logically, the selectivity is more evident in the differential activity maps; on the other hand the intermingled

patches responsive to other fingers are more noticeable in the direct paradigm. This suggests that the fingers activity distribution in M1 for the motor execution follows a somatotopic distributed pattern, in the sense that there are finger specific regions (grids) that also include smaller regions to encode other fingers as well.

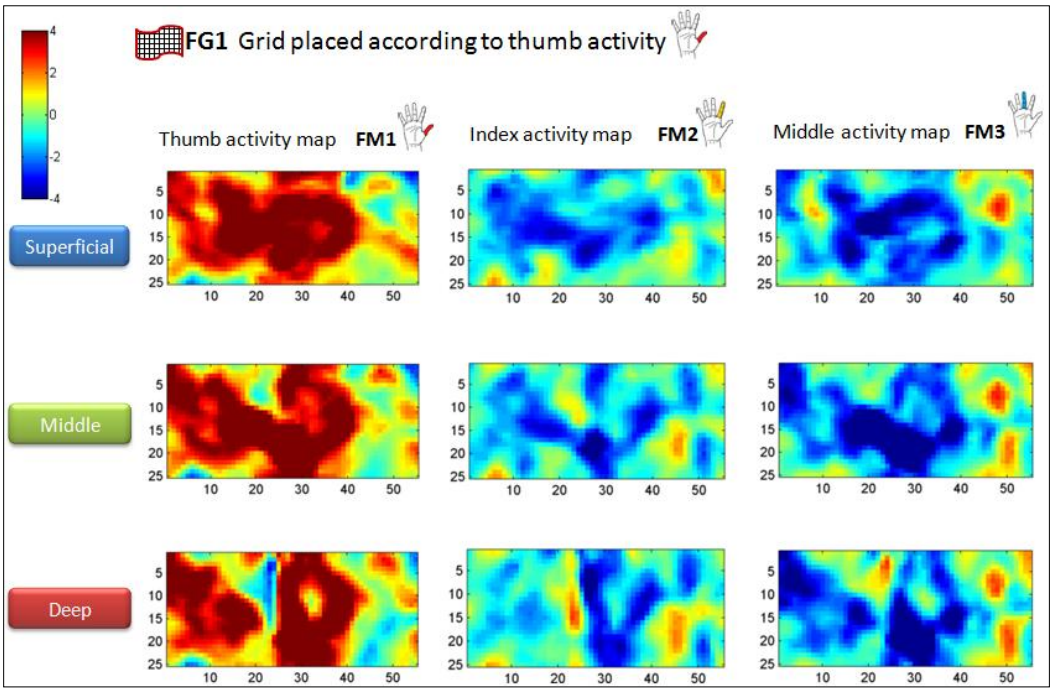

Figure 6.1– Differential activity maps of thumb finger grid in single subject [S9]. The maps above show the t-values for different fingers activity maps – thumb (left column); index finger (middle column) and middle finger (right column). Rows show activity in different layers of the cortical sheet (top-superficial to bottom-deep). Note the high selectivity of FG1 to thumb activity and also that the activity is stronger in the superficial layers compared with the deeper ones.

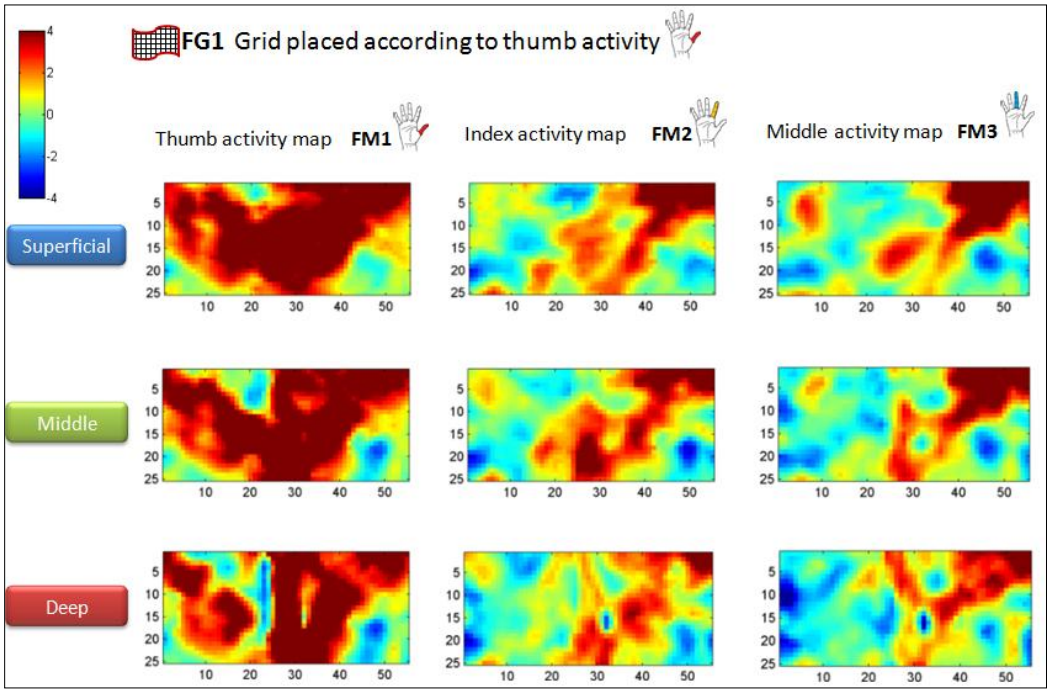

Figure 6.2 – Direct activity maps of thumb finger grid in single subject [S9]. The maps above show the t-values for different fingers activity maps – thumb (left column); index finger (middle column) and middle finger (right column). Rows show activity in different layers of the cortical sheet (top-superficial to bottom-deep). Note the high selectivity of FG1 to thumb activity and the intermingled patches responsive to other fingers, also for all fingers the activity is stronger in the superficial layers compared with the deeper ones.

Below, this relation between the activity pattern of different fingers and the finger used in grid's placement will be analyzed in terms of number of active pixels (t-value > 3) and peak of average BOLD responses. The annex contains other finger activity maps examples for both grids from the direct paradigms for motor execution.

Active pixels

To analyze the number of active pixels of the direct paradigm we used a repeated measure ANOVA with three factors: finger grid (FG1 and FG3), finger map (thumb and middle) and depth (superficial, middle and deep).

The results of the ANOVA test indicated that, for both grids (FG1 and FG3), the number of active pixels is significantly different between matching and un-matching grid/activity maps [$F(1,12)=20.2$; $P < 0.0001$] (in this case an activity map is considered to match when it is plotted in the respective finger grid, for instance if thumb activity map – FM1 is sampled in FG1 exists a match between the grid placement and the activity map; which means that, following the example, the plotting of the middle activity map – FM3 in the same grid represents the un-match). The post-hoc comparisons demonstrated that the matching grid/activity maps has a bigger number of active pixels (M=243; SD= 119) compared with the un-matching (M=35; SD=23) in FG1 ($P < 0.01$), however this effect wasn't significant for the other finger grid – FG3. This interaction is represented in Figure 6.3.

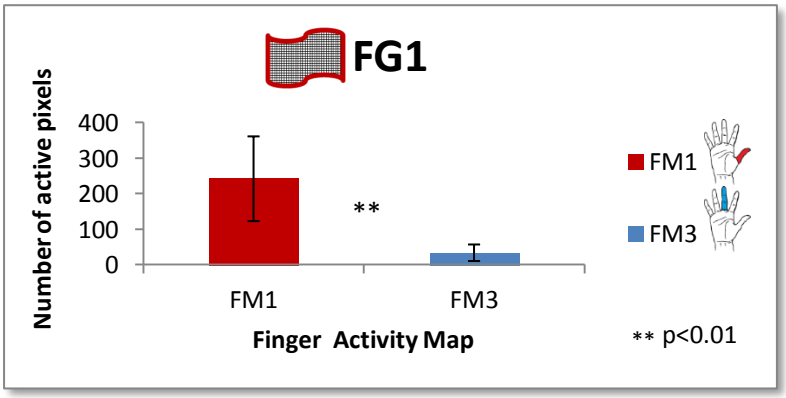

Figure 6.3 – Number of active pixels averages for different finger maps (FM1 and FM3) in FG1.

This supports the somatotopic pattern for finger activity, in the sense that different grids show a stronger response for a specific finger, thus grids are finger specific. Besides this somatotopic idea, this result proposes that the thumb is a more independent finger than the middle, in the sense that his region is even more specific.

Percent signal change – BOLD response

To analyze the peak of BOLD response we employed a repeated measure ANOVA with three factors: finger grid (FG1 and FG3), finger map (thumb and middle) and depth (superficial, middle and deep).

The results of the ANOVA test indicated that, for both grids (FG1 and FG3) the peak of BOLD response was significantly different between matching and un-matching grid/activity maps [$F(1,12)=7.6$; $P < 0.05$]: the match between grid and activity map has a higher peak compared with the un-match in FG1 ($P < 0.08$) and in FG3 ($P < 0.08$ This effect is shown in Figure 6.4. In FG1 the matching grid/activity maps has a higher peak of BOLD response (M=6.38; SD=3.18) compared with

the un-matching (M=3.30; SD=1.66). The same happens in FG3, where the match case shows a higher maximum of percent signal change (M=6.80; SD=4.06) than the un-match (M=3.85; SD=2.36). This relation is illustrated in Figure 6.5 and Figure 6.6.

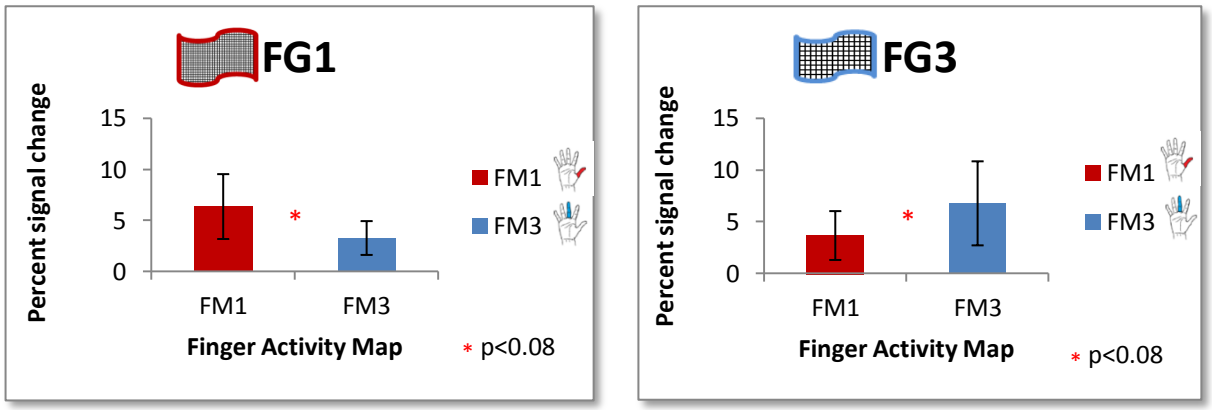

Figure 6.4 - Percent signal change peak averages for different finger maps (FM1 and FM3) in both finger grids (FG1 - left and FG3 - right)

This suggests that the fingers activity distribution in M1 for the motor execution follows a somatotopic pattern, in the sense that different regions (grids) show a bigger response for a specific finger.

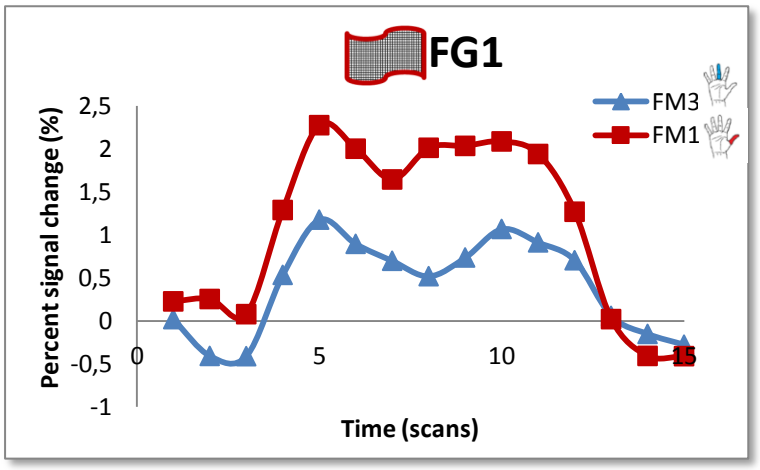

Figure 6.5 – Average BOLD response of all subjects for two finger maps (thumb - FM1 and middle - FM3) in FG1. Note that the percent signal change is much higher for the matching finger, in this case the thumb finger.

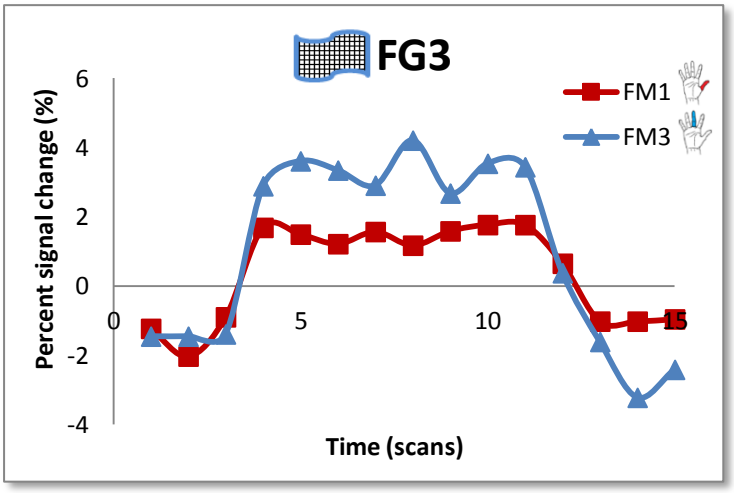

Figure 6.6 – Average BOLD response of all subjects for two finger maps (thumb - FM1 and middle - FM3) in FG3. Note that the percent signal change is much higher for the matching finger, in this case the middle finger.

Overall, the results indicated that 1. Grids showed some finger specificity, representing the expected somatotopic hot spots. 2. Despite this particular characteristic regarding the grids specificity, the results also point to the involvement of non-specific fingers in the grids. Thus, the results match our predictions of a somatotopic distributed pattern for fingers activity.

6.1.2 Somatotopy between layers

In this subchapter we will describe the results for the functional representation of single fingers between different cortical depths (superficial, middle and deep).
As presented above we used two types of data (number of active pixels and peak of BOLD signal) to analyse the of activity pattern organization in different layers.
According to our hypothesis, their organization is based in a mixture of somatotopy and distributed organizations, also we predict that this pattern varies with the cortical layers, being more distributed in the superficial layers and more specific in the deeper layers.

Active pixels

In order to understand what is encoded by each finger grids (FG1 and FG3), pixels of the direct activity maps were distributed by the different cortical layers in two main families – active ($t \geq 3$) and non active ($t < 3$). The active pixels were sub-divided into shared (activated by more than one finger) and specific (only activated by one finger) pixels.

The pixel distribution analysis was performed for each subject separately and then averaged across individuals of different layers for each grid to generate a distribution chart for each grid's layers (Figure 6.7).

Interestingly, the majority of the pixels within the grid (75,5% on average), more than two thirds, were not activated and from the charts analysis, the percentage of the non-activated pixels seams to increase with depth.

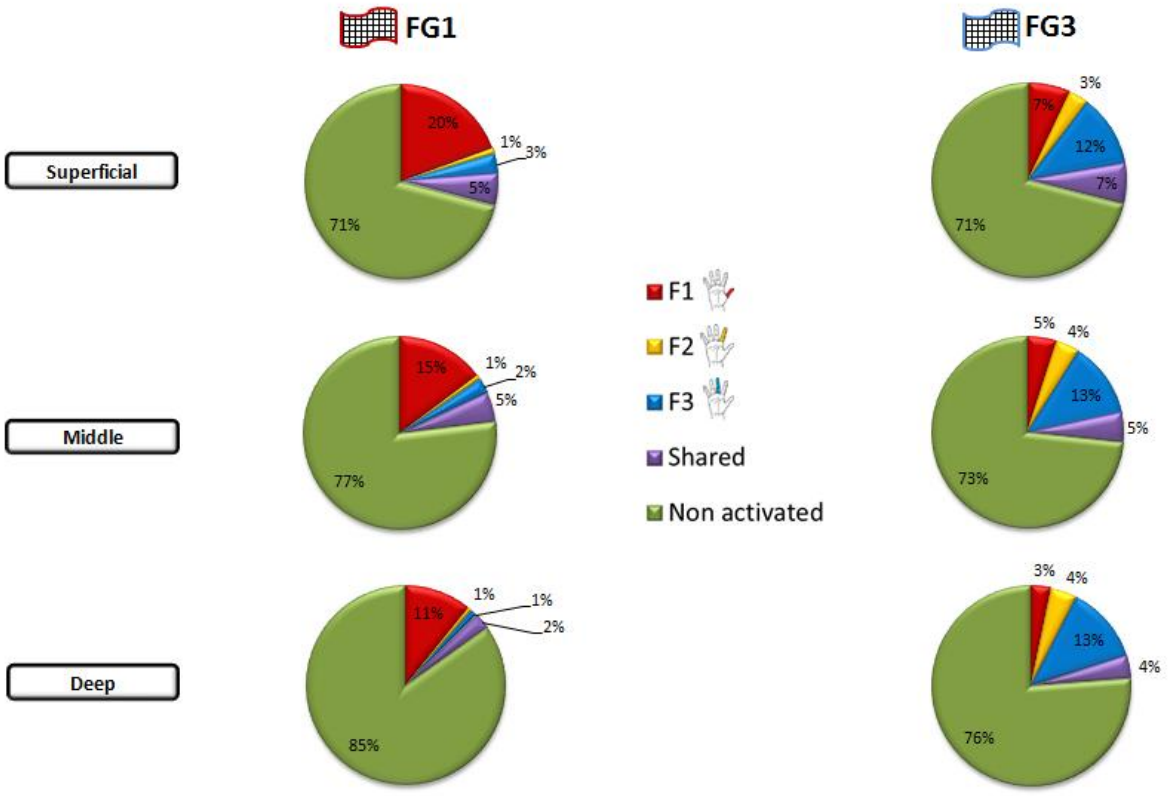

Figure 6.7 – Distribution of the pixels for the ME: average of all subjects. The rows indicate the cortical layer (top-superficial to bottom-deep) and the columns the finger grid (FG1 in the left and FG3 in the right). Note the massive portion of non-activated pixels and how it increases in depth.

To go further in the analysis of the number of active pixels we used a repeated measure ANOVA with three factors: finger grid (FG1 and FG3), finger map (thumb and middle) and depth (superficial, middle and deep).

The results of the ANOVA test indicated that the number of active pixels is significantly different in diverse layers [$F(2,24)=9.9$; $P < 0.001$]. In addition, these layer specific differences were found separately in the each finger grid and as a main effect, the last one is presented in Figure 6.8. The post-hoc comparisons showed that the superficial layer has a larger number of active pixels of (M=183; SD=) compared with the middle (M=150; SD=) ($P < 0.05$) and deeper (M=116; SD=) ($P < 0.001$) layers; subsequently, the middle layer has more active pixels than deeper layer ($P < 0.05$). This effect is noticeable in Figure 6.9. Suggesting that the deeper layers may have a more focal encoding of the movement than the superficial layers. Also, for all the cortical layers the number of non-active pixels of the higher resolution maps is considerably larger than what we were expecting. This suggests that using high resolution imaging, the region that we activated for finger movement using the lower resolution imaging may actually have different response properties, not directly encoding this type of finger movements.

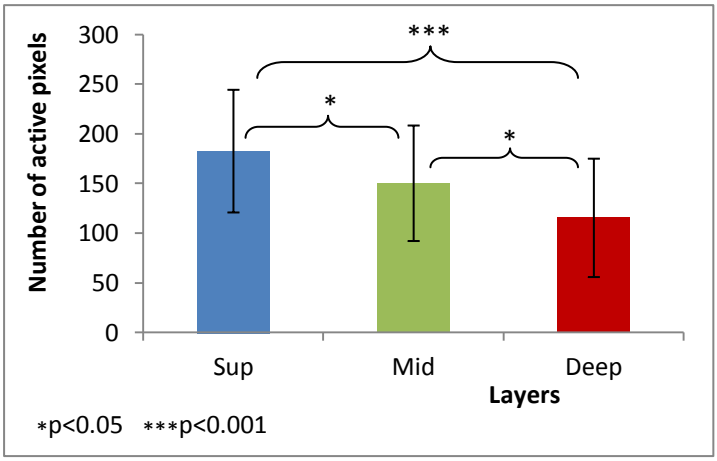

Figure 6.8 – Number of active pixels average in the three cortical layers (superficial, middle and deep). Note the sequential decrease of the number of active pixels with the depth increase.

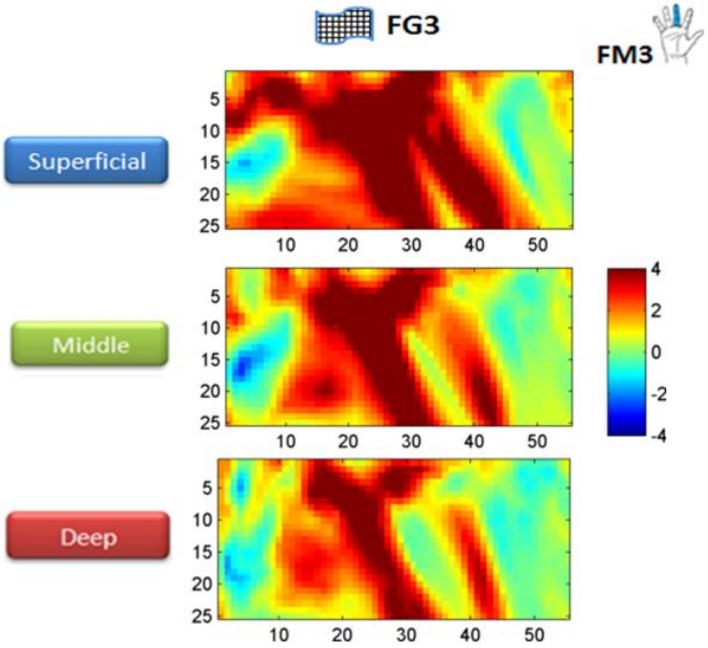

Figure 6.9 –Illustrative example of the number of active pixels decrease with depth in FM3 of FG3 of the direct paradigm for a single subject [S6]

In the active pixel's distribution (Figure 6.10), it is clear the predominance of finger specific pixels related with the placement of the grid (for instance in FG1 superficial layer 67% of the active pixels are specifically activated for the thumb – F1). From the figure analysis, it is clear that despite the grid specificity, all the types of pixels are activated in one grid: shared, matching and un-matching finger specific pixels.

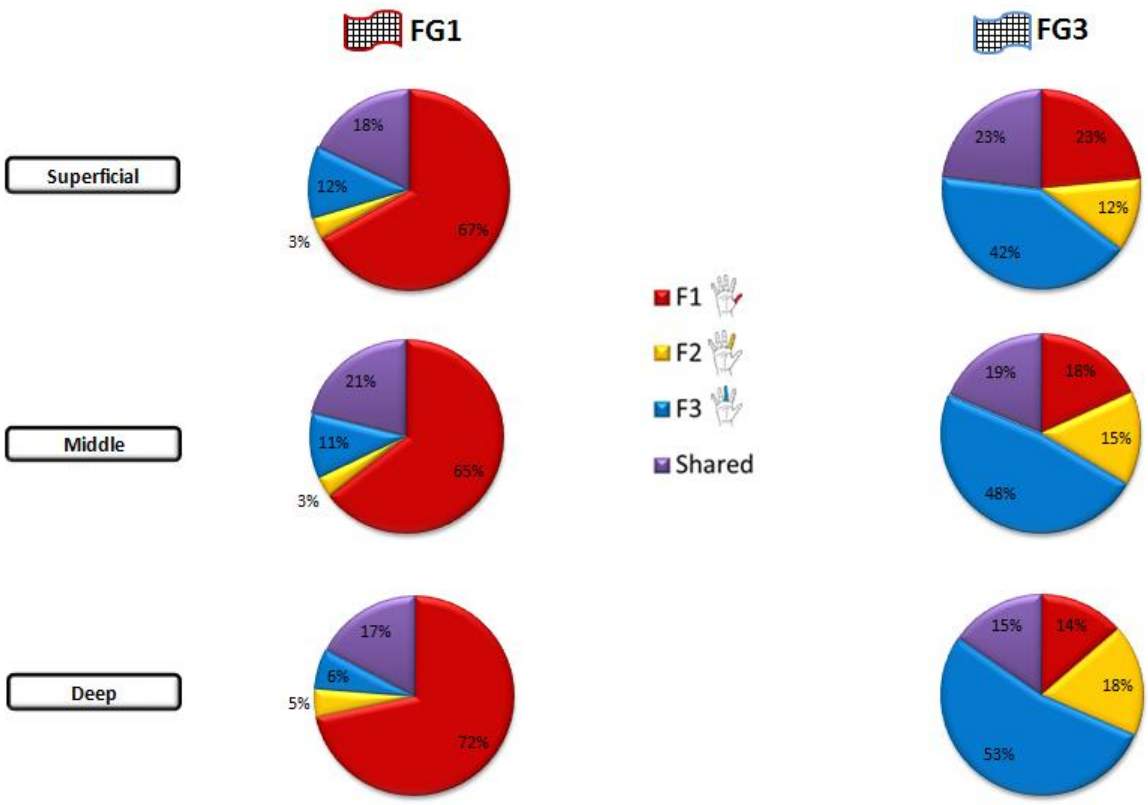

Figure 6.10 - Distribution of the active pixels for the ME: average of all subjects. The rows indicate the cortical layer (top-superficial to bottom-deep) and the columns the finger grid (FG1 in the left and FG3 in the right). Note the increase of the matching specific finger with depth and the decreased percentage of the shared pixels in the deeper layers.

This shows that while the grids are clearly dominated by the finger activity which they were selected (suggesting a somatotopic hotspot) representation of other fingers is clearly present in the high resolution images. Furthermore, this distribution proposes that the thumb is a more independent finger than the middle, in the sense that his grid is even more specific.

Peak of percent signal change – BOLD response

With the intention to improve the understanding of the different finger regions – grids, a percent signal change analysis was performed for each subject separately, culminating in the generation of an average BOLD response for each layer and each finger per grid.
The different fingers BOLD responses were then averaged across individuals of different layers for each grid to create a general BOLD response for each layer of both grids; examples are illustrated in Figure 6.11 and Figure 6.12.

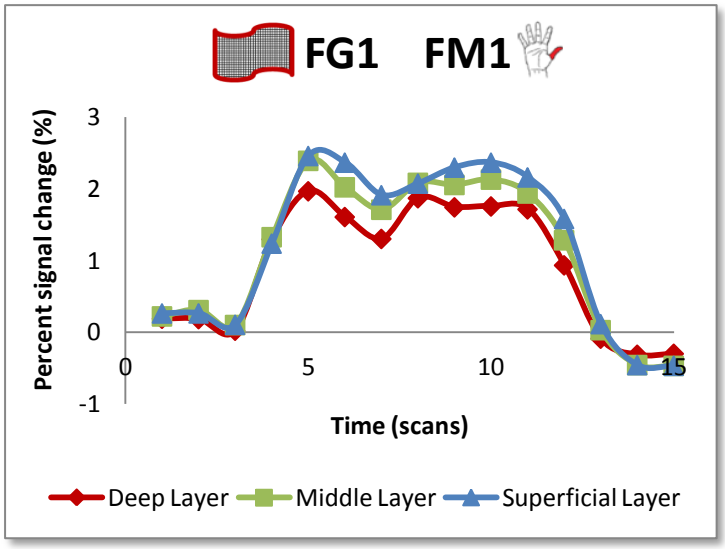

Figure 6.11 –Average BOLD response of all subjects of thumb in FG1 for the three cortical layers (superficial, middle and deep). Note the sequential difference of the BOLD response between the three depths.

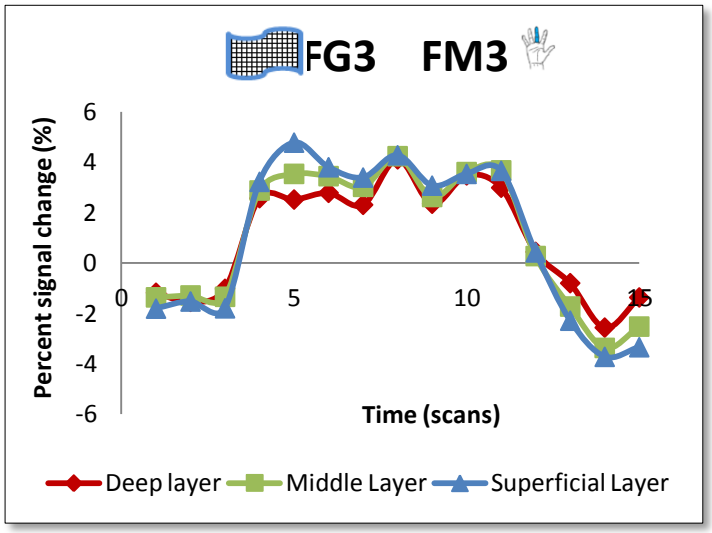

Figure 6.12 –Average BOLD response of all subjects of middle finger in FG3 for the three cortical layers (superficial, middle and deep). Note that the peak percent signal change is higher for the superficial layers, than for the deeper layers.

To analyze the peak of BOLD response data from the different subjects we used a repeated measure ANOVA with three factors: finger grid (FG1 and FG3), finger map (thumb and middle) and depth (superficial, middle and deep).

The ANOVA results test revealed a significant difference for the peak of BOLD response in different layers was demonstrated [$F(2,24)=6.99$; $P < 0.01$] (Figure 6.13): the superficial and middle layers have higher peaks of percent signal change (M=5.7%; SD=3.47% and M=5.2%; SD=3.13% respectively) than the deeper layer ($P < 0.01$ and $P < 0.05$ respectively), which has 4.2% of percent signal change (M=4.2%; SD=2.57%). Suggesting that deeper layers are less stimulated and consequently less responsive compared with the superficial ones.

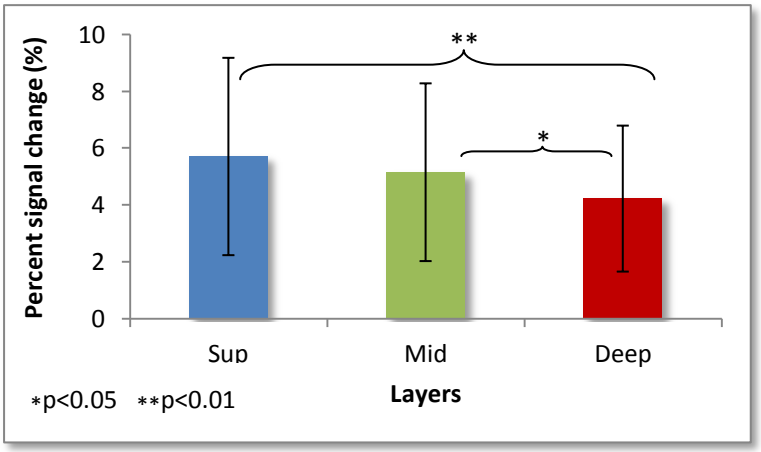

Figure 6.13 – Peak of BOLD response average for the three different layers (superficial, middle and deep). Note the sequential decrease of the peak of BOLD response with depth.

In summary, the results demonstrate that 1. The grid area stimulated by the lower resolution imaging in fact includes a large number of non-activated pixels. 2. There is a cortical difference in terms of layers response - superficial layers are more responsive than the deeper ones. 3. Despite the grid specificity, all types of pixels are activated in one grid: shared, matching and un-matching finger specific pixels. Therefore, the results match our predictions of a difference regarding the functional representations for fingers activity; however no distinction was found in the organization pattern of the three cortical layers, which is contrary to what we hypothesized.

6.1.3 Correlation between finger activity maps

Along this subchapter we will describe the results for the spatial relationship between different finger presentations. In order to attain different tests for the fingers activity organization in M1, the correlation between different fingers activity maps of the direct paradigm was performed.
Considering our hypothesis of a somatotopic distributed organization model for fingers, we predict that all fingers are correlated in terms of activity maps; furthermore sequential fingers activity maps should be more correlated, not only because of a somatotopic model, but also due to an increased similarity between the distributed patterns of finger specific regions.

To examine the different correlation indexes we used a repeated measure ANOVA with three factors: finger grid (FG1 and FG3), finger map pair (thumb/index, index/middle and middle/thumb) and depth (superficial, middle and deep).

The ANOVA results test demonstrated a significant interaction between adjacent and non-adjacent fingers [$F(2,24)=18.2$; $P < 0.0001$]: in the sense that adjacent fingers are strongly correlated than the non-adjacent. The thumb and index finger show a higher correlation (M=0.49; SD=0.1) than the thumb and the middle finger (M=0.24; SD=0.12) ($P < 0.0001$); the same happens with the remaining pair of adjacent fingers activity maps – index and middle fingers – that have a correlation index of M=0.50; SD=0.12 (Figure 6.14) ($P < 0.0001$). This suggests that there is a distributed pattern of fingers activity, because all finger maps are positively correlated. In addition, there is a difference between adjacent and non-adjacent fingers correlations, in the sense that adjacent fingers are strongly

correlated than the non-adjacent, pointing to the somatotopic feature of activity organization. Overall, this result sustains our predictions.

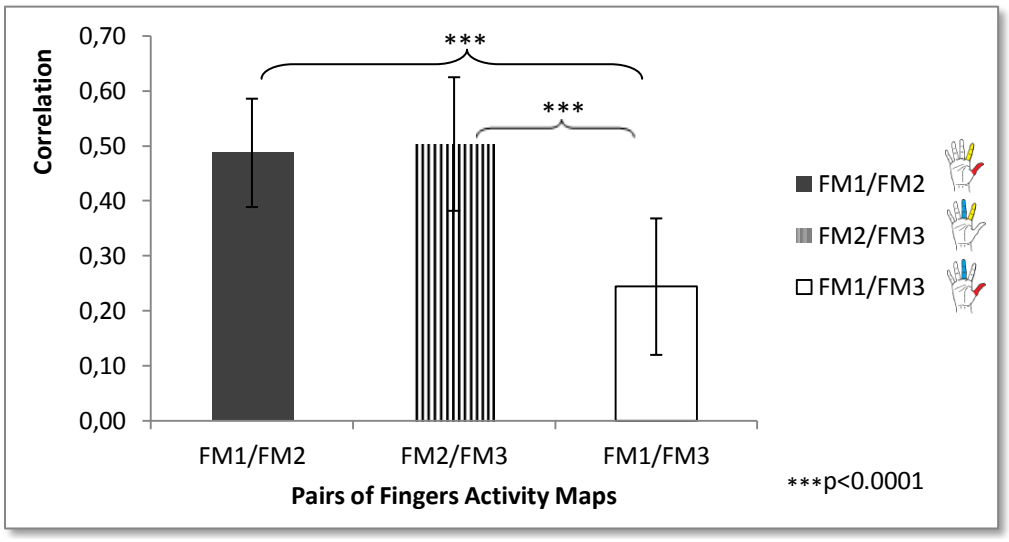

Figure 6.14 – Correlation indexes averages between the different finger maps of activity. Note that all the fingers are correlated and there is a difference of the correlation level between sequential (adjacent) and non-sequential fingers.

Moreover, the correlation index between adjacent fingers activity maps differed between matching and un-matching states of adjacent fingers pair with the finger grid [$F(2,24)=6.1$; $P < 0.01$] (in this case a grid and a pair of adjacent fingers activity maps are considered to match when one of the fingers that belongs to the pair correspond to the finger used for the grid placement, for instance the pair of fingers thumb and index - FM1/FM2 - shows a matching and un-matching situations respectively with the FG1 and FG3). The post-hoc comparisons demonstrated that the matching states between the finger grid and the pairs of adjacent fingers have smaller correlation indexes compared with the un-matching ones. In FG1 ($P < 0.01$), the match state has an index correlation of M=0.41; SD=0.08, whereas the un-matched state shows M=0.52; SD=0.09 of correlation (Figure 6.15). However, this effect did not reach the significance in FG3 ($P < 0.08$). This suggests that, despite all sequential fingers are strongly connected in one specific region – the grid; the matching finger of this specific region is more independent of the other fingers, pointing to the grid specificity.

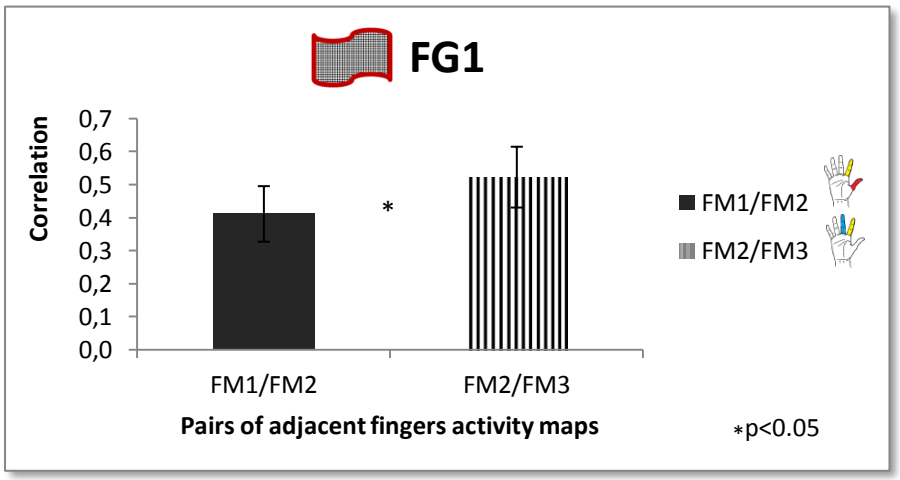

Figure 6.15 – Correlation indexes average between adjacent finger activity maps in FG1. Note that the matching map finger (in this case FM1) is less correlated with the adjacent finger map (FM2) than the un-matching finger map (FM3).

Briefly, the results express that 1. All fingers have a strong connection, supporting the expected distributed pattern of organization. 2. The relation between fingers is dependent of their spatial distance: adjacent fingers are strongly correlated than the non-adjacent, sustaining the idea of finger somatotopic hot spots.

6.2 Depth Structures

In this subchapter we will address the question of the columnar structures within M1. While this kind of structures has already been shown in the monkeys M1 (Amirikian and Georgopoulos, 2003), there is no evidence of their existence in the human M1. Here we addressed this question by examining: 1. The spatial relationship between different layer presentations using grid correlations for different measures. 2. The connectivity of the pixels regarding their directionality preference for three directions (in-plane – x and y and depth - z).

We conjectured that 1. All the layers show a strong relation, being this connection more relevant between the neighbour layers. 2. The preferred direction for the pixels conectivity is the depth.

6.2.1 Layer connections

In this sub-chapter we will describe the results for the spatial relationship between different layer presentations. In order to attain different tests to evaluate this relation between layers different measures were used to correlate the three cortical layers: activity maps (t-values), percent signal change average and the mean of the untreated time course. All the measurements were performed for both grids of each subject's cortical layers, to later be used in a correlation test.

Considering our hypothesis of the existence of depth structures in M1, we predict that all layers are correlated; furthermore sequential layers should be more correlated than distant layers, following the idea of a cortical continuity in depth.

Activity maps

To study the different correlation levels between different layer's activity maps of the direct paradigm we used a repeated measure ANOVA with three factors: finger grid (FG1 and FG3), finger map (thumb and middle) and layer pair (superficial/middle, middle/deep and deep/superficial).

The analysis of these correlation values revealed a significant interaction between adjacent and non-adjacent layers [$F(2,24)=842.46$; $P < 0.00001$], in the sense that adjacent layers are strongly correlated. The superficial and middle layers show a higher correlation (M=0.65; SD=0.12) than the superficial and the deep layers (M=0.36; SD=0.12) ($P < 0.00001$); the same happens with the remaining pair of adjacent layers – middle and deep layers – that have a correlation index of M=0.59; SD=0.12 (Figure 6.16) ($P < 0.00001$). The results indicate that, as expected, adjacent layers have a stronger connectivity than more distant layers.

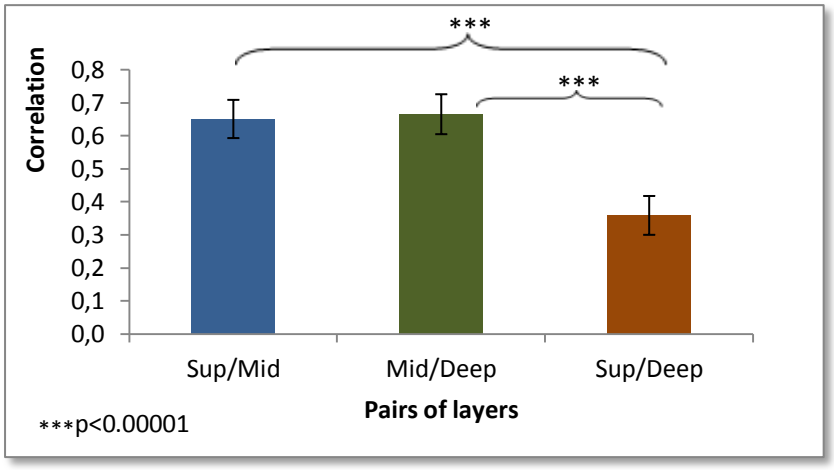

Figure 6.16 - Correlation indexes average of the t-maps for different pairs of layers (superficial/middle, middle/deep and deep/superficial).

Percent signal change – BOLD response

To inspect the different correlation indexes between the average percent signal change (BOLD response) of the cortical layers, we used a repeated measure ANOVA with three factors: finger grid (FG1 and FG3), finger map (thumb and middle) and layer pair (superficial/middle, middle/deep and deep/superficial).

The ANOVA analysis shows a significant effect for the adjacent layers [$F(2,24)=161.39$; $P < 0.00001$]. The superficial and middle layers have a bigger correlation index (M=0.64; SD=0.09) than the superficial and the deep layers (M=0.42; SD=0.1) ($P < 0.00001$); the same happens with the remaining pair of adjacent layers – middle and deep layers – that show a correlation of M=0.65; SD=0.1 (Figure 6.17) ($P < 0.00001$).

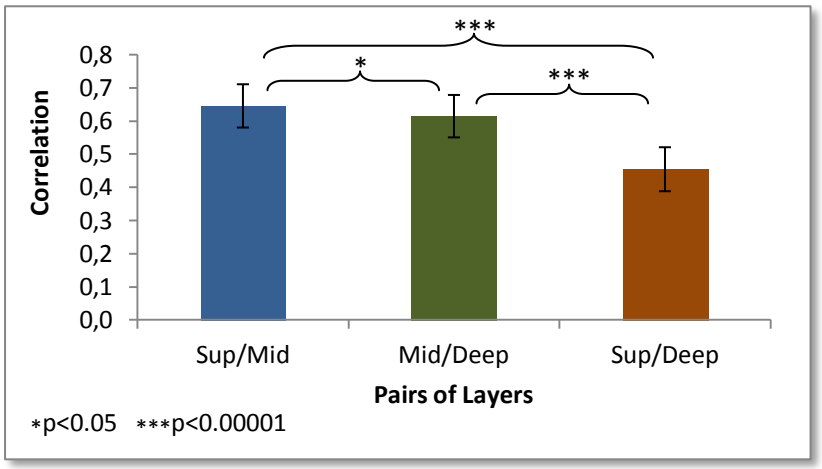

Figure 6.17 - Correlation values averages between the average BOLD responses of different pairs of layers (superficial/middle, middle/deep and deep/superficial).

This result supports the prediction of a stronger connectivity for adjacent layers than for more distant layers. Additionally, there is a significant difference between the superficial and deeper layer pairs ($P < 0.05$): the superficial layer pair – superficial and middle layers – has a higher correlation value than the deeper layer pair – middle and deeper layers.

Mean of the time course signal

To examine the different correlation indexes we used a repeated measure ANOVA with two factors: finger grid (FG1 and FG3) and layer pair (superficial/middle, middle/deep and deep/superficial).

The analysis of the correlation values between different layer's mean time course signal shows a significant interaction between adjacent and non-adjacent layers, was also found in the index correlation analysis of the mean time courses between different layers [$F(2,12)=17.1$; $P < 0.001$]. Adjacent layers show a stronger correlation index (Figure 6.18): the superficial and middle layers show a higher correlation (M=0.65; SD=0.03) than the superficial and the deep layers (M=0.41; SD=0.3) ($P < 0.001$); the same happens with the remaining pair of adjacent layers – middle and deep layers – that have a correlation index of M=0.63; SD=0.04 ($P < 0.001$). This finding also supports our hypothesis of a higher connectivity for sequential layers than for more separated layers.

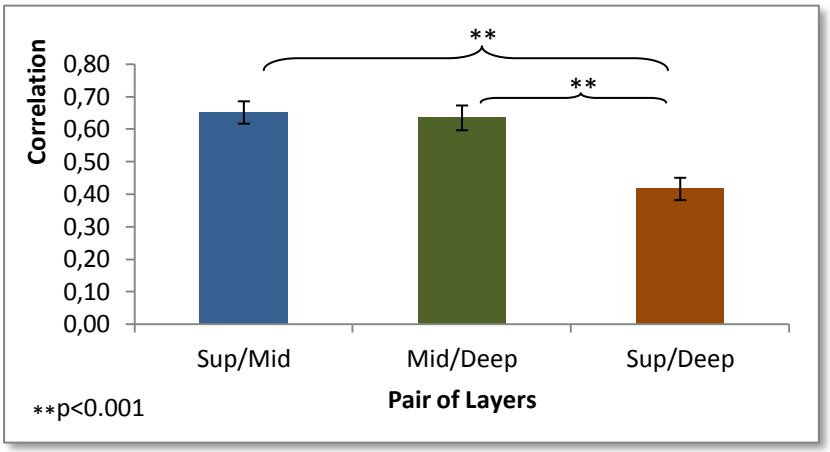

Figure 6.18 - Correlation values averages between different layer's mean time course signals

In summary, the results demonstrate that 1. All layers have a strong connection. 2. The relation between layers is dependent of their spatial distance: adjacent layers are strongly correlated than the non-adjacent, sustaining the idea of depth continuity along the cortex.

6.2.2 Directionality Preference of Functional Connectivity

Along this sub-chapter we will show the results for the directionality preference of the pixels connectivity. In order to test their preference, time course correlations were be performed between blocks of four pixels (to avoid up-sampling contamination) in three neighbor dimensions: in-plane directions (x and y) and depth direction (z). We conjecture that depth is the preferred direction in terms of pixels connectivity.

The analysis of the correlation between the blocks of four pixels in different neighbor dimensions was performed for each subject separately and then used for a statistic analysis. Note that the neighbor dimensions of the in-plane direction are not spatially separated as the neighbor depth direction; considering the mean cortical thickness for all the subjects of 1.88 mm for FG1 and 1.84 mm for FG3 (Appendix – Table 2), the average spacing of two neighbors in the depth direction is 0.5 mm for both finger grids, which corresponds exactly to the size of one voxel.

A t-test was performed to evaluate the difference between the in-plane dimensions (x and y) and the depth (z dimension). The t-test revealed a significant difference between the in-plane dimensions and the depth dimension (Figure 6.19) ($P < 0.05$). The in-plane direction (M=0.68; SD=0.016) shows significant lower correlations between the blocks of pixels than the depth direction (M=0.73; SD=0.04).

Besides the significance shown by the t-test statistics, the blocks of pixels correlated in depth direction are spatially separated by at least 0.5 mm, while the pixels correlated in the other two dimensions have no spatial gap between them. Thus, it is clear that M1 has a massive directionality preference for the depth direction. This result points to the existence of functional depth structures in primary motor cortex, similar to columnar structures in V1 with diameters bellow 1000 nm, because the resolution used to study this directionality was an isometric space of 1 mm^2 (0.5 mm x 0.5 mm - the size of one block of four pixels).

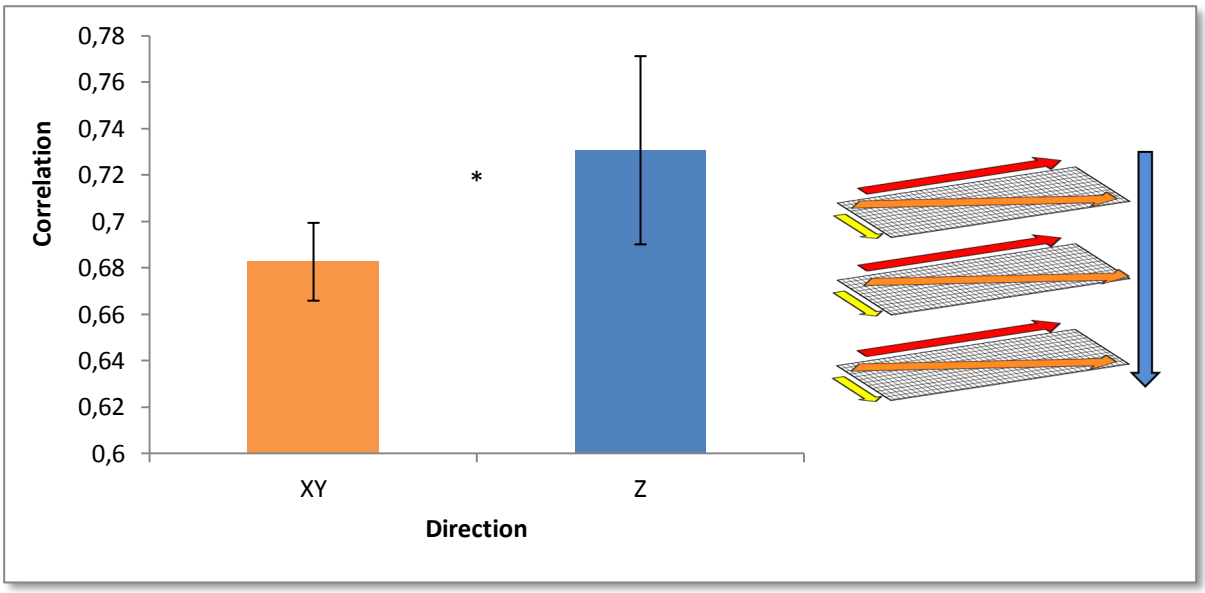

Figure 6.19– Correlation indexes averages between pixel's signals for different dimensions (a scheme to illustrate the dimensions is visible in the right: the orange arrow corresponds to the in-plane dimensions – x and y; the blue arrow corresponds to the depth dimension – z). Note the preference for the depth direction.

Briefly, the result expresses that depth is the preferred direction for the pixels connectivity, sustaining the expected existence of depth structures in human M1.

6.3 Imagery in M1

In this subchapter we will address the question of the motor imagery in M1. There is a debate among the scientific community about the involvement of motor imagery in M1: while some studies point to a relation between movement imagery and M1 (Porro et al., 2000; Roth et al., 1996; Sharma et al., 2008), other experiments show that this task is not involved with M1 (Binkofski et al., 2000; Hanakawa et al., 2003). Here we addressed this question by examining the finger activity maps of motor imagery in each finger specific grid (FG1 and FG3) placed according the motor activity (using two measures – the number of active pixels and the percent signal change peak measure).

We predict that 1. There is some activity in the motor imagery maps, furthermore we hypothesise that this activity is more relevant in the matching finger map, in other words the specific finger of the grid. 2. The deeper layers are not responsive to the motor imagery task.

In order to study the involvement of motor imagery in M1, in each finger specific grid (FG1 and FG3) placed according the motor activity the different (direct and differential) finger activity maps of motor imagery were sampled.

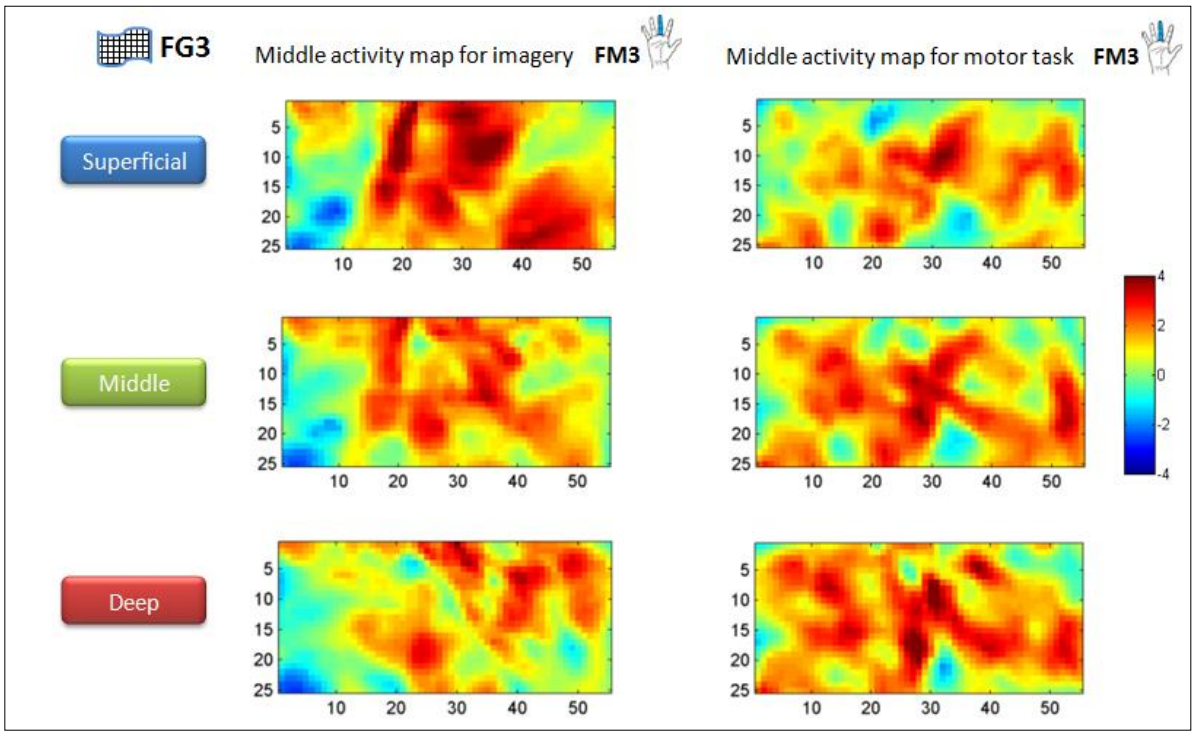

Figure 6.20– Direct activity maps of two tasks (motor imagery and motor execution-ME) for the middle finger grid (FG3) of a single subject [S3]. The maps above show the t-values for different task activity maps – motor imagery (left column) and ME (right column). Rows show activity in different layers of the cortical sheet (top-superficial to bottom-deep).

Our results reveal that there is evidence of motor imagery activity in the motor finger specific grids; two examples are illustrated in the figures above and below respectively (Figure 6.20 and Figure 6.21). The first figure shows the activity maps of middle finger for motor imagery and motor execution (ME) in the middle finger grid - FG3. The second image illustrates the activity maps of thumb finger for motor imagery and motor execution (ME) in the thumb finger grid – FG1. From both figures it is clear the existence of a smooth motor imagery activity in the fingers motor areas and also the increased involvement of imagery in the superficial layer.

With the intention of improve the understanding of the different finger regions – grids, a percent signal change analysis was performed for each subject separately, culminating in the generation of an average BOLD response for each layer and each finger per grid. Using the peak of BOLD response measure in an repeated measures ANOVA analysis with two factors - finger grid (FG1 and FG3) and cortical layer (superficial, middle and deep) - no statistical evidence was found regarding the grid specificity [$F(1,6)=1.879$; $P < 0.22$] and differences between layers [$F(2,12)=1.503$; $P < 0.262$]. Note that we only tested the peak of BOLD response of the matching finger of each grid (for FG1 the FM1 and for FG3 the FM3).

Also for each finger map in each grid, the number of active pixels was counted, however this measure revealed a big variance between subjects and also the resultant set is not significantly larger than zero.

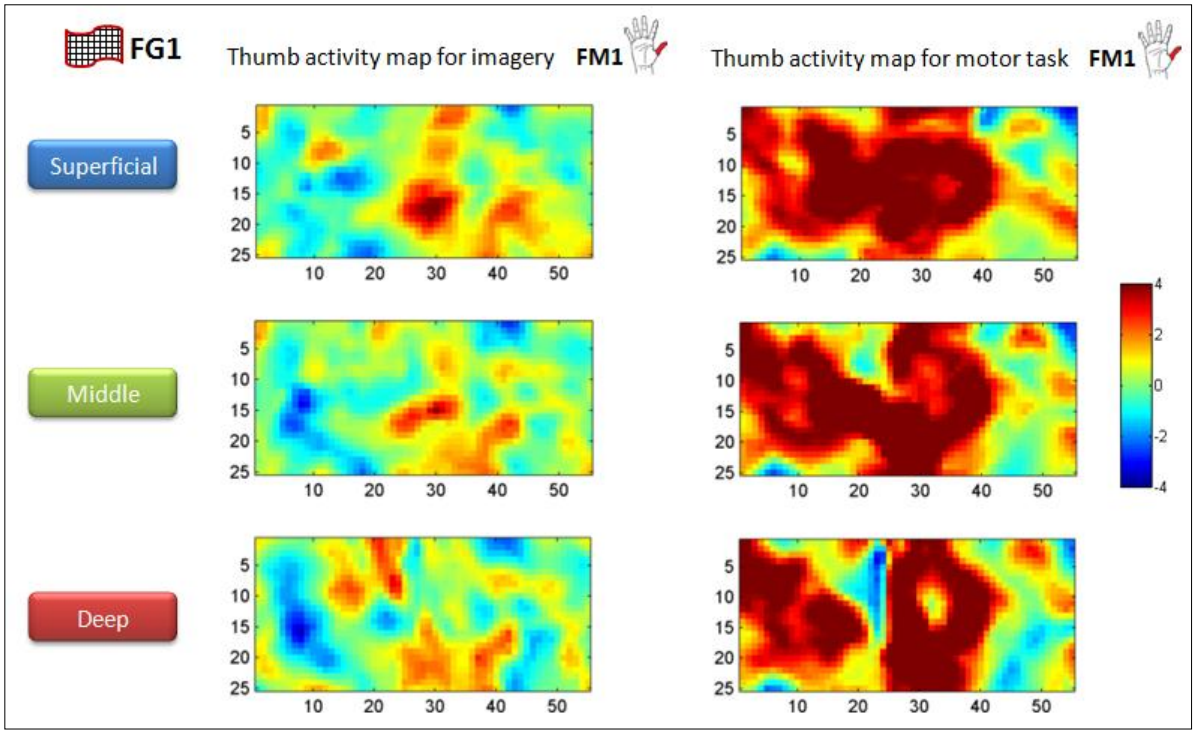

Figure 6.21 – Differential activity maps of two tasks (motor imagery and motor execution-ME) for the thumb finger grid (FG1) of a single subject [S9]. The maps above show the t-values for different task activity maps – motor imagery (left column) and ME (right column). Rows show activity in different layers of the cortical sheet (top-superficial to bottom-deep).

Overall, the results demonstrate that 1. There is some activity in the imagery maps, however differing from our hypothesis there is no grid specificity for the motor imagery. 2. Contrary to our hypothesis, there is no difference of activity between the three cortical layers.

6.4 Visual activity in M1

Along this subchapter we will focus on the results related with the movement observation in M1. There is a debate among the scientific community about the involvement of vision in M1: while some studies point to a relation between movement observation and M1, other experiments show that this task is not involved with M1. Here we addressed this question by examining the finger activity maps of movement observation in each finger specific grid (FG1 and FG3) placed according the motor activity (using two measures – the number of active pixels and the percent signal change peak measure).

We predict that 1. There is some activity in the movement observation maps, furthermore we hypothesise that this activity is more relevant in the matching finger map, in other words the specific finger of the grid. 2. The output layers (the deeper ones) show less activity in the movement observation task, once no movements are being performed

To facilitate the understanding of the involvement of visual activity in M1, in each finger specific grid (FG1 and FG3) placed according the motor activity the different (direct and differential) finger activity maps of movement observation were sampled.

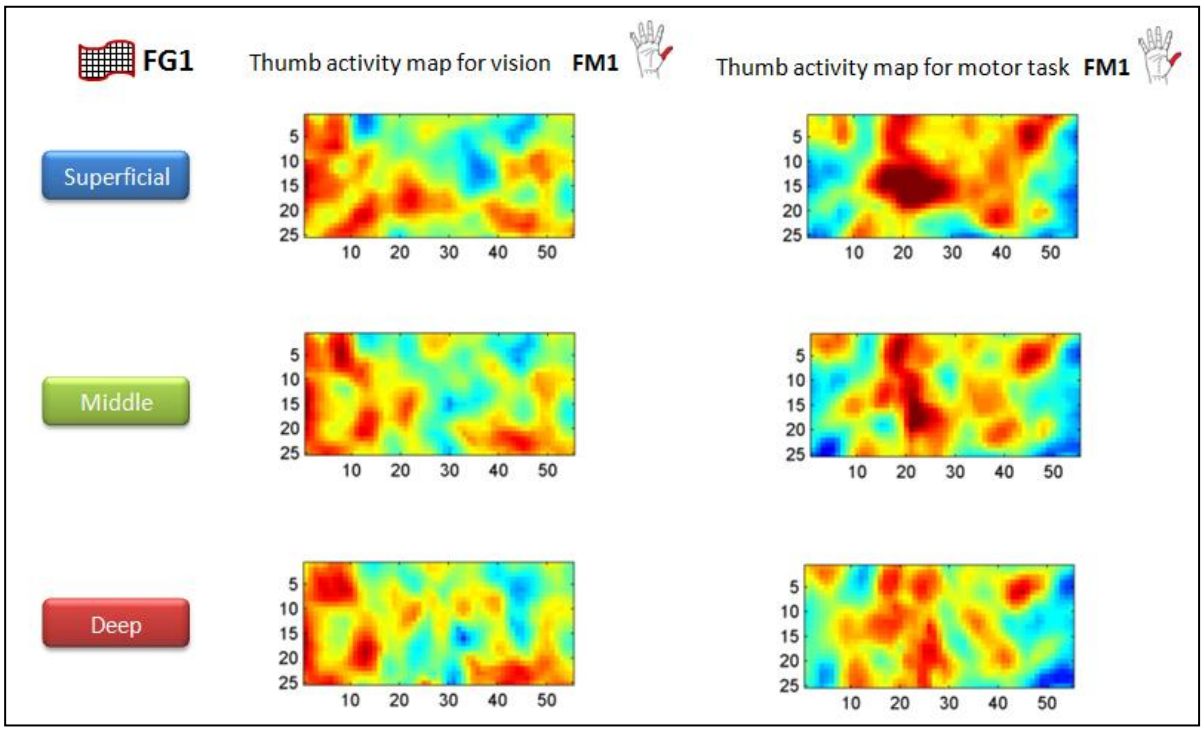

Figure 6.22 – Direct activity maps of two tasks (movement observation - MO and motor execution-ME) for the thumb grid (FG1) of a single subject [S6]. The maps above show the t-values for different task activity maps – MO (left column) and ME (right column). Rows show activity in different layers of the cortical sheet (top-superficial to bottom-deep).

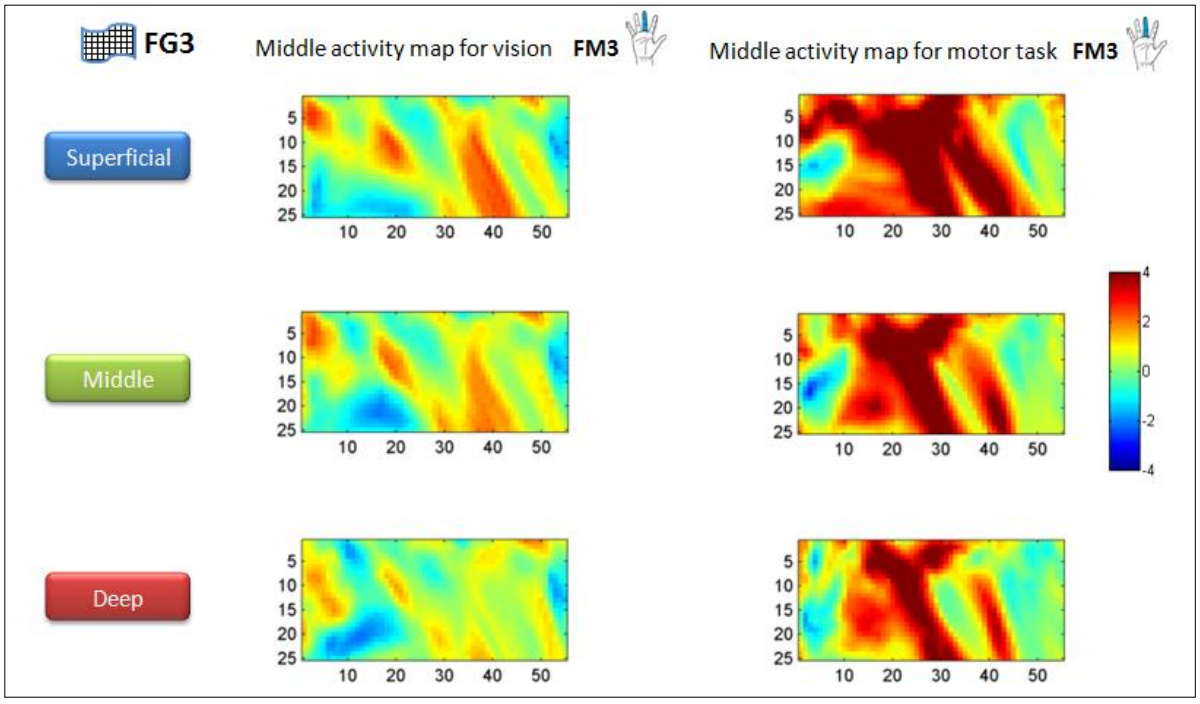

Figure 6.23 – Direct activity maps of two tasks (movement observation - MO and motor execution-ME) for the middle finger grid (FG3) of a single subject [S6]. The maps above show the t-values for different task activity maps – MO (left column) and ME (right column). Rows show activity in different layers of the cortical sheet (top-superficial to bottom-deep).

Our results indicate the existence of visual activity in the motor finger specific grids; two examples are illustrated in the figures above (Figure 6.22 and Figure 6.23). In both figures, it is clear the existence of a smooth visual activity in the fingers motor areas and also the increased involvement of this activity in the superficial layer, although this last feature is more evident in the last figure.

In order to improve the understanding of the different finger regions – grids, a percent signal change analysis was performed for each subject separately, culminating in the generation of an average BOLD response for each layer and each finger per grid. Using the peak of BOLD response measure in an repeated measures ANOVA analysis with two factors - finger grid (FG1 and FG3) and cortical layer (superficial, middle and deep) - no statistical evidence was found regarding the grid specificity [$F(1,4)=0.363$; $P < 0.58$] and differences between layers [$F(2,8)=0.438$; $P < 0.66$]. Note that we only tested the peak of BOLD response of the matching finger of each grid (for FG1 the FM1 and for FG3 the FM3).

Also for each finger map in each grid, the number of active pixels was measured; yet the results showed to vary a lot between subjects and also the resulting sample is not significantly larger than zero.

Overall, the attained results demonstrate that 1. There is some activity in the visual maps, although differing from our hypothesis no grid specificity was found for movement observation. 2. There is no difference of activity between the three cortical layers, which is a contrary finding according to our predictions.

6.5 Task related differences

In this subchapter we will address the question of the relation between the three tasks – motor imagery, movement execution and movement observation. Since M1 is related with all three tasks, we would like to understand how they are connected. Here we addressed this question by examining 1. The correlation level between the activity maps of different tasks. 2. The influence of the matching of finger maps in the correlation level of two tasks.

We predict that 1. The motor imagery and movement observation (MO) are related with the motor execution (ME). 2. The motor imagery and MO are not correlated. 3. The superficial cortical layers show a higher correlation between tasks, than the deeper ones. 4. The relation between tasks is finger dependent: the matching finger maps between ME and the other two tasks shows a stronger relation than the un-matching case.

In order to study the relation of different tasks, the correlation index between the direct activity maps of different tasks was performed for each subject covering all possible combinations of finger maps and grids.

To study the different correlation levels between different task's activity maps we used a repeated measures ANOVA with two factors: task pair (motor/imagery, motor/visual and imagery/visual) and layers (superficial, middle and deep). Note that we only tested two task pairs in one ANOVA test, thus three tests were made to cover all the possible combinations and also the correlation values used correspond to only the matching maps of middle and thumb fingers between the different tasks, for instance for one grid the matching values correspond to the correlation indexes between two tasks activity maps of the thumb and also the correlation indexes between two tasks activity maps of the middle finger.

The analysis of these correlation values demonstrated significant differences between task pairs (Figure 6.24). First of all, there is a stronger connection between motor and imagery tasks (M=0.12; SD=0.1) than visual and imagery (M=-0.03; SD=0.06) [$F(1,19)=7.56$; $P < 0.05$]. Statistics also show a weaker correlation between visual and imagery tasks compared with motor and visual tasks correlation (M=0.16; SD=0.07) [$F(1,19)=10.58$; $P < 0.001$]. This result follows our hypothesis, suggesting that both – imagery and visual tasks – are related with the motor activity, however they are not correlated between them.

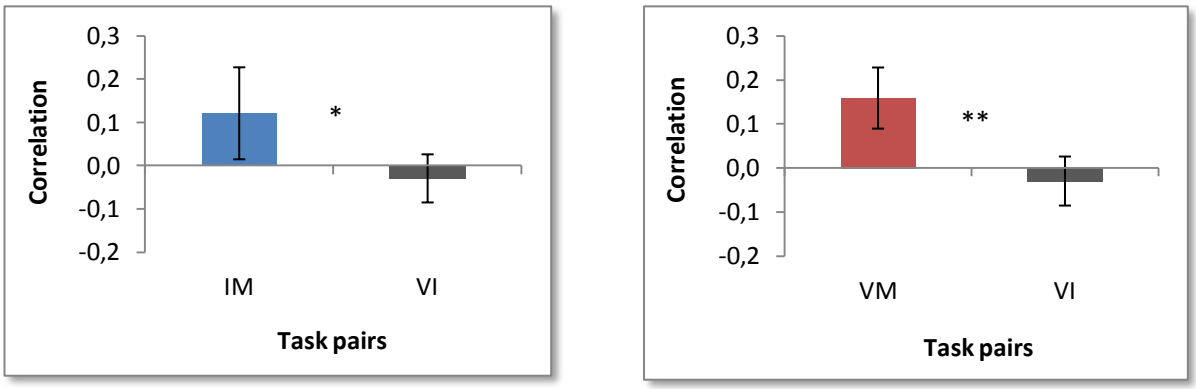

Figure 6.24 – Average correlation values between the matching activity maps of different task pairs: on left imagery and motor tasks (IM) compared with imagery and visual tasks (VI); on right visual and motor tasks (VM) compared with imagery and visual tasks (VI)

To test the influence of the matching of finger maps in the correlation level of two tasks, we used a repeated measure ANOVA with two factors: type of task pair (matching and un-matching) and layers (superficial, middle and deep). Note that we only tested one task pair in one single ANOVA test, thus two tests were made to inspect the correlation level regarding the finger dependency between MO and ME and also between motor imagery and ME.

This ANOVA analysis revealed an interaction between matching and un-matching finger activity map pairs of MO and ME [$F(1,19)=24.27$; $P < 0.0001$] (Figure 6.25). The result points to a positive correlation between matching finger activity map pairs of M=0.15; SD=0.06 (same fingers for motor and visual tasks) and to a negative correlation between un-matching finger activity map pairs of M=-0.17; SD=0.07 (different fingers for motor and visual tasks). Additionally, this ANOVA analysis also revealed a significant decrease of the correlation level from the middle to the deeper layer ($p< 0.05$). This result follows two of our hypotheses: first suggest that MO and ME relation is finger dependent; finally it also indicates that the deeper layers are not so correlated with the motor activity. This interaction between matching and un-matching finger activity map pairs wasn't found for motor imagery.

Despite that the grids analysis of single task point to an inexistence of finger grid specificity and thus a lack of somatotopic like motor pattern, which probably would bring the erroneous suggestion that motor execution and movement observation are two unrelated tasks. Although, apart from ME do show grid specificity and MO doesn't, first there is a strong relation between the two, judging from the correlation index between the finger activity maps and more importantly this high correlation is driven by the matching fingers between the two tasks, because the un-matching fingers situation reveals the contrary – a negative correlation index. So, we suggest that MO and ME share the same pattern of functional organization regarding the fingers movement.

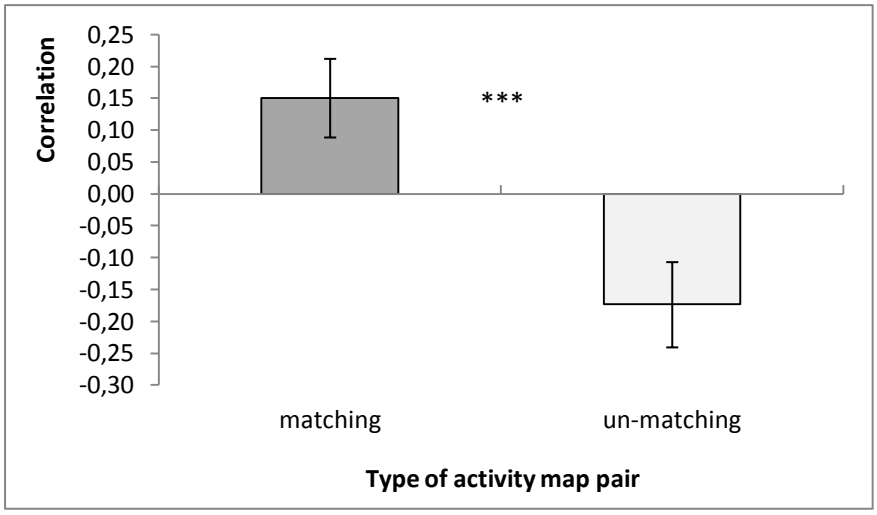

Figure 6.25 – Average correlation values between matching finger activity map pairs and un-matching finger activity map pairs of MO and ME

In summary, the results indicate that 1. Motor imagery and MO are connected with the motor execution, as expected. 2. Movement observation and motor imagery have no relation, how we predicted. 3. The connection between MO and ME is decreased in the deeper layers; however we also hypothesized the same for motor imagery. 4. The relation between MO and ME is dependent on the matching/un-matching fingers factor, because, as we theorized, is stronger for the matching fingers. Although, the relation between motor imagery and ME is not finger dependent, the contrary of what we expected.

7 Discussion

In this chapter the results of the different main themes - somatotopy; depth structures and non-motor tasks - will be discussed and also the project limitations as well as future perspectives will be presented.

7.1 Somatotopy

The existence of a distributed organization regarding the fingers representation in M1 has long been a point of discussion. The present study reveals a distributed pattern intermingled with somatotopic "hot spots" for single fingers activity in different cortical layers of M1. We demonstrate that within the cortical area of a finger specific grid, representations of the three fingers (thumb, index and middle fingers) are highly related and there is a considerable amount of active pixels that is only activated by other fingers showing or not overlap between them (at least with one of three). Despite overlap, grids are finger specific, thus these representations maintain distinct centers – somatotopic hot spots. Finally, the functional representation of single fingers varies between different cortical depths, being more responsive in the superficial layers.

We explored whether single finger representations have a somatotopic pattern, by analysing the finger grids specificity. The level of finger grid specificity revealed is slightly different based upon whether the number of active pixels or the peak of BOLD response is used for statistics. Both measures revealed a main effect showing a response increase for the grid matching finger, pointing to a somatotopic pattern, however for the active pixels this interaction was only significant for the thumb finger grid (FG1) and for the peak of BOLD response this effect was almost significant for both finger grids. This difference can be due to the extreme generality of the BOLD response, which is based in the average of all the pixels from one grid comparing with the specificity of pixels analysis. Also, the average of active pixels distribution between the three layers reveals that 62% of the active pixels in FG1 are only active for the thumb and that 49.3% of the active pixels in FG3 are only activated by the middle finger. Joining this difference between the percentage of the two fingers and the fact that only the FG1 showed grid specificity from the active pixel analysis, we propose that the thumb is a more independent finger than the middle, in the sense that his region is even more specific. In addition, the correlation level between different finger representations reveals that adjacent fingers are strongly correlated than the non-adjacent, pointing to the somatotopic feature of activity organization. Note that exclusion of the fingers overlap, by using the differential activity maps, logically would demonstrate more difference between fingers regions (Dechent and Frahm, 2003), revealing only a somatotopic organization, therefore to consider the entire activity all the maps statistics only involved the data from the direct activity maps. The finding of somatotopic hot spots between the fingers is concordant with the classical views (Penfield and Boldrey, 1937; Penfield and Rasmussen, 1950) and recent studies (Beisteiner et al., 2001; Dechent and Frahm, 2003a; Hluštík et al., 2001; Lotze et al., 2000). However, only two of the referred studies are based on a similar finger tapping task (Lotze et al., 2000; Dechent and Frahm, 2003), while others applied a task of flexion-extension movements of fingers (Beisteiner et al., 2001; Hluštík et al., 2001).

Second, we investigated whether single fingers representations overlap with each other in M1. We found from different measures that there is a strong relation between the representation of different fingers, suggesting a distributed organization: on average 19% of the active pixels of one grid are activated by more than one finger representation - all the types of pixels are activated in one grid (shared, matching and un-matching finger specific pixels); all the finger representations are strongly correlated. The discovery of distributed organization for single fingers is concordant with recent

studies (Grafton et al., 1991; Indovina and Sanes, 2001; Sanes et al., 1995; Schieber, 1999), although none of these studies used the finger tapping task. So this study is exclusive in the finding of a distributed pattern for fingers activity organization using a single finger tapping task.

Basically, combining the two findings, we state that single fingers encoding in M1 is distributed pattern intermingled with somatotopic "hot spots". Following the piano analogy made by Schieber (Schieber, 2001), we propose that all possible neuronal combinations (regarding the finger's movements) can be made within each finger's cortical specific region (in this case the grids): the majority of neurons function is to code movements related with the correspondent finger (the hot-spots) and in the same area there are other neurons that encode some features of other fingers movements. The purpose of the hot-spot is to ensure a fine individuated control of the movement, in terms of strength and direction, on other hand the distribution guarantees coordinated movements, an idea shared by Dechent (Dechent and Frahm, 2003b).

Regarding the functional representation of single fingers between different cortical depths, we discovered that there is a cortical difference in terms of response intensity – the number of active pixels and the peak of BOLD response analysis indicated the existence of a stronger response in the superficial layers. However, the level of difference between layers varies with the type of measure: the number of active pixels reveals that the three laminas have distinct response intensities, being more intense in the superficial and sequentially decreasing the strength of response in the other layers; on other hand the peak of BOLD response only shows a distinction in the response level between the deeper and the other two layers, being less responsive in the deep layer. Once again, the slight difference in the two measures results can be due to the extreme generality of the BOLD response, which is based in the average of all the pixels from one grid comparing with the specificity of pixels analysis. Usually this increased response in the superior layers is explained by vessels contamination (Chen et al., 2013), although in this study this explanation is not valid, because we assured their exclusion. Also, we discovered that there is no variance in the organization pattern for fingers activity between different layers. Suggesting the difference is not in the type of organization, but in the level of response, therefore we propose that the deeper layers are less stimulated and consequently less responsive than the superficial ones; probably due to the stronger specificity of deeper layers less but more specific stimulus are needed to induce the processing of motor execution; contrary the superficial layers due to their more distributed feature, receive a more general kind of stimulus and filter them in a specified fashion to the deep layers.

7.2 Depth Structures

The cortical columnar structures are the fruit of a well-established theory to define the elementary level of the functional organization of cerebral cortex, which has been proven in some cerebral areas (Yacoub et al., 2008; Zimmermann et al., 2011b), although no evidence of these structures has been found in the human M1. The present study reveals the existence of columnar like structures in the primary motor cortex. We demonstrate that all the cortical layers are strongly related in terms of functional signal and activity maps. Furthermore, there is a directionality preference in the depth regarding the functional connectivity.

We studied the connections of the three cortical layers, by analyzing the correlation level of the activity maps, the BOLD response and the mean time course signal between different depths. All the measures analysis revealed that all layers have a strong correlation, although the correlation level is dependent of their spatial distance: adjacent layers are strongly correlated than the non-adjacent, sustaining the idea of depth continuity along the cortex. This result is concordant with (Asanuma and

Rosén, 1972; Jankowska et al., 1975). However, only the BOLD response correlation analysis shows a distinction between adjacent layers, being less correlated in the deep layer. Once again, the slight difference in the three measures results can be due to the fact that besides BOLD response results from an average of all pixels in one grid and consequently is a more general measure, this signal is treated; contrary to the raw signal, which is also based in the average of all the pixels.

Regarding the directionality preference of pixels functional connectivity, we found a directionality preference for the depth direction with a correlation index in depth of 0.73. Thus, we propose the existence of depth structures in primary motor cortex, in a columnar level with diameters bellow 1000 nm, because the resolution used to study this directionality was an isometric space of 1 mm^2 (0.5 mm x 0.5 mm - the size of one block of four pixels). At this stage, we can only speculate about the source of the directionality preference – blood supply, cortical columns or it could also be that each cortical column has each exclusive blood supply. To our knowledge, this study is unique in investigation the columnar properties of a primary motor cortex area sampled in multiple layers. The close resemblance of our findings to conclusions reached in electrophysiology recordings in animals (Amirikian and Georgopoulos, 2003), however, provides support for our observations.

7.3 Non-motor tasks

From a classical view, M1 is responsible for the final cortical output of movement commands, while recent studies point to more complex roles for M1 in orchestrating motor-related information. The present study shows that non-motor tasks such as motor imagery and movement observation (MO) also activate the primary motor cortex. Additionally, motor imagery and MO are connected with the motor execution and these two non-motor tasks have no relation. Specifically, MO and ME correlation level shows a decrease in the deeper layers and their correlation index is finger dependent.

First we separately explored the activity level of both non-motor tasks – motor imagery and MO – in the selected finger motor regions – grids. We discovered some activity in the both maps, although no grid specificity was found. These results are concordant with other studies that have shown motor imagery (Porro et al., 2000; Roth et al., 1996; Sharma et al., 2008) and movement observation activity (Grezes, 1998; Nishitani and Hari, 2000) in the M1. However, none of the referred investigations have used the fingers tapping for motor imagery or movement observation; regarding the techniques there are several techniques applied among these studies – lower resolution fMRI (Porro et al., 2000; Roth et al., 1996; Sharma et al., 2008), MEG (Nishitani and Hari, 2000); positron emission tomography - PET (Grezes, 1998). Grezes and colleagues found that movement observation in the M1 is activated by meaningful actions and not by meaningless movements, also Nishitani and Hari state the existence of M1 activity provoked by meaningful visual observation. Yet, our study shows M1 activity for meaningless actions, we propose that M1 responds to all types of recognized actions, being more responsive to meaningful movements. Regarding the different cortical layers, no difference was found in terms of activity intensity, we propose that deep layers are also activated, except the responsive neurons for these on-motor tasks are different from the ones activated by the movement performance. Besides the inexistence of grid specificity in these non-motor tasks we found that the number of active pixels (for the defined threshold of three) is not significantly larger than zero, this result can be explained by the difference subject skills not only in terms of imagery but also in terms of visual recognition, which is also prominent by the exceptional variance of this measure from subject to subject.

Finally, we studied the connections of the non-motor tasks with the motor execution, by analyzing the correlation level of the activity maps. We found that both tasks are positively correlated with ME

and that there is no relation between motor imagery and MO. Additionally, ME and MO correlation indexes are increased if both fingers are congruent. This finding is similar to TMS studies that show congruence between the observed motor behavior and the evoked motor output (Strafella and Paus, 2000; Gangitano et al., 2001). To our knowledge, this study is unique in investigation the non-motor tasks properties in the human primary motor cortex area for multiple layers. Therefore, this study it also indicates that the correlation level between MO and ME decreases in the deeper layers, probably due to the inexistence of movement performance. Yet, this decrease of correlation is not directly translated in a decrease of response intensity.

7.4 Limitations and Future Work

During the development of this project certain limitations were encountered, which can be avoided or solved in future studies.

Regarding the cortical sampling choices we didn't sampled grids in the index finger region because the activity of this finger was not considered sufficient along all the subjects, besides with this extra grid the three grids would have undesired overlap regions, therefore this lack of grid is not considered a project limitation.

Our scanning resolution is not high enough to resolve cortical columns in M1, although it appears to be sufficient to reliably resolve large scale axis of functional connectivity direction with an estimated size of at least 1mm. Also, because of the curvature of the cortical gray matter, the vertical organization of cortical columns may not perfectly transverse the different layers along lines perpendicular to the surface, a problem that is encountered also in electrophysiology, but due to uncertainties in angle of electrode penetration (Diogo et al., 2003).

The selection of the volunteers only followed the age and handiness standards; however it is known that the capacity to perform telekinetic imagery is a skill, which can be improved by training (Sacco et al., 2006). Even better, nowadays the brain computer interfaces (BCI) users fulfill the standards of a good imagery performance (Ang et al., 2010; Neuper et al., 2006), thus we propose that future studies use another principle.

Finally, we suggest that future projects use EEG or electromyography to assure that no movement is being performed during motor imagery and movement observation, once in this project we could only evaluate that by observation.

8 Conclusion

In general, the study presented in this thesis accomplishes its principal objective – study the functional properties of primary motor cortex, with aim to answer the following questions:

- Is there a somatotopic or distributed representation for fingers in M1?
- Are there any depth structures in human M1?
- Is M1 activated by action observation?
- Is M1 activated by motor imagery?

The attained results reveal that: 1. Primary motor cortex has a distributed pattern intermingled with somatotopic “hot spots” for single fingers activity in different cortical layers; 2. There are evidences for columnar structures existence in M1; 3. Non-motor tasks such as motor imagery and action observation also activate this cortex.

Overall, we conclude that the primary motor cortex has much more un-expected complex roles regarding the processing of movement related information, not only due to their involvement in tasks that do not imply muscle movement, but also due to their intriguing organization pattern.

References

Amirikian, B., and Georgopoulos, A.P. (2003). Modular organization of directionally tuned cells in the motor cortex: Is there a short-range order? Proc. Natl. Acad. Sci. *100*, 12474–12479.

Ang, K.K., Guan, C., Chua, K.S.G., Ang, B.T., Kuah, C., Wang, C., Phua, K.S., Chin, Z.Y., and Zhang, H. (2010). Clinical study of neurorehabilitation in stroke using EEG-based motor imagery brain-computer interface with robotic feedback. Conf. Proc. Annu. Int. Conf. IEEE Eng. Med. Biol. Soc. IEEE Eng. Med. Biol. Soc. Conf. *2010*, 5549–5552.

Asanuma, H., and Rosén, D.I. (1972). Topographical organization of cortical efferent zones projecting to distal forelimb muscles in the monkey. Exp. Brain Res. *14*, 243–256.

Baldissera, F., Cavallari, P., Craighero, L., and Fadiga, L. (2001). Modulation of spinal excitability during observation of hand actions in humans. Eur. J. Neurosci. *13*, 190–194.

Beisteiner, R., Windischberger, C., Lanzenberger, R., Edward, V., Cunnington, R., Erdler, M., Gartus, A., Streibl, B., Moser, E., and Deecke, L. (2001). Finger Somatotopy in Human Motor Cortex. NeuroImage *13*, 1016–1026.

Benjamini, Y., and Hochberg, Y. (1995). Controlling the False Discovery Rate: A Practical and Powerful Approach to Multiple Testing. J. R. Stat. Soc. Ser. B Methodol. *57*, 289–300.

Binkofski, F., Amunts, K., Stephan, K.M., Posse, S., Schormann, T., Freund, H.-J., Zilles, K., and Seitz, R.J. (2000). Broca's region subserves imagery of motion: A combined cytoarchitectonic and fMRI study. Hum. Brain Mapp. *11*, 273–285.

Blamire, A.M., Ogawa, S., Ugurbil, K., Rothman, D., McCarthy, G., Ellermann, J.M., Hyder, F., Rattner, Z., and Shulman, R.G. (1992). Dynamic mapping of the human visual cortex by high-speed magnetic resonance imaging. Proc. Natl. Acad. Sci. U. S. A. *89*, 11069–11073.

Blasdel, G.G., and Salama, G. (1986). Voltage-sensitive dyes reveal a modular organization in monkey striate cortex. Nature *321*, 579–585.

Bonhoeffer, T., and Grinvald, A. (1991). Iso-orientation domains in cat visual cortex are arranged in pinwheel-like patterns. Nature *353*, 429–431.

Bourekas, E.C., Christoforidis, G.A., Abduljalil, A.M., Kangarlu, A., Chakeres, D.W., Spigos, D.G., and Robitaille, P.M. (1999). High resolution MRI of the deep gray nuclei at 8 Tesla. J. Comput. Assist. Tomogr. *23*, 867–874.

Boxerman, J.L., Bandettini, P.A., Kwong, K.K., Baker, J.R., Davis, T.L., Rosen, B.R., and Weisskoff, R.M. (1995). The intravascular contribution to fmri signal change: monte carlo modeling and diffusion-weighted studies in vivo. Magn. Reson. Med. *34*, 4–10.

Brodal, P. (2010). The central nervous system: structure and function (New York: Oxford University Press).

Buccino, G., Binkofski, F., Fink, G.R., Fadiga, L., Fogassi, L., Gallese, V., Seitz, R.J., Zilles, K., Rizzolatti, G., and Freund, H.-J. (2001). Action observation activates premotor and parietal areas in a somatotopic manner: an fMRI study. Eur. J. Neurosci. *13*, 400–404.

Buckner, R.L. (1998). Event-related fMRI and the hemodynamic response. Hum. Brain Mapp. *6*, 373–377.

Buxton, R.B. (2009). An introduction to functional magnetic resonance imaging principles and techniques (Cambridge: Cambridge University Press).

Carter, M., and Shieh, J.C. (2010). Guide to research techniques in neuroscience (Burlington, MA: Academic Press).

Carter, R., Aldridge, S., Page, M., Parker, S., Frith, C.D., Frith, and Shulman, M.B. (2009a). The human brain book (London; New York, N.Y.: DK Pub.).

Carter, R., Aldridge, S., Page, M., Parker, S., Frith, C.D., Frith, and Shulman, M.B. (2009b). The human brain book (London; New York, N.Y.: DK Pub.).

Chen, G., Wang, F., Gore, J.C., and Roe, A.W. (2013). Layer-specific BOLD activation in awake monkey V1 revealed by ultra-high spatial resolution functional magnetic resonance imaging. NeuroImage *64*, 147–155.

Cheng, K., Waggoner, R.A., and Tanaka, K. (2001). Human Ocular Dominance Columns as Revealed by High-Field Functional Magnetic Resonance Imaging. Neuron *32*, 359–374.

Cochin, S., Barthelemy, C., Lejeune, B., Roux, S., and Martineau, J. (1998). Perception of motion and qEEG activity in human adults. Electroencephalogr. Clin. Neurophysiol. *107*, 287–295.

Cochin, S., Barthelemy, C., Roux, S., and Martineau, J. (1999). Observation and execution of movement: similarities demonstrated by quantified electroencephalography. Eur. J. Neurosci. *11*, 1839 –1842.

Cohen-Seat, G., Gastaut, H., Faure, J., and Heuyer, G. (1954). Etudes expérimentales de l'activité nerveuse pendant la projection cinématographique. Rev Int Filmol *5*, 7–64.

Crick, F., and Jones, E. (1993). Backwardness of human neuroanatomy. Nature *361*, 109–110.

Decety, J. (1996). The neurophysiological basis of motor imagery. Behav. Brain Res. *77*, 45–52.

Dechent, P., and Frahm, J. (2000). Direct mapping of ocular dominance columns in human primary visual cortex. Neuroreport *11*, 3247–3249.

Dechent, P., and Frahm, J. (2003a). Functional somatotopy of finger representations in human primary motor cortex. Hum. Brain Mapp. *18*, 272–283.

Dechent, P., and Frahm, J. (2003b). Functional somatotopy of finger representations in human primary motor cortex. Hum. Brain Mapp. *18*, 272–283.

Dechent, P., Merboldt, K.-D., and Frahm, J. (2004). Is the human primary motor cortex involved in motor imagery? Cogn. Brain Res. *19*, 138–144.

Deichmann, R., Gottfried, J.A., Hutton, C., and Turner, R. (2003). Optimized EPI for fMRI studies of the orbitofrontal cortex. NeuroImage *19*, 430–441.

Desimone, R., Albright, T.D., Gross, C.G., and Bruce, C. (1984). Stimulus-selective properties of inferior temporal neurons in the macaque. J. Neurosci. *4*, 2051–2062.

Diogo, A.C.M., Soares, J.G.M., Koulakov, A., Albright, T.D., and Gattass, R. (2003). Electrophysiological imaging of functional architecture in the cortical middle temporal visual area of Cebus apella monkey. J. Neurosci. Off. J. Soc. Neurosci. *23*, 3881–3898.

Duong, T.Q., Kim, D.-S., Uğurbil, K., and Kim, S.-G. (2001). Localized cerebral blood flow response at submillimeter columnar resolution. Proc. Natl. Acad. Sci. *98*, 10904–10909.

Duyn, J.H. (2012). The future of ultra-high field MRI and fMRI for study of the human brain. NeuroImage *62*, 1241–1248.

Economo, C., and Triarhou, L.C. (2009). Cellular structure of the human cerebral cortex (Basel; New York: Karger).

Edelman, R.R. (2006). Clinical magnetic resonance imaging Vol. 1. Vol. 1. (Philadelphia, PA: Saunders Elsevier).

Fadiga, L., Fogassi, L., Pavesi, G., and Rizzolatti, G. (1995). Motor facilitation during action observation: a magnetic stimulation study. J. Neurophysiol. *73*, 2608–2611.

Fadiga, L., Craighero, L., and Olivier, E. (2005). Human motor cortex excitability during the perception of others' action. Curr. Opin. Neurobiol. *15*, 213–218.

Friston, K.J., Holmes, A.P., Worsley, K.J., Poline, J.-P., Frith, C.D., and Frackowiak, R.S.J. (1994). Statistical parametric maps in functional imaging: A general linear approach. Hum. Brain Mapp. *2*, 189–210.

Gallese, V., Fadiga, L., Fogassi, L., and Rizzolatti, G. (1996). Action recognition in the premotor cortex. Brain *119*, 593–609.

Galuske, R.A.W., Schlote, W., Bratzke, H., and Singer, W. (2000). Interhemispheric Asymmetries of the Modular Structure in Human Temporal Cortex. Science *289*, 1946–1949.

Gangitano, M., Mottaghy, F.M., and Pascual-Leone, A. (2001). Phase-specific modulation of cortical motor output during movement observation. Neuroreport *12*, 1489–1492.

Gastaut, H.J., and Bert, J. (1954). EEG changes during cinematographic presentation (Moving picture activation of the EEG). Electroencephalogr. Clin. Neurophysiol. *6*, 433–444.

Genovese, C.R., Lazar, N.A., and Nichols, T. (2002). Thresholding of Statistical Maps in Functional Neuroimaging Using the False Discovery Rate. NeuroImage *15*, 870–878.

Gerardin, E., Sirigu, A., Lehéricy, S., Poline, J.-B., Gaymard, B., Marsault, C., Agid, Y., and Bihan, D.L. (2000). Partially Overlapping Neural Networks for Real and Imagined Hand Movements. Cereb. Cortex *10*, 1093–1104.

Geva, T. (2006). Magnetic resonance imaging: historical perspective. J. Cardiovasc. Magn. Reson. Off. J. Soc. Cardiovasc. Magn. Reson. *8*, 573–580.

Ghose, G.M., and Ts'o, D.Y. (1997). Form processing modules in primate area V4. J. Neurophysiol. *77*, 2191–2196.

Goldman-Rakic, P.S., and Schwartz, M.L. (1982). Interdigitation of contralateral and ipsilateral columnar projections to frontal association cortex in primates. Science *216*, 755–757.

Goodyear, B.G., and Menon, R.S. (2001). Brief visual stimulation allows mapping of ocular dominance in visual cortex using fMRI. Hum. Brain Mapp. *14*, 210–217.

Grafton, S.T., Woods, R.P., Mazziotta, J.C., and Phelps, M.E. (1991). Somatotopic mapping of the primary motor cortex in humans: activation studies with cerebral blood flow and positron emission tomography. J. Neurophysiol. *66*, 735–743.

Graham C. Wiggins, D Phil; Daniel K. Sodickson, MD, PhD, *MReadings: Ultra High Field MRI*, MAGNETOM Flash, 1/2011

Grezes, J. (1998). Top down Effect of Strategy on the Perception of Human Biological Motion: A Pet Investigation. Cogn. Neuropsychol. *15*, 553–582.

Guillot, A., Collet, C., Nguyen, V.A., Malouin, F., Richards, C., and Doyon, J. (2008). Functional neuroanatomical networks associated with expertise in motor imagery. NeuroImage *41*, 1471–1483.

Hadjikhani, N., Liu, A.K., Dale, A.M., Cavanagh, P., and Tootell, R.B.H. (1998). Retinotopy and color sensitivity in human visual cortical area V8. Nat. Neurosci. *1*, 235–241.

Hanakawa, T., Immisch, I., Toma, K., Dimyan, M.A., Van Gelderen, P., and Hallett, M. (2003). Functional properties of brain areas associated with motor execution and imagery. J. Neurophysiol. *89*, 989–1002.

Hari, R., Forss, N., Avikainen, S., Kirveskari, E., Salenius, S., and Rizzolatti, G. (1998). Activation of human primary motor cortex during action observation: A neuromagnetic study. Proc. Natl. Acad. Sci. *95*, 15061–15065.

Herculano-Houzel, S. (2009). The Human Brain in Numbers: A Linearly Scaled-up Primate Brain. Front. Hum. Neurosci. *3*.

Hluštík, P., Solodkin, A., Gullapalli, R.P., Noll, D.C., and Small, S.L. (2001). Somatotopy in Human Primary Motor and Somatosensory Hand Representations Revisited. Cereb. Cortex *11*, 312–321.

Hotelling, H. (1953). New Light on the Correlation Coefficient and its Transforms. J. R. Stat. Soc. Ser. B Methodol. *15*, 193–232.

Hubel, D.H., and Wiesel, T.N. (1959). Receptive fields of single neurones in the cat's striate cortex. J. Physiol. *148*, 574–591.

Hubel, D.H., and Wiesel, T.N. (1977). Ferrier lecture. Functional architecture of macaque monkey visual cortex. Proc. R. Soc. Lond. Ser. B Contain. Pap. Biol. Character R. Soc. G. B. *198*, 1–59.

Hübener, M., Shoham, D., Grinvald, A., and Bonhoeffer, T. (1997). Spatial Relationships among Three Columnar Systems in Cat Area 17. J. Neurosci. *17*, 9270–9284.

Huck, S.W., and McLean, R.A. (1975). Using a repeated measures ANOVA to analyze the data from a pretest-posttest design: A potentially confusing task. Psychol. Bull. *82*, 511–518.

Huettel, S.A., Song, and McCarthy (2009). Functional magnetic resonance imaging (Sunderland (MA): Sinauer Associates).

Imaios, *e-MRI*, 2008-2014. [http://www.imaios.com/en/e-Courses/e-MRI] (21 November 2013)

Indovina, I., and Sanes, J.N. (2001). On somatotopic representation centers for finger movements in human primary motor cortex and supplementary motor area. NeuroImage *13*, 1027–1034.

Jankowska, E., Padel, Y., and Tanaka, R. (1975). The mode of activation of pyramidal tract cells by intracortical stimuli. J. Physiol. *249*, 617–636.

Jeannerod, M. (1994). The representing brain: Neural correlates of motor intention and imagery. Behav. Brain Sci. *17*, 187–202.

Jeannerod, M. (2001). Neural Simulation of Action: A Unifying Mechanism for Motor Cognition. NeuroImage *14*, S103–S109.

Jeannerod, M., Arbib, M.A., Rizzolatti, G., and Sakata, H. (1995). Grasping objects: the cortical mechanisms of visuomotor transformation. Trends Neurosci. *18*, 314–320.

Jellema, T., Baker, C.I., Wicker, B., and Perrett, D.I. (2000). Neural Representation for the Perception of the Intentionality of Actions. Brain Cogn. *44*, 280–302.

Jenkinson, M., Bannister, P., Brady, M., and Smith, S. (2002). Improved optimization for the robust and accurate linear registration and motion correction of brain images. NeuroImage *17*, 825–841.

Kandel, E.R., Schwartz, J.H., and Jessell, T.M. (2000). Principles of neural science (New York: McGraw-Hill, Health Professions Division).

Krieg, W.J.S. (1946). Connections of the cerebral cortex. I. The albino rat. A. Topography of the cortical areas. J. Comp. Neurol. *84*, 221–275.

Kuhtz-Buschbeck, J.P., Mahnkopf, C., Holzknecht, C., Siebner, H., Ulmer, S., and Jansen, O. (2003). Effector-independent representations of simple and complex imagined finger movements: a combined fMRI and TMS study. Eur. J. Neurosci. *18*, 3375–3387.

Kwan, H.C., MacKay, W.A., Murphy, J.T., and Wong, Y.C. (1978). Spatial organization of precentral cortex in awake primates. II. Motor outputs. J. Neurophysiol. *41*, 1120–1131.

Kwong, K.K., Belliveau, J.W., Chesler, D.A., Goldberg, I.E., Weisskoff, R.M., Poncelet, B.P., Kennedy, D.N., Hoppel, B.E., Cohen, M.S., and Turner, R. (1992). Dynamic magnetic resonance imaging of human brain activity during primary sensory stimulation. Proc. Natl. Acad. Sci. U. S. A. *89*, 5675–5679.

Lim, K.O., and Pfefferbaum, A. (1989). Segmentation of MR brain images into cerebrospinal fluid spaces, white and gray matter. J. Comput. Assist. Tomogr. *13*, 588–593.

Lorente De Nó, R. (1938a). Synaptic stimulation of motoneurons as a local process. J. Neurophysiol. *1*, 195–206.

Lorente De Nó, R. (1938b). Synaptic stimulation of motoneurons as a local process. J. Neurophysiol. *1*, 195–206.

Lotze, M., Seggewies, G., Erb, M., Grodd, W., and Birbaumer, N. (2000). The representation of articulation in the primary sensorimotor cortex. Neuroreport *11*, 2985–2989.

Maeda, F., Kleiner-Fisman, G., and Pascual-Leone, A. (2002). Motor facilitation while observing hand actions: specificity of the effect and role of observer's orientation. J. Neurophysiol. *87*, 1329–1335.

Marques, J.P., and Gruetter, R. (2013). New Developments and Applications of the MP2RAGE Sequence - Focusing the Contrast and High Spatial Resolution R1 Mapping. PLoS ONE *8*, e69294.

Marques, J.P., Kober, T., Krueger, G., van der Zwaag, W., Van de Moortele, P.-F., and Gruetter, R. (2010). MP2RAGE, a self bias-field corrected sequence for improved segmentation and T1-mapping at high field. NeuroImage *49*, 1271–1281.

De Martino, F., Esposito, F., van de Moortele, P.-F., Harel, N., Formisano, E., Goebel, R., Ugurbil, K., and Yacoub, E. (2011). Whole brain high-resolution functional imaging at ultra high magnetic fields: an application to the analysis of resting state networks. NeuroImage *57*, 1031–1044.

McRobbie, D.W. (2007). MRI from picture to proton (Cambridge, UK; New York: Cambridge University Press).

Menon, R.S. (2002). Postacquisition suppression of large-vessel BOLD signals in high-resolution fMRI. Magn. Reson. Med. *47*, 1–9.

Menon, R.S., Ogawa, S., Strupp, J.P., and Uğurbil, K. (1997). Ocular dominance in human V1 demonstrated by functional magnetic resonance imaging. J. Neurophysiol. *77*, 2780–2787.

Mountcastle, V.B. (1997). The columnar organization of the neocortex. Brain J. Neurol. *120 (Pt 4)*, 701–722.

Mountcastle, V.B. (1957). Modality and topographic properties of single neurons of cat's somatic sensory cortex. J. Neurophysiol. *20*, 408–434.

Nair, D.G., Purcott, K.L., Fuchs, A., Steinberg, F., and Kelso, J.A.S. (2003). Cortical and cerebellar activity of the human brain during imagined and executed unimanual and bimanual action sequences: a functional MRI study. Cogn. Brain Res. *15*, 250–260.

Neuper, C., Müller-Putz, G.R., Scherer, R., and Pfurtscheller, G. (2006). Motor imagery and EEG-based control of spelling devices and neuroprostheses. In Progress in Brain Research, Christa Neuper and Wolfgang Klimesch, ed. (Elsevier), pp. 393–409.

Nichols, T.E., and Holmes, A.P. (2002). Nonparametric permutation tests for functional neuroimaging: A primer with examples. Hum. Brain Mapp. *15*, 1–25.

Nishitani, N., and Hari, R. (2000). Temporal dynamics of cortical representation for action. Proc. Natl. Acad. Sci. *97*, 913–918.

Nishitani, N., and Hari, R. (2002). Viewing lip forms: cortical dynamics. Neuron *36*, 1211–1220.

De No, L. (1938). The cerebral cortex: architecture, intracortical connections and motor projections. In Physiology of the Nervous System, J. Fulton, ed. (Oxford University Press), pp. 291–301.

Ogawa, S., Lee, T.M., Kay, A.R., and Tank, D.W. (1990). Brain magnetic resonance imaging with contrast dependent on blood oxygenation. Proc. Natl. Acad. Sci. U. S. A. *87*, 9868–9872.

Ogawa, S., Tank, D.W., Menon, R., Ellermann, J.M., Kim, S.G., Merkle, H., and Ugurbil, K. (1992). Intrinsic signal changes accompanying sensory stimulation: functional brain mapping with magnetic resonance imaging. Proc. Natl. Acad. Sci. U. S. A. *89*, 5951–5955.

Ogawa, S., Menon, R.S., Tank, D.W., Kim, S.G., Merkle, H., Ellermann, J.M., and Ugurbil, K. (1993). Functional brain mapping by blood oxygenation level-dependent contrast magnetic resonance imaging. A comparison of signal characteristics with a biophysical model. Biophys. J. *64*, 803–812.

Di Pellegrino, G., Fadiga, L., Fogassi, L., Gallese, V., and Rizzolatti, G. (1992). Understanding motor events: a neurophysiological study. Exp. Brain Res. *91*, 176–180.

Penfield, W., and Boldrey, E. (1937). Somatic Motor and Sensory Representation in the Cerebral Cortex of Man as Studied by Electrical Stimulation. Brain *60*, 389–443.

Penfield, W., and Rasmussen, T. (1950). The cerebral cortex of man; a clinical study of localization of function (Oxford, England: Macmillan).

Perrett, D.I., Harries, M.H., Bevan, R., Thomas, S., Benson, P.J., Mistlin, A.J., Chitty, A.J., Hietanen, J.K., and Ortega, J.E. (1989). Frameworks of analysis for the neural representation of animate objects and actions. J. Exp. Biol. *146*, 87–113.

Perrett, D.I., Hietanen, J.K., Oram, M.W., Benson, P.J., and Rolls, E.T. (1992). Organization and Functions of Cells Responsive to Faces in the Temporal Cortex [and Discussion]. Philos. Trans. R. Soc. Lond. B. Biol. Sci. *335*, 23–30.

Pfurtscheller, G., and Lopes da Silva, F.H. (1999). Event-related EEG/MEG synchronization and desynchronization: basic principles. Clin. Neurophysiol. *110*, 1842–1857.

Poldrack, R.A., Mumford, J.A., and Nichols (2011). Handbook of functional MRI data analysis (New York: Cambridge University Press).

Porro, C.A., Cettolo, V., Francescato, M.P., and Baraldi, P. (2000). Ipsilateral involvement of primary motor cortex during motor imagery. Eur. J. Neurosci. *12*, 3059–3063.

Powell, T.P., and MOUNTCASTLE, V.B. (1959). Some aspects of the functional organization of the cortex of the postcentral gyrus of the monkey: a correlation of findings obtained in a single unit analysis with cytoarchitecture. Bull. Johns Hopkins Hosp. *105*, 133–162.

Qi, H.-X., Stepniewska, I., and Kaas, J.H. (2000). Reorganization of Primary Motor Cortex in Adult Macaque Monkeys With Long-Standing Amputations. J. Neurophysiol. *84*, 2133–2147.

Rizzolatti, G., and Craighero, L. (2004). The Mirror-Neuron System. Annu. Rev. Neurosci. *27*, 169–192.

Rizzolatti, G., and Luppino, G. (2001). The Cortical Motor System. Neuron *31*, 889–901.

Rizzolatti, G., Fadiga, L., Gallese, V., and Fogassi, L. (1996a). Premotor cortex and the recognition of motor actions. Brain Res. Cogn. Brain Res. *3*, 131–141.

Rizzolatti, G., Fadiga, L., Matelli, M., Bettinardi, V., Paulesu, E., Perani, D., and Fazio, F. (1996b). Localization of grasp representations in humans by PET: 1. Observation versus execution. Exp. Brain Res. *111*, 246–252.

Rizzolatti, G., Fogassi, L., and Gallese, V. (2001). Neurophysiological mechanisms underlying the understanding and imitation of action. Nat. Rev. Neurosci. *2*, 661–670.

Lee Rodgers, J., and Nicewander, W.A. (1988). Thirteen Ways to Look at the Correlation Coefficient. Am. Stat. *42*, 59–66.

Roth, M., Decety, J., Raybaudi, M., Massarelli, R., Delon-Martin, C., Segebarth, C., Morand, S., Gemignani, A., Décorps, M., and Jeannerod, M. (1996). Possible involvement of primary motor cortex in mentally simulated movement: a functional magnetic resonance imaging study. Neuroreport *7*, 1280–1284.

Sacco, K., Cauda, F., Cerliani, L., Mate, D., Duca, S., and Geminiani, G.C. (2006). Motor imagery of walking following training in locomotor attention. The effect of "the tango lesson."NeuroImage *32*, 1441–1449.

Salomon, R., Bleich-Cohen, M., Hahamy-Dubossarsky, A., Dinstien, I., Weizman, R., Poyurovsky, M., Kupchik, M., Kotler, M., Hendler, T., and Malach, R. (2011). Global functional connectivity deficits in schizophrenia depend on behavioral state. J. Neurosci. Off. J. Soc. Neurosci. *31*, 12972–12981.

Sanes, J.N., Donoghue, J.P., Thangaraj, V., Edelman, R.R., and Warach, S. (1995). Shared neural substrates controlling hand movements in human motor cortex. Science *268*, 1775–1777.

Scheibel, M.E., Tomiyasu, U., and Scheibel, A.B. (1977). The aging human betz cell. Exp. Neurol. *56*, 598–609.

Schieber, M.H. (1995). Muscular production of individuated finger movements: the roles of extrinsic finger muscles. J. Neurosci. *15*, 284–297.

Schieber, M.H. (1999). Somatotopic gradients in the distributed organization of the human primary motor cortex hand area: Evidence from small infarcts. Exp. Brain Res. *128*, 139–148.

Schieber, M.H. (2001). Constraints on somatotopic organization in the primary motor cortex. J. Neurophysiol. *86*, 2125–2143.

Schieber, M.H., and Hibbard, L.S. (1993). How somatotopic is the motor cortex hand area? Science *261*, 489–492.

Schünke, M., Schulte, E., and Schumacher, U. (2010). Thieme atlas of anatomy. (Stuttgart; New York: Thieme).

Senden, M. (2012). Structural connectivity allows for multi-threading during rest: The structure of the cortex leads to efficient alternation between resting state exploratory behavior and default mode processing. NeuroImage *60*, 2274–2284.

Sharma, N., Jones, P.S., Carpenter, T.A., and Baron, J.-C. (2008). Mapping the involvement of BA 4a and 4p during Motor Imagery. NeuroImage *41*, 92–99.

Shmuel, A., and Grinvald, A. (1996). Functional Organization for Direction of Motion and Its Relationship to Orientation Maps in Cat Area 18. J. Neurosci. *16*, 6945–6964.

Shmuel, A., Yacoub, E., Chaimow, D., Logothetis, N.K., and Ugurbil, K. (2007). Spatio-temporal point-spread function of fMRI signal in human gray matter at 7 Tesla. NeuroImage *35*, 539–552.

Snell, R.S. (2010). Clinical neuroanatomy (Philadelphia: Wolters Kluwer Health/Lippincott Williams & Wilkins).

Solodkin, A., Hlustik, P., Chen, E.E., and Small, S.L. (2004). Fine Modulation in Network Activation during Motor Execution and Motor Imagery. Cereb. Cortex *14*, 1246–1255.

Song, A.W., Wong, E.C., Tan, S.G., and Hyde, J.S. (1996). Diffusion weighted fMRI at 1.5 T. Magn. Reson. Med. *35*, 155–158.

Speck, O., Stadler, J., and Zaitsev, M. (2008). High resolution single-shot EPI at 7T. Magma N. Y. N *21*, 73–86.

Squire, L.R. (2013). Fundamental neuroscience (Amsterdam; Boston: Elsevier/Academic Press).

Strafella, A.P., and Paus, T. (2000). Modulation of cortical excitability during action observation: a transcranial magnetic stimulation study. Neuroreport *11*, 2289–2292.

Strominger, N.L., Demarest, R.J., and Laemle, L.B. (2012). Noback's Human Nervous System, Seventh Edition: Structure and Function (Totowa, NJ: Humana Press).

Talairach, J., and Tournoux, P. (1988). Co-Planar Stereotaxic Atlas of the Human Brain: 3-D Proportional System: An Approach to Cerebral Imaging (Thieme Classics) (Thieme).

Tanner, M., Gambarota, G., Kober, T., Krueger, G., Erritzoe, D., Marques, J.P., and Newbould, R. (2012). Fluid and white matter suppression with the MP2RAGE sequence. J. Magn. Reson. Imaging *35*, 1063–1070.

Tootell, R.B., Silverman, M.S., Switkes, E., and Valois, R.D. (1982). Deoxyglucose analysis of retinotopic organization in primate striate cortex. Science *218*, 902–904.

Tootell, R.B., Silverman, M.S., Valois, R.D., and Jacobs, G.H. (1983). Functional organization of the second cortical visual area in primates. Science *220*, 737–739.

Tootell, R.B.H., Hadjikhani, N., Hall, E.K., Marrett, S., Vanduffel, W., Vaughan, J.T., and Dale, A.M. (1998). The Retinotopy of Visual Spatial Attention. Neuron *21*, 1409–1422.

Triantafyllou, C., Hoge, R.D., Krueger, G., Wiggins, C.J., Potthast, A., Wiggins, G.C., and Wald, L.L. (2005). Comparison of physiological noise at 1.5 T, 3 T and 7 T and optimization of fMRI acquisition parameters. NeuroImage *26*, 243–250.

Vaughan, J.T., Garwood, M., Collins, C.M., Liu, W., DelaBarre, L., Adriany, G., Andersen, P., Merkle, H., Goebel, R., Smith, M.B., et al. (2001). 7T vs. 4T: RF power, homogeneity, and signal-to-noise comparison in head images. Magn. Reson. Med. Off. J. Soc. Magn. Reson. Med. Soc. Magn. Reson. Med. *46*, 24–30.

Vovk, U., Pernus, F., and Likar, B. (2007). A review of methods for correction of intensity inhomogeneity in MRI. IEEE Trans. Med. Imaging *26*, 405–421.

Weliky, M., Bosking, W.H., and Fitzpatrick, D. (1996). A systematic map of direction preference in primary visual cortex. Nature *379*, 725–728.

Woolrich, M.W., Ripley, B.D., Brady, M., and Smith, S.M. (2001). Temporal autocorrelation in univariate linear modeling of FMRI data. NeuroImage *14*, 1370–1386.

Woolsey, C.N., SETTLAGE, P.H., MEYER, D.R., SENCER, W., PINTO HAMUY, T., and TRAVIS, A.M. (1952). Patterns of localization in precentral and "supplementary" motor areas and their relation to the concept of a premotor area. Res. Publ. - Assoc. Res. Nerv. Ment. Dis. *30*, 238–264.

Wriessnegger, S.C., Kurzmann, J., and Neuper, C. (2008). Spatio-temporal differences in brain oxygenation between movement execution and imagery: A multichannel near-infrared spectroscopy study. Int. J. Psychophysiol. *67*, 54–63.

Yacoub, E., Shmuel, A., Pfeuffer, J., Van De Moortele, P.-F., Adriany, G., Ugurbil, K., and Hu, X. (2001). Investigation of the initial dip in fMRI at 7 Tesla. NMR Biomed. *14*, 408–412.

Yacoub, E., Shmuel, A., Logothetis, N., and Uğurbil, K. (2007). Robust detection of ocular dominance columns in humans using Hahn Spin Echo BOLD functional MRI at 7 Tesla. NeuroImage *37*, 1161–1177.

Yacoub, E., Harel, N., and Uğurbil, K. (2008). High-field fMRI unveils orientation columns in humans. Proc. Natl. Acad. Sci. *105*, 10607–10612.

Zimmermann, J., Goebel, R., De Martino, F., van de Moortele, P.-F., Feinberg, D., Adriany, G., Chaimow, D., Shmuel, A., Uğurbil, K., and Yacoub, E. (2011a). Mapping the Organization of Axis of Motion Selective Features in Human Area MT Using High-Field fMRI. PLoS ONE *6*, e28716.

Zimmermann, J., Goebel, R., De Martino, F., van de Moortele, P.-F., Feinberg, D., Adriany, G., Chaimow, D., Shmuel, A., Uğurbil, K., and Yacoub, E. (2011b). Mapping the Organization of Axis of Motion Selective Features in Human Area MT Using High-Field fMRI. PLoS ONE *6*, e28716.

Van der Zwaag, W., Francis, S., Head, K., Peters, A., Gowland, P., Morris, P., and Bowtell, R. (2009). fMRI at 1.5, 3 and 7 T: Characterising BOLD signal changes. NeuroImage *47*, 1425–1434.

Annex

Characterization of the grid's thickness

Below we present the average values of the grid's thickness for each subject and for each grid.

Table 2 – Average values of grid's thickness for each subject

Subject\Grid	FG1	FG3	Total
S1	1,655369	1,662321	1,658845
S2	1,506268	1,009246	1,257757
S3	1,941867	2,338102	2,139985
S4	1,894587	1,606344	1,750465
S5	1,320445	1,498198	1,409322
S6	1,867866	1,39956	1,633713
S7	1,975156	1,895188	1,935172
S8	1,421237	1,97428	1,697758
S9	2,235186	2,014034	2,12461
S10	2,30327	1,407502	1,855386
S11	3,354868	3,894956	3,624912
S12	1,64796	1,43269	1,540325
S13	1,361017	1,807432	1,584224
Average	**1,883469**	**1,841527**	**1,862498**

Examples of functional activity of motor execution in M1

In this section we show other examples of the direct functional maps for ME.

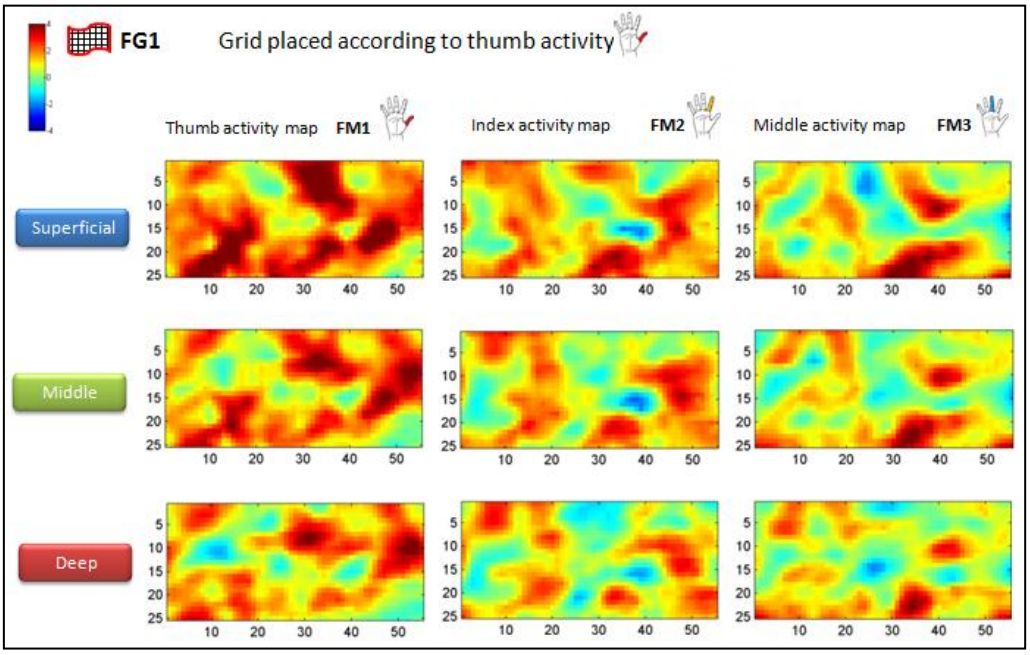

Figure I - Activity maps of thumb grid in single subject [S2] using the direct paradigm.

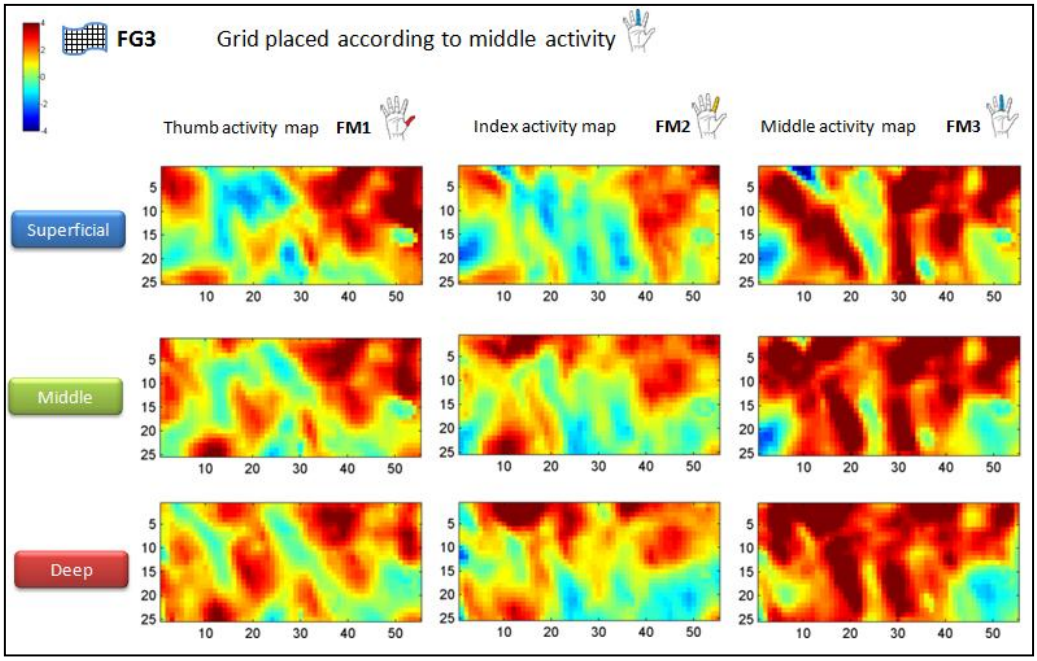

Figure II - Activity maps of middle finger grid in single subject [S4] using the direct paradigm.

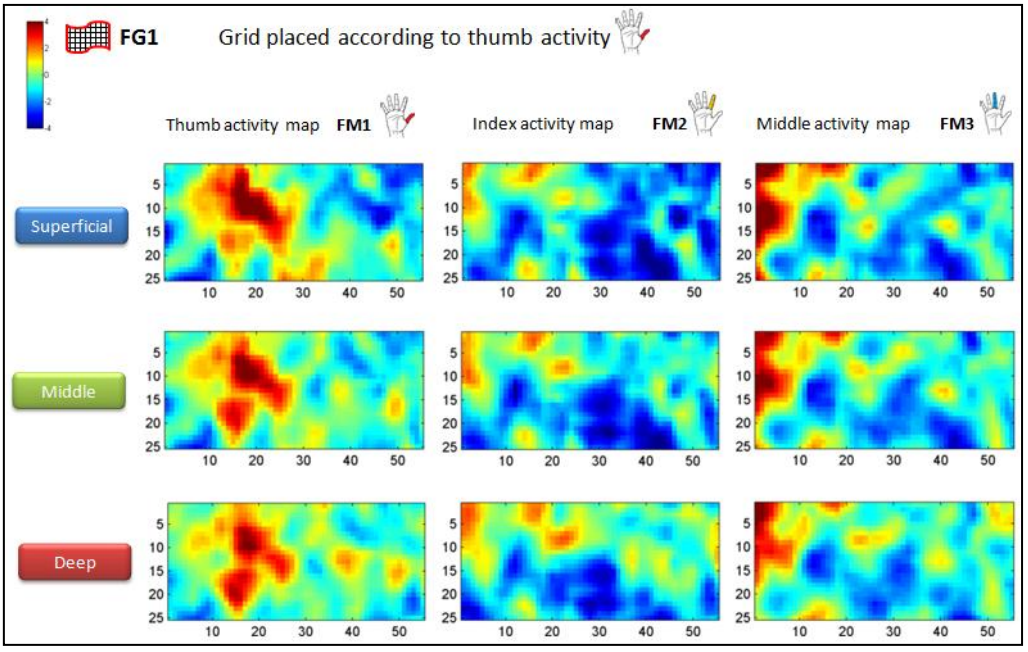

Figure III - Activity maps of thumb grid in single subject [S5] using the direct paradigm.

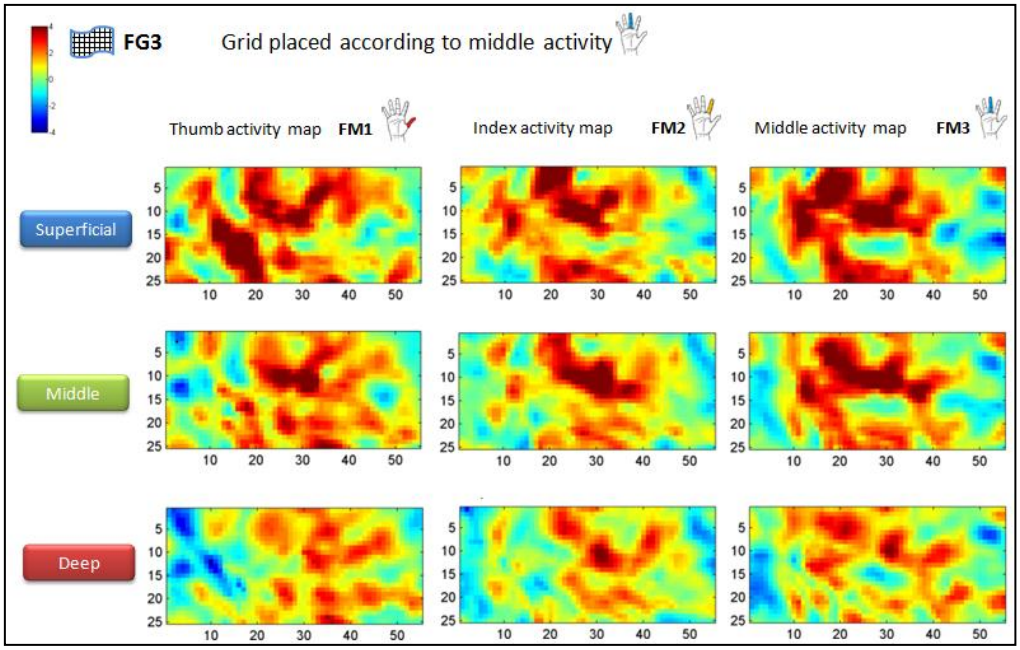

Figure IV - Activity maps of middle finger grid in single subject [S7] using the direct paradigm.

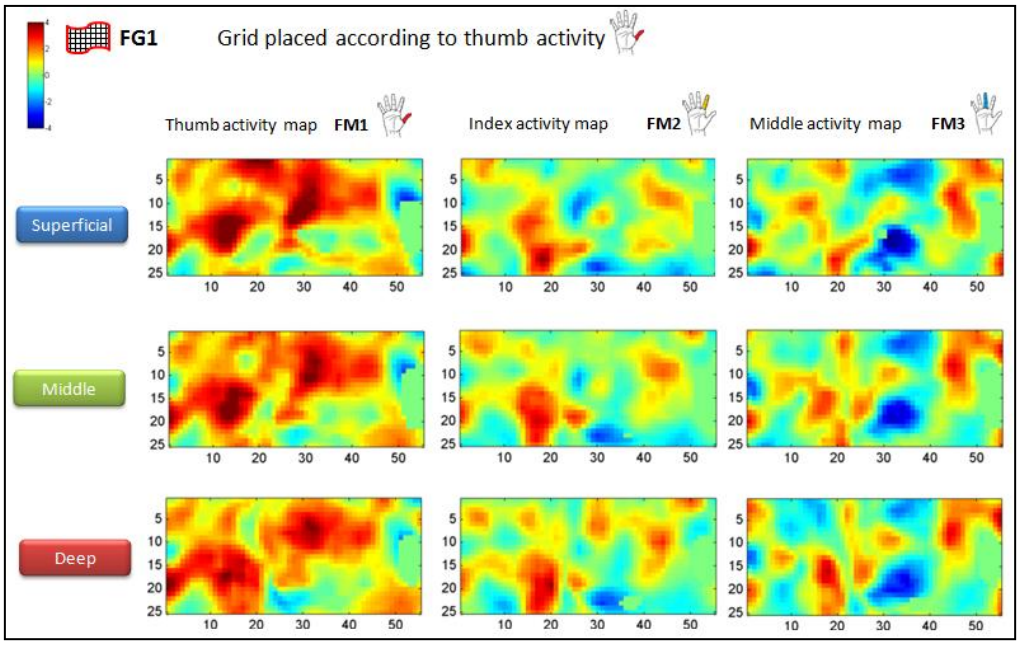

Figure V - Activity maps of thumb grid in single subject [S3] using the direct paradigm.

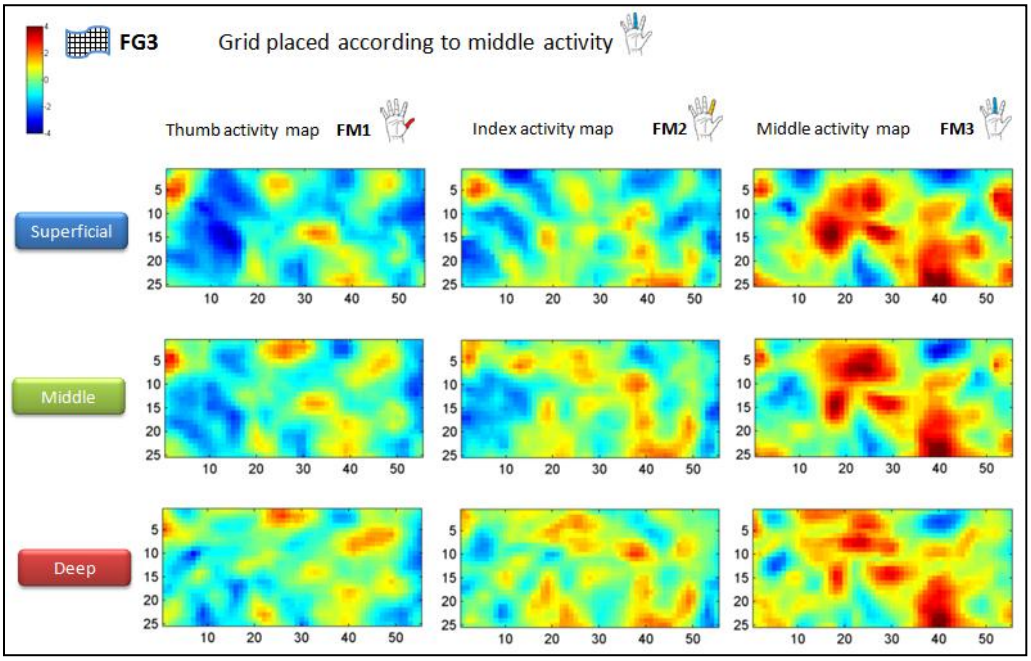

Figure VI - Activity maps of middle finger grid in single subject [S1] using the direct paradigm.

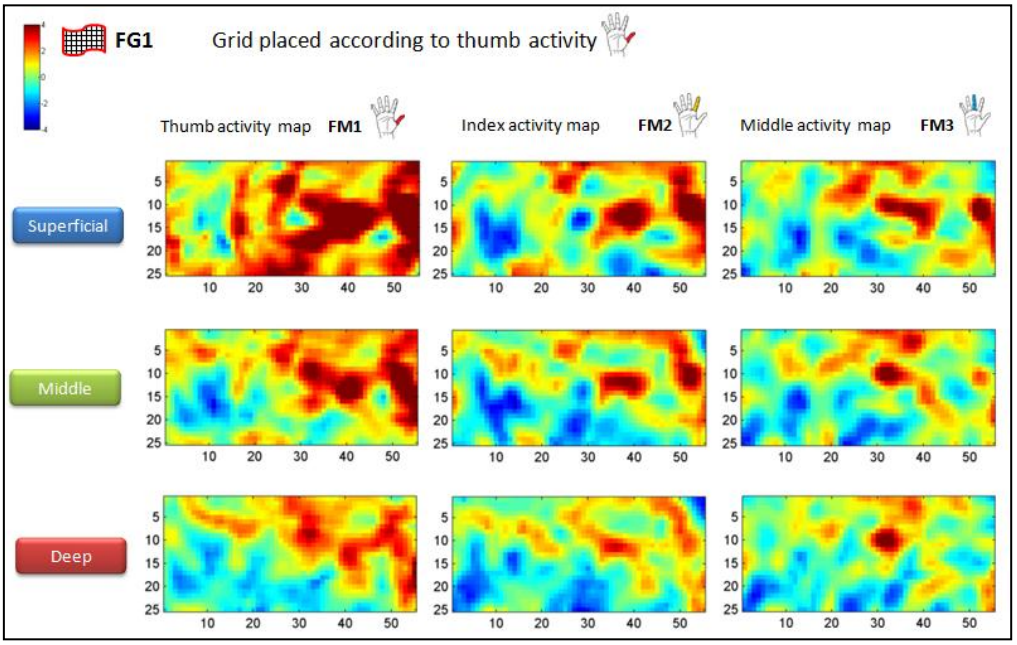

Figure VII - Activity maps of middle finger grid in single subject [S7] using the direct paradigm.

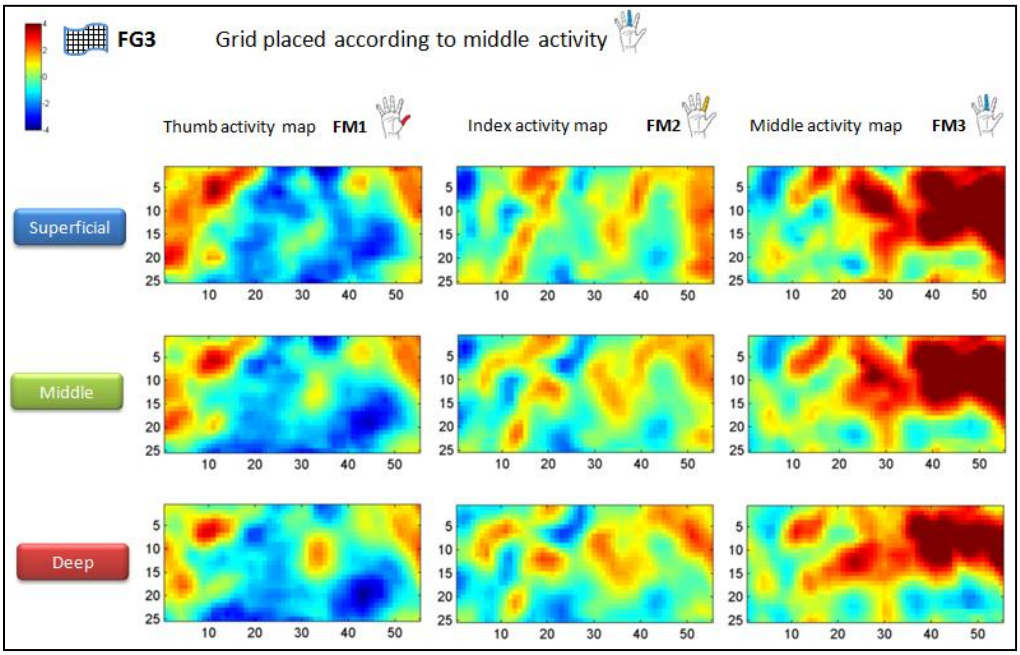

Figure VIII - Activity maps of middle finger grid in single subject [S10] using the direct paradigm.

Catarina Pereira Amado
Abril 2014